MSc thesis

Investigation of a concrete deck connection in reusable composite floor system

Luxi Jiang

Civil Engineering

Steel and Timber Structures

TU Delft

DELFT UNIVERSITY OF TECHNOLOGY

MASTER THESIS

MSC CIVIL ENGINEERING

STEEL AND TIMBER STRUCTURES

Investigation of a concrete deck connection in reusable composite floor system

Authors:
Luxi Jiang (5614228)

Assessment Committee:
Prof.dr. Milan Veljkovic
Dr. Florentia Kavoura
Dr. Yuguang Yang

January 25, 2024

TU Delft Delft University of Technology

CONTENTS

ABSTRACT

In the construction industry, composite structures combining concrete and steel are commonly employed in floor systems due to their exceptional performance in compression and tension. With a growing emphasis on sustainability and Life Cycle Assessment (LCA), this thesis introduces a novel concept: a modularised floor system consisting of reusable concrete deck and composite beam.

This research focuses on analysing the behaviour of an innovative demountable "concrete to concrete" by FEA. A connection between the composite beam and concrete deck connected by a shear connector (bolt). The goal is to understand the mechanical behaviour of such connections.

This design differs from cast-in-situ traditional composite floor systems by having a concrete deck divided into three separate parts that are connected by bolted shear connectors. The composite floor consists of composite girders and concrete decks.
A key advantage of this system is the ability to extract the concrete deck from existing floor systems, offering economic benefits and reducing carbon emissions over its life cycle.

The mechanical performance of the newly designed connection between two concrete segments (a composite beam and a concrete deck) is examined through a shear and bending model using Abaqus Software.

The shear model does not represent a real case loading, and it is introduced to gain confidence in the numerical analysis due to the absence of experimental data in this research. The specimen consists of two concrete blocks being pulled apart. These blocks are connected by a demountable shear connector (bolt) in the middle.

A three-point bending model presents the mechanical behaviour and realistic potential failure modes of the innovative demountable "concrete to concrete" connection. It consists of three connected concrete segments. This model reveals failure modes, including cracking at the "re-entrant corners" of the connection points, crushing of concrete at the mid-plane of the connection and under the bolt nut, and transverse concrete cracking originating from the bolt hole, refer to Figure 6.26.

To enhance the structural behavior of this modularised floor system, several methods are investigated. First, adding steel plates at the connections effectively mitigates concrete crushing at the mid-plane and prevents cracking at the re-entrant corners. Second, relocating the connection to zero-bending moment positions results in a notable reduction

in the three failure modes, improving loading capacity by about 10%.

*Furthermore, the environmental impact of this novel design is noteworthy. With the assumption given in this thesis, for an area of 5.67m*8m concrete deck, reusing the newly designed concrete deck can result in a savings of approximately 4.2 tonnes of CO_2 emissions per subsequent life cycle. Similarly, reusing concrete decks from existing buildings can lead to a reduction of around 2.33 tonnes of CO_2 emissions per life cycle with this size of the floor.*

Based on the assumptions made in this research, the results suggest that the newly designed concrete deck may have a lower loading capacity than traditional concrete slabs. However, its potential economic and environmental advantages make it a promising topic for future investigations.

Keywords: demountable, concrete deck, "concrete to concrete" connection, modularised floor system, bolted shear connector, second cycle of life, life cycle assessment

ACKNOWLEDGEMENTS

The past two years, and particularly the last eleven months, have been challenging as I worked on this thesis. However, I was fortunate to encounter wonderful individuals who gave me strength on continuing my work.

I would like to extend my deepest gratitude to all those who assisted me in completing this master's thesis.
First and foremost, I am grateful to my Graduation Committee; I owe a heartfelt thank you to Prof. Dr. Milan Veljkovic, who was also my supervisor for the case study project. He encouraged me into the topic of reusable connections. His encouragement and professional guidance were pivotal, especially when I faced uncertainties or had questions. His insights significantly improve the quality of my work.
I would also like to thank my daily supervisor Dr. Florentia Kavoura for her continuous support throughout my thesis journey, her insightful opinions, and constructive suggestions in each of our meetings were instrumental; My thanks also extend to Dr. Yuguang Yang, for joining the committee and providing his professional insights on concrete structures.

Additionally, I want to express my sincere appreciation to my friend, Yufei Zhang. Since her arrival at the TU Delft, her assistance in modeling has been exceptional. Her willingness to always make time to share her insights whenever I faced questions has been a tremendous help.
I am equally grateful to Haodong Qiu, who provided not only emotional support but also practical advice during challenging moments of my thesis. The journey would have been unimaginably difficult without the support and companionship of all my friends.

Last but not least, my utmost gratitude would go to my parents. They have always had faith in me, respected my choices, and offered their support and encouragement unconditionally. Without their enduring faith and support, I would never been able to finish my studies.

Luxi Jiang
Delft, January 2024

1

INTRODUCTION

Concrete and steel are the most widely used materials in construction, but are also recognised as some of the most environmentally detrimental materials. Steel and concrete, contributing to 7% and 6% of CO2 emissions, respectively, collectively account for 12-13% of global emissions [40][65].

Over recent decades, the pressing need for a sustainable environment has surged, driving engineers to seek innovative ways to reuse/recycle structural components and reduce carbon emissions. According to Rijksbreed programma Circulaire Economie (2015) "Net Zero by 2050" [41], the Netherlands has set the target to achieve a balance between greenhouse gasses emission into the atmosphere and the amount removed by means of natural process or through technologies.

Floor systems in buildings are often cast in situ. Prefabrication is seen as a more sustainable construction process. This concept is not used in concrete floor system and relatively seldom in composite (steel-concrete) structures.

Within the scope of this thesis research, the fundamental focus will be on designing an innovative demountable "concrete to concrete connection", a connection between the steel-concrete composite beam and concrete deck, and understanding the mechanical behaviour of such connections. This can be described as a new type of connection which allows a relatively thin concrete deck to be dismounted and reused in the other structures after the first cycle of life, thus contributing to the circular economy. A similar solution for a so-called half joint concrete is well-known in concrete structures [5][12][75], but cannot be directly used in floor system applications.

1

1.1. INTRODUCTION

DUE to the concrete and steel properties of high resistance against compression and tension, respectively, they are often used simultaneously to maximize resistance in elements, as seen in examples like reinforced concrete slabs or composite floor systems.

There are several methods for combining steel and concrete elements together for a composite floor system, most commonly using permanent connections. The most widely used shear connectors are the headed studs which are welded to the top flange of the steel beam and embedded into the concrete slab, see section 2.1. Composite floor systems are typically not demountable since they are cast at the construction site. Consequently the steel beam and concrete floor can only be disconnected with destructive methods.

The majority of floor systems are:
- a monolithic concrete floor system, which consists of concrete beams and concrete decks (reinforced), shown in Figure 1.1 (a), and
- a composite floor system, which consists of composite beams and concrete slabs/composite slabs, which can be seen in Figure 1.1(b).

Transversal re-bars and other potential details are not drawn here since this is a simplified illustration of the floor systems. These two floor systems are based on casting concrete in situ, so the beams cannot be disconnected from the slabs with a non-destructive way.

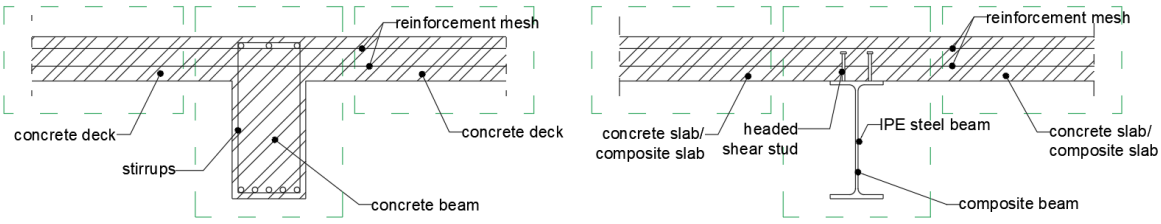

(a) Monolithic concrete floor system (reinforced) (b) Composite floor system (reinforced)

Figure 1.1: Two types of cast in situ floor systems often used in buildings

In this thesis, see in Figure 1.1, the following distinction between concrete slab and concrete deck is used:
- a concrete slab refers to a monolithic reinforced concrete element;
- a concrete deck is a reinforced concrete element that forms part of a composite floor structure.

Normally, the (a) monolithic concrete floor system shown in Figure 1.1 cannot be reused after its first life cycle since it is cast in situ, the structure is often demolished, and the concrete members possibly could be recycled.
The proposed demountable connector in this research aims to allow for the reuse of

the monolithic concrete deck of the concrete floor system (shown in Figure 1.1 (a)) and the composite floor system (shown in Figure 1.1 (b)). By separating the floor system along the green dashed lines shown, the aforementioned concrete components (decks and slabs) could eventually be reused instead of recycled. As a side note, reusing of these elements normally requires a check of the original reinforcement design.

Within the scope of this thesis, reusing the concrete beam from a monolithic concrete floor system (shown in Figure 1.1 (a)) is not considered, since the beam is the critical load-bearing component. Reuse of concrete beams requires detailed information and it is left out of scope for the MSc thesis.

The main goal of this research is to enhance the modularisation of concrete floor systems and their integration into a circular built environment.

1.2. MOTIVATION

Research shows that the cement production process for concrete causes high amounts of CO_2 release, up to 5 to 6% on a global scale, see subsection 2.2.1. To slow down climate change, reduce air pollutants, and maintain biodiversity, immediate action against gas emissions should be taken.

Therefore, when the building reaches the end of its service life, it is considered to keep structural elements as much as possible in the life cycle (second cycle of life and further) and a feasible solution is needed to perform such reusable action. Even if the elements are planned to be demolished, strive to take the construction material and reuse/recycle it as much as possible.

Disconnecting the concrete deck from existing building and combining it with a composite beam prevents the fabrication of a new concrete element, as mentioned in section 1.1.

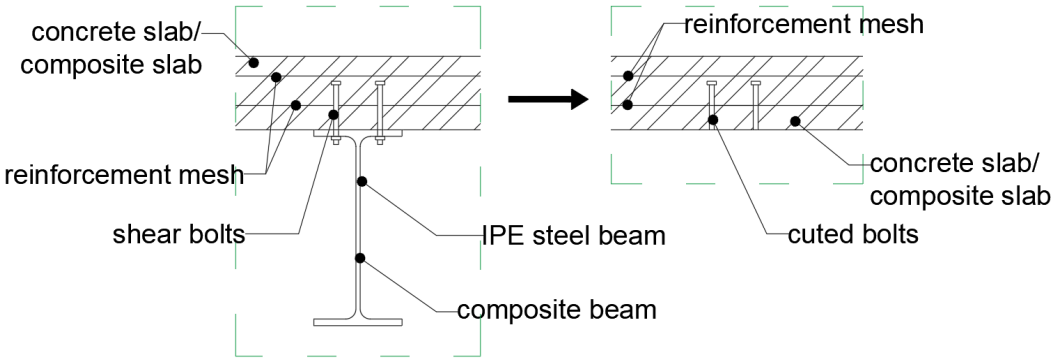

Figure 1.2: Reusing concrete slab cut from the composite floor system

1

See Figure 1.2 above for illustration in case the bolts are used in a prefabricated composite floor system. If bolts are used instead of headed shear studs in the concrete floor system as shown, the concrete deck can be easily separated from the steel beam, but bolts should be cut, and the concrete slab can be sawed to appropriate measures. By doing so, the concrete deck can be reused. Therefore, embedded CO_2 emissions will be saved, which will be discussed in section 7.

The concrete elements (concrete deck and steel-concrete composite beam) can be integrated by adding steel plates at both the top and bottom surfaces of the concrete end sections, as shown in Figure 1.3. These plates are connected by bolts which go through the concrete elements. A number of bolts should be determined to facilitate a secure and effective connection.

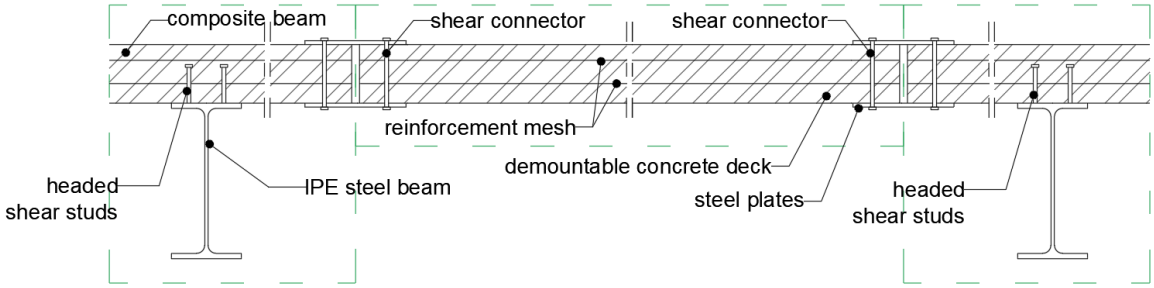

Figure 1.3: Combined concrete deck and composite beam

In such a way, the concrete deck taken from existing buildings can be connected to a composite beam. By doing so, the reusable action can be achieved by having a modular floor system. Of course, proper design of cut concrete slab should be proved either by FEA or hand calculation methods.

In this thesis, the author prioritised developing a newly designed composite floor system, consisting of a composite beam and concrete deck and investigating such a "concrete to concrete" connection. For the first stage of investigation, a reliable numerical model must be developed.
The numerical model is validated by a “simple” loading in shear and by a realistic loading in bending.

For subsequent stages, attention can shift towards re-utilizing the concrete deck, which has been cut off from an existing floor system, by connecting it to a composite beam, as shown in Figure 1.3, thereby creating a modularised floor system. This research is an important step for this type of system, particularly concentrating on the behaviour of the connections and the load-bearing capacity of such "concrete to concrete" joints.

1.3. PROBLEM STATEMENT

Most floor systems are built on-site with concrete designed for only one life cycle, leading to demolition at the end of use. However, introducing a demountable floor system allows for the prefabrication of both the composite beam and the concrete deck. This approach enables these components to be reused beyond their initial life cycle.

This thesis centres on a novel composite floor system design, which connects concrete deck with a composite beam. These two elements are connected using demountable shear connectors (bolts) at the concrete dapped-end joints, as depicted in Figure 1.4.

It is assumed here that this concrete deck is only bearing load in one direction, which is the transversal direction, and the composite beam will bear load in the longitudinal direction.

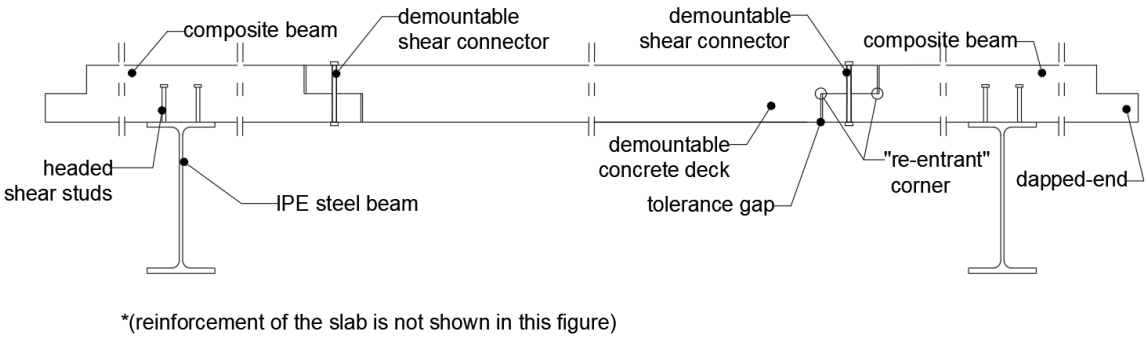

Figure 1.4: Three elements of a composite floor system connected through a demountable shear connector (bolt)

An increasing number of research studies are being undertaken on demountable conditions [25], and among these, composite floor systems have become a noteworthy subject of investigation.

It is observed that the majority of existing demountable connection solutions primarily concentrate on shear connectors placed on steel beams, such as headed shear studs and bolts, as referenced in [26]. There are studies dedicated to concrete half (dapped-end) joints, as discussed in section 2.7, but these do not involve the use of shear connectors. However, very few solutions exist for demountable shear bolt connections between concrete elements.

Therefore, it is necessary to investigate the demountable connections between composite beams and concrete decks and understand the mechanical behaviour of such connections.

A key question is about fundamental aspects such as the shape and dimensions of the concrete elements.

It is also necessary to design a correct and adequate arrangement of reinforcement of the deck, especially at the dapped end to provide adequate tension and compression resistance for concrete decks.
Furthermore, it is important to understand the mechanisms by which connectors can effectively withstand and transfer shearing and bearing forces.
Lastly, the analysis of loads, stresses and deflection of the concrete decks is performed.

It is important to mention that cutting concrete decks straight line from existing floor systems will result in a concrete deck used in a smaller span compared to a standard concrete system. The concrete deck will not be designed to carry end bending moment resistance and the spans will be designed so the existing reinforcement is sufficient. However, locally, at the connection around bolts, it will be a challenging question since no dedicated reinforcement design is available. The design of concrete to the concrete connection between the composited beam and the used concrete slab is left out of the scope of this thesis.

Research on a short reinforced concrete cantilever is being done on a much larger scale than the concrete deck in this MSc thesis, for example, for bridges, as discussed in section 2.7. The goal of the FE model used in this research is to provide an initial estimate of the effectiveness of the “thin slab” design.

The reinforcement design done in this research is a modified version of the reinforcement design shown in the literature review in section 2.7. It is challenging to implement complicated designs from references shown in section 2.7.3, and therefore, a preliminary study is done within the scope of this thesis.

1.4. RESEARCH OBJECTIVE

The principal research objectives of this thesis are directed towards investigating the feasibility and analysing the failure mechanisms of the proposed demountable "concrete to concrete" connections in "thin concrete slabs".
Specifically, the research seeks to determine whether such connections can be successfully implemented in a demountable floor system and to identify the factors that contribute to their potential failure.

As mentioned before, the demountable "concrete to concrete" connection can vary depending on whether it involves a reused concrete deck from existing buildings or a fully new floor system design, as shown in Figure 1.3 and Figure 1.4. However, for both floor systems, the structural elements must be designed with the capability to be reused after their primary life cycle:
(1) Newly-made demountable connection concrete deck with tailor-made reinforcement.
(2) In the same system consisting of composite beams and concrete decks, the existing concrete decks can be used. This concrete deck can be cut out of the concrete floor system after the first life cycle and connected to a composite beam for reuse.

The most practical method would be the second approach which can maximise the reduction of emissions and also be the most cost-effective solution. Because the modifications are applied to existing structural elements, instead of newly produced elements, refer to discussion in section 7.

However, since this demountable method of connections and such a modular floor system which consists of prefabricated composite beam and concrete deck, is a novel idea, hence extensive research should be performed accordingly.

Understanding the mechanical behaviour of the connection between the segments is important. Therefore, it is decided that the mechanical behaviour of the connection should be investigated in a newly produced demountable concrete deck with tailor-made reinforcement.

This way, the fundamental failure modes of the "concrete to concrete" demountable connection can be determined. This knowledge is interesting even for the “concrete to concrete” connection in which an existing concrete deck is used.

Therefore, this research will focus on the first alternative mentioned above:
the connection behaviour of the tailor-made demountable concrete decks

To accomplish this objective, several topics are investigated. The main aspects are summarised as follows:

1. Define the shape and dimensions of the demountable connection concrete decks.
2. Propose a tailor-made reinforcement for the concrete decks, especially at the location of the connections.
3. Investigate the mechanical behaviour of the demountable connection.
4. Propose possible improvements for the demountable connection.

Additional efforts are necessary for the existing concrete decks to be redesigned into a demountable floor system. In the concrete floor system, only top and bottom reinforcement mesh exist in most cases. Cutting concrete decks will result in a "bending weak" connection at the ends.

1.5. RESEARCH METHODOLOGY

This thesis is carried out only by Finite Element Method (FEM), by using Abaqus software. A detailed discussion of numerical modelling is in chapter 4. The corresponding laboratory experiments are proposed for future studies.

The following subsections will describe the methodologies applied in this thesis research.

1.5.1. LITERATURE REVIEW

A comprehensive literature review will be conducted to gain a deeper understanding of the current challenge.

This review will provide characteristics of concrete and steel as construction materials, including their material properties, see section **??** and 2.4.
There will be examples of conventional composite floor systems in section 2.1, with recycle possibilities of concrete after demolishing in section 2.2.2. Also, the background of essential tasks for reducing gas emissions produced by construction materials are provided.
Additionally, it will include examinations of relevant research works closely aligned with the scope of this document, see section 2.5 and 2.6. Examples of half-joint concretes that have a similar configuration to the proposed model are given in section 2.7.

1.5.2. PRELIMINARY STUDY

Before conducting an in-depth analysis, a simplified preliminary study is conducted using the finite element method for structural analysis and design software AxisVM [10].

This study aims to compare the difference between a conventional deck and demountable deck, such as displacement or flexural moments obtained from the models in section 3.2.2. Furthermore, sensitivity analyses are performed in section 3.2.4, to see the influence of changing the thickness of the deck or changing the spacing of the bolts in the longitudinal direction.

In this stage, linear elastic analysis is performed.

1.5.3. MECHANICAL BEHAVIOUR OF THE DEMOUNTABLE CONNECTION UNDER SHEARING

A "concrete to concrete" connection is very complicated, and the reason for developing a shear model is to have a step-by-step increase in the level of complexity of the proposed structure to gain confidence in the numerical modelling rather than being a realistic loading condition. This is a case relevant for the numerical analysis, since there are no experiments available for such a floor system.

For this model, two concrete blocks are connected by a shear connector (bolt). Two ends are pulled away from each other simultaneously in the horizontal direction as shown in Figure 1.5.

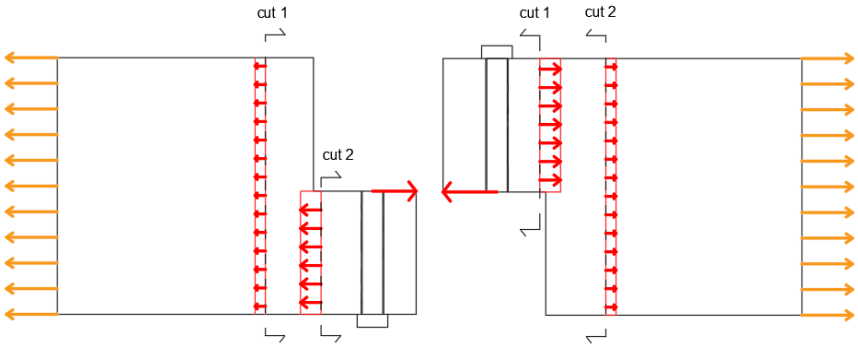

Figure 1.5: Shear transfer in "concrete to concrete" connection

Figure 1.5 shows the shear transfer in the "concrete to concrete" connection; the size of the arrows indicates the magnitude of the force. (Noted that the reinforcement is not shown in this figure).

Section 5.1 aims to discuss how bolts resist shear force and the damage caused by bent bolts pulling from concrete blocks.

In this stage, plastic non-linear analysis is performed.

1.5.4. DETAILED STUDY OF DEMOUNTABLE CONNECTION UNDER BENDING

After gaining experience and confidence from the shear model, a bending model was built and analysed. The mechanical behaviour and accompanying failure modes of this innovative demountable "concrete to concrete connection" under three-point bending is the most critical aspect for investigation, and thus, chapter 5 is in the main focus of the thesis research.

After looking at the previous shear model, the concrete deck with a demountable shear connector can be built and checked with the assigned dimensions, material properties, and reinforcement plan.

A segment of the transfer of bending moment is shown in Figure 1.6 around the "concrete to concrete" connection. (Note that the reinforcement is not shown in this figure).

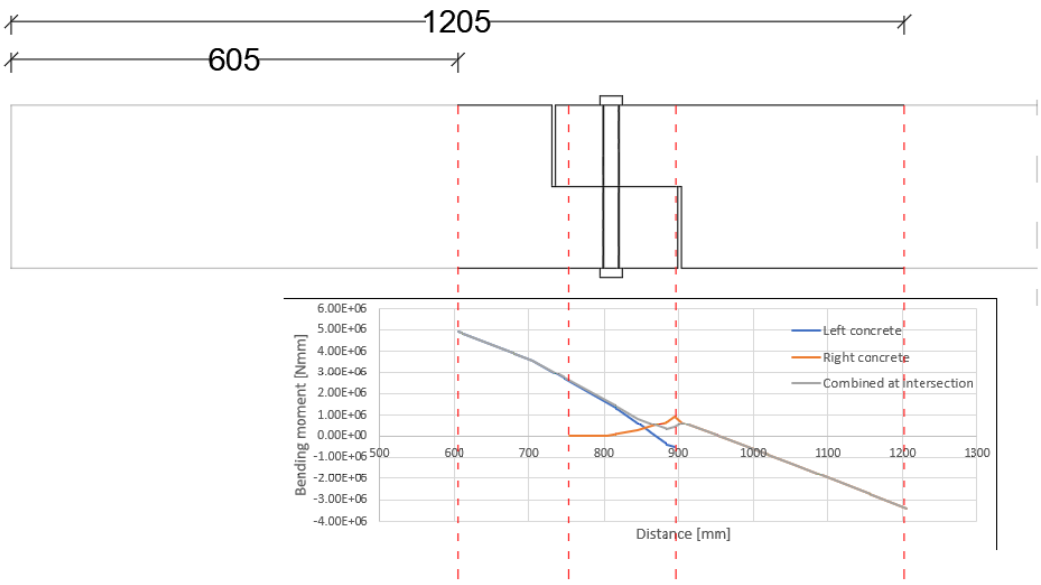

Figure 1.6: Bending transfer in "concrete to concrete" connection

The investigation into the behaviour of the connection involves multiple aspects.
1. Section 5.2 details the influence of the edge distance of the bolt hole, which is the distance between the centre of the shear bolt and the edge of the concrete dapped-end.
2. This study investigates the impact of adding steel plates at the dapped end corners of a concrete deck on the failure modes of the connection. This topic is explored in section 6.1. Additionally, the research examines whether the connection's position affects its performance. Specifically, the study analyses if the connection is located in an area experiencing a bending moment or at a position with zero bending moment, as discussed in section 6.2.

Deflection, load-displacement curves, failure modes, and other aspects are included in section 5.2. In this stage, non-linear analysis is also performed.

1.5.5. DISCUSSION OF THE RESULTS AND POTENTIAL IMPROVEMENTS IN THE CONNECTION

After obtaining results from the above-mentioned models in chapter 5, a series of analyses and comparisons can be conducted. Improvements in the failure modes on such connections can also be developed accordingly. Conclusions, therefore, can be drawn based on the numerical outputs.

1.5.6. FUTURE STUDIES

The results obtained in the previous chapters through the numerical modelling of the demountable connector in shear and bending concluded that further investigation is needed.
The novel demountable floor system design established in this research lays the groundwork for enabling the reuse of concrete decks which are cut off from existing buildings.

In this last chapter of the thesis, recommendations for further research that will aim at the improvement of the evaluation of technical performance, as well as the analysis of the behaviour and details of this demountable connector, are discussed.
Additionally, this chapter explores potential alternative types of demountable "concrete to concrete" connections, which are further elaborated in section 8.2.2.

2

Literature Review

2.1. COMPOSITE FLOOR SYSTEM

DUE to the high resistance of concrete and steel against compression and tension respectively, they are often used simultaneously to maximize the resistance of elements, such as in reinforced concrete decks or composite floor systems.

A composite floor system consists of concrete slab sitting on top of a steel beam (cast in trapezoidal sheet), connected with shear connections, such as headed studs. It combines the advantages of steel in tension and concrete in compression, achieving a cost-effective floor system solution.

The idea of a composite floor system is to have compression on top and tension on the bottom, Therefore, placing a concrete slab on top of the steel beams leverages the resistance advantages of both elements.

In this thesis research, the structure considered is a newly designed concrete deck connected to a composite beam by a demountable shear connector (bolt), achieving a modularised floor system.

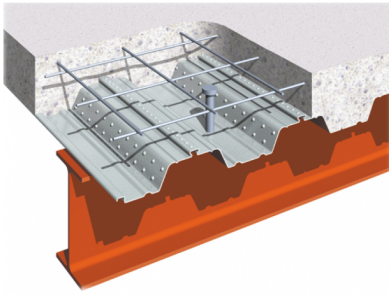

Figure 2.1: New composite floor system ComFlor from Steel & Tube

As mentioned by Giovanni Brambilla et al [13] , the most widely used shear connectors are headed studs, which are welded to the top flange of the steel beam and embedded into the concrete slab.

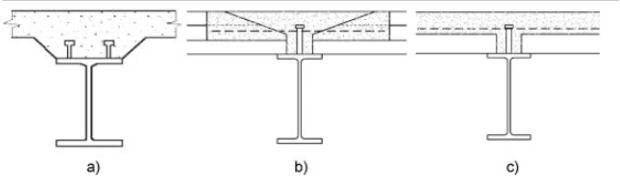

Figure 2.2: Welded headed studs applied as shear connectors in profiled decking system (a), hollow core sections (b) and solid slab with topping (c)

Although the deconstruction of composite floor system is still problematic, due to the monolithic behaviour offered by current shear connector practices, numerous researches efforts are underway. One solutions for a demountable composite floor system is a precast concrete slab sitting on top of the steel beam, connected using pre-tensioned High-Strength Friction-Grip (HSFG) bolts, as shown in the Figure below.

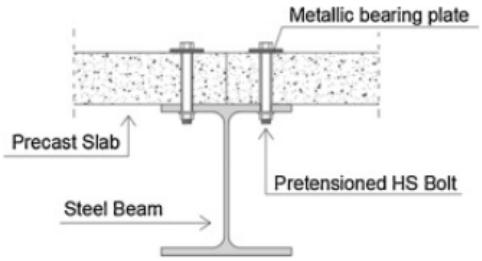

Figure 2.3: Steel concrete composite beam with HSFG bolts.

Research from Giovanni Brambilla et al shows that structures with a demountable composite floor system are the most environmentally friendly solution among all options. The saving of emissions/resources ware quantified for each impact category. For example, the greenhouse gas emissions saving from the demountable system compared to the conventional systems ware quantified at least 80kg CO_2-eq/m2, and the saving of primary energy resources was estimated at least 800MJ/m2.

However, the focus of this thesis is on the design of an innovative demountable connection between concrete deck and composite beam and understanding the mechanical behaviour of such connection.

2.2. CIRCULARITY

2.2.1. EMISSION REDUCTION

RESEARCH shows that the iron and steel industry is one of the largest industrial emitters of CO_2 accounting for about 7% of global anthropogenic CO_2 emissions[76].

in addition, concrete also produces a relatively high embodied energy, from excavation, manufacture, transportation, and even for demolition.
The cement production process releases high amounts of CO_2, contributing up to 5 to 6% on global scale. (In Netherlands, the typical cement used is 25% CEMI + 75% GGBFS.).

"...CO_2 emission, global warming and its resultant effect (climate change) are serious environmental problems that need urgent scientific attention, thereby calling for a reduction in CO_2 emissions in all sectors of human activity, including power generation. ...Also, this chapter revealed that CO_2 emission does not directly result in climate change.

Instead, it first depletes the ozone layer, leading to global warming (the greenhouse effect), then climate change." —— Kelvin O. Yoro et al. [1]

It is widely accepted that there is a pressing need to reincorporate concrete waste back into the production cycle by maximizing its reuse rate in new concrete mixes.

Certain actions can be taken:
– Focusing more on the performance side of the products, instead of the robustness. By changing size of aggregates, the water-cement ratio, and adding admixtures, the performance of the concrete can be manipulated.
– Once the building needs to be taken down, keep elements as much as possible in the life cycle. Even when the elements need to be demolished, take the materials and reuse/re-cycle as much as possible.

2.2.2. CIRCULAR ECONOMY

THE building industry is responsible for major societal impact, with 40% of total energy use and 30% of the global amount of waste. Moreover, the concrete business is a major source of excess material.

We aim for circular developments to change from a linear, open-ended economy to a circular, closed-loop economy where materials retain their value, resources are maintained and zero landfill is produced.

Figure 2.4: Circular economy by European Parliament[61]

Circular building process requirements:

1. No (hardly) use of primary resources
2. Reuse of materials and elements (half products)
3. Recycling of resources (secondary resources)

[1] Parts of this chapter have been published in Chapter 1 - CO_2 emission sources, greenhouse gases, and the global warming effect page 3-28, (2020) [76].

4. "Up-cycling": no loss of functional performance
5. No/low emissions of harmful (for health + environment) compounds

According to the 2015 'Climate Change Conference' in Paris [58], targets are set to achieve a reduction of greenhouse gas emissions by 50% in 2050 and EU should be fully greenhouse gas emission-neutral in 2100 (100% renewable energy sources).

Two definitions are explained: reuse and recycle.
– Reusing means using second-hand (half) products for the production of new products/constructions. – Recycling means using the old product as raw materials (secondary resources) for the production of new (half) products.

It is important to foam a circularity in the building industry: Circular building means "... using and reusing buildings, areas and infrastructure without unnecessarily depleting natural resources, polluting the living environment and affecting ecosystems. Carrying out construction such that it is economically justifiable and contributes to the welfare of people and animals. Here and there, now and later." [2].

Design for deconstruction and reuse structures is a cornerstone of the circular economy. Current practice generally involves demolishing buildings without regard for preserving the integrity and value of components for reuse. Only by designing buildings for deconstruction can we make reuse of buildings and building components more commonplace and commercially viable.

Precast construction offers numerous benefits to different stakeholders of the value chain in the construction industry.
Bolted connections provide fast and safe assemblies of precast concrete elements and also allow easier disassembly. In addition, the elements are usually manufactured in factories where the quality and precision are controlled.

Alternative building solution include the use of renewable materials:
• Renewable materials are substances derived from a living tree, plant, animal or ecosystem which has the ability to regenerate itself. A renewable material can be produced again and again.
• Biodegradable materials are substances that will decompose in a natural environment.

Taking an example of concrete decks:
The reuse of concrete depends on the quality and remaining life span of the concrete. It is important to design elements with demountable possibility, for example with bolted connection. Hence, wet connections should not be used.
With the demount possibility, at the end of first service life, concrete decks can be demounted easily with no or little damage to the deck, which gives the chance to reuse it in new buildings.
The main focus of this thesis is to design such connection that provides adequate strength

[2] Parts of this chapter have been published in Transitieagenda Circulaire Bouweconomie, (2050) [59].

and durability of the reused concrete deck which is connected to a composite beam by a demountable shear connector (bolt).

In relation to the strength and durability of recycled concrete aggregates, an example of an experiment taken from Somayeh Lotfi et al 2014 [52] regarding the C2CA Project shows the difference between concrete aggregate recycled from demolished building and new aggregate concrete at the end-of-life service.

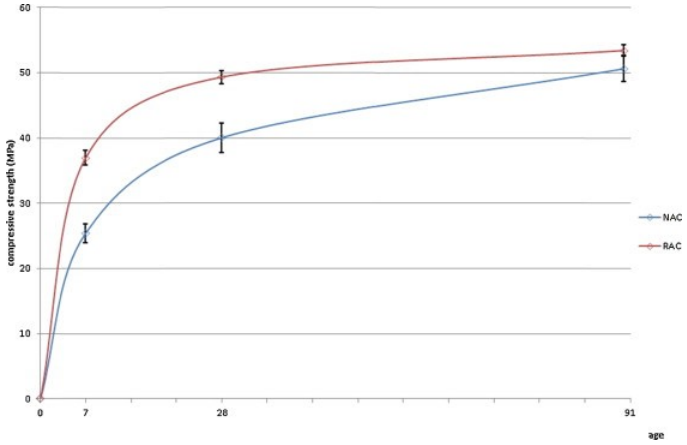

Figure 2.5: Comparison between compressive strength of NAC (blue) and RAC (red) in different ages [52]

In the first demonstration case of the new technology, recycled aggregate was tested in new concrete (RAC) to investigate the workability, compressive strength and durability compared to concrete made from natural aggregate (NAC). The RAC showed 30% higher compressive strength after 7 days.

It is believed that the favorable development of strength of the recycled aggregate is caused by changes in the surface of the particles as a result of the intensive liberation process. The results of the freeze–thaw resistance, however, showed that the recycled concrete performed less well than NAC but fulfilled the requirements for F100 class [52].

Taking the example of steel elements:
The typical recycled rate of steel material is 90%, with the average rate being 95% In the case of hot-rolled I beams, the rate of recycle can even go up to 99%, according to the "Recycling and Reuse Survey" in England in 2000.

"..., reclaim and direct reuse significantly reduces potential upstream and downstream environmental impact. In an earlier study, the authors have shown that increasing the share of reusing steel decking could decrease the average aggregated embodied Global Warming Potential (GWP) of steel elements in the construction by 21%."- Ajayebi et al [17].

Designers can take the following considerations to increase the possibility of reuse:

1. Using bolted connections to allow disassembly of structures during deconstruction.
2. Ensuring easy and permanent access to connections.
3. Using long-span beams, which offer greater flexibility of use and can be reused by cutting them to new lengths.

Although up until now, it is still a challenge to satisfy both reusability and aesthetic needs at the same time.

Recycling steel elements after the first service life requires secondary steel-making, producing extra energy emission, as well as extra labor cost, which can be downside of recycling steel products.

2.3. LIFE CYCLE ASSESSMENT

LIFE cycle assessment, developed in 1960s, is a wildly used tool for the quantification of mid- and endpoint impacts (human health, ecosystem health, resources scarcity) on construction elements and complete built structures.

LCA adheres to the principal standards of the ISO 14040 series. These standards provide guidance on:
LCA principles and framework (ISO 14040);
LCA requirements and guidelines (ISO 14044).

Cradle-to-gate vs cradle-to-cradle:
An important scoping decision in LCA and embodied carbon studies is determining which parts of the product life cycle to include.

Studies that assess the environmental impact from the moment the product is being produced until it leaves the factory are called cradle-to-gate studies.

Meanwhile, studies encompassing the entire life cycle of a product, including production, use phase, and end-of-life phase where the product is demolished to be reused and recycled, are known as ‘cradle-to-cradle’ studies.

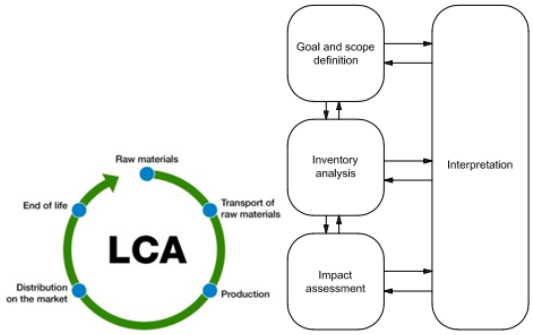

Figure 2.6: LCA steps [49][33]

LCA can be used to calculate the external (environmental) costs of a product through the following steps:

1. Definition of goal and scope and functional unit of the LCA.
2. Compiling an inventory of relevant energy and material inputs and environmental releases (outputs) associated with a defined system. Releases can be solid wastes or emissions to air or water. 'process tree' can be made in this step.
3. LCIA (life cycle impact assessment): Evaluating the potential impacts associated with these inputs and releases, e.g., the global warming impact from CO_2 and other greenhouse gas emissions.
4. Interpreting the results of the environmental impact of a product to help make informed decisions.

2.4. MATERIAL PROPERTIES

THE stress-strain relationship of concrete, both in compression and tension, is a fundamental characteristic defining its structural behavior. Understanding this relationship is crucial in structural design, enables engineers to predict concrete behavior under varying loads, thereby facilitating the design of safe and robust structures that can withstand these loads.

If the ductile property is not considered, the material's strength increases gradually during the plastic phase while stiffness remains constant. However, when a ductile damage model is considered, it is assumed that the material's strength decreases as damage increases. Correspondingly, stiffness also diminishes with an increase in the damage parameter d_c. When using Abaqus to simulate a material's ductile damage model, it is usually necessary to input the range of the material's strength degradation, represented by the displacement at failure. A smaller value for this parameter indicates a more brittle characteristic, while a larger value signifies a more ductile characteristic.

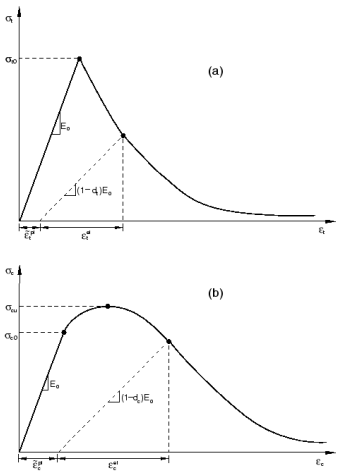

Figure 2.7: Concrete in tension and compression behaviour

2.4.1. CONCRETE IN COMPRESSION

Concrete is predominantly used in compression, making its compressive stress-strain behaviour a major interest. This is one of the most important material characteristics of concrete. Many studies experimentally clarified the influence of compressive strength and other parameters, such as types of coarse aggregate, on the stress-strain curve of concrete (K. Watanabe et al.)[44].
According to Eurocode 2, concrete strength classification is based on the characteris-

tic cylinder strength f_{ck}, determined through a compressive test conducted at 28 days using a compressive testing machine. The classification ranges from lower values to a maximum of C90/105, varying according to national annexes.

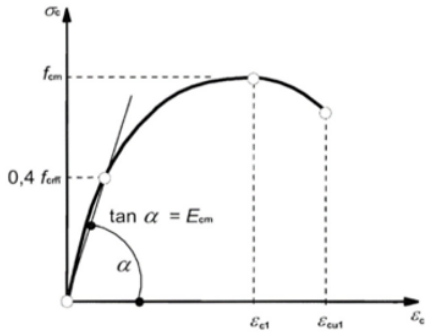

Figure 2.8: Schematic representation of the stress-strain relation for structural analysis according to Eurocode 2

Barbosa et al [11] state that, "In compression, the stress-strain curve for concrete is linearly elastic up to about 30 percent of the maximum compressive strength. Above this point, the stress increases gradually up to the maximum compressive strength. After it reaches the maximum compressive strength σ_{cu}, the curve descends into a softening region, and eventually crushing failure occurs at an ultimate strain ϵ_{cu}"

2.4.2. CONCRETE IN TENSION

The tensile strain capacity of concrete, defined as the material's ability to withstand deformation without cracking, is crucial for minimizing the risk of cracking under service load conditions.
The tensile strength of the concrete increases over time, peaking at around 28 days of curing. According to Leonhardt F. [50], its tensile strength is related to compressive cylinder strength f_c and can be computed as formula:

$$f_{tm} = 0.34 \times f_c^{\frac{2}{3}} \tag{2.1}$$

Laboratory data from H. Busch, analysed by Leonhardt. F later on, suggests that it is possible to adjust the coefficient in this equation to 0.22 and 0.45 to derive the values representing the 5th and 95th percentiles, respectively, of the tensile strength, f_t. The tensile strength of concrete is slightly higher in flexure.

Another important parameter is the tensile strain, ϵ_t„ when the strain exceeds 0.010 to 0.012 percent, concrete cracks. Notably, tensile strain is independent of concrete strength[50].

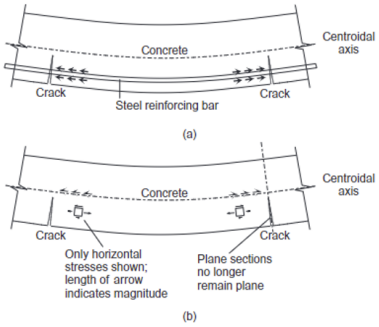

Figure 2.9: (a) stress transfer through bond; (b) shearing action of curvature [60]

When reinforced concrete cracks, its stiffness decreases but does not drop to zero, as the uncracked region still carry some tensile stresses and provide stiffness to the overall behaviour of the structure. This phenomenon is known as tension stiffening.

According to P. L. Ng et al., tensile stresses in concrete can be induced in two ways: through the bond between steel re-bars and concrete, which provides stress transfer, and the shearing action of the uncracked concrete in tension zones.

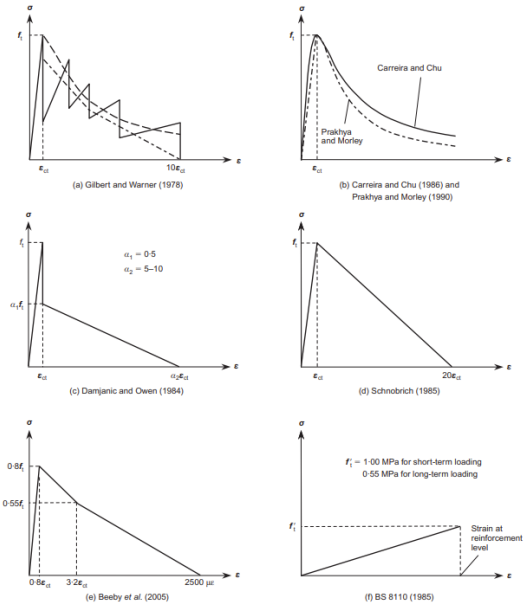

Figure 2.10: Tensile stress block [48]

Accurately measuring tensile stresses in cracked concrete is challenging, Several dif-

ferent tensile stress blocks have been developed by researchers, typically involving a method of trial and error which that proposes a certain tensile stress block and determines unknown parameters by fitting curves to load-deflection data obtained from experimentation.

Figure 2.10 (a) shows the three stress blocks that proposed by Gilbert and Warner. Among these, the bi-linear descending curve fits experimental results well. It consist of a straight line with a slope of E_c reaching the top f_t, then drops vertically to $0.6f_t$, and descends in a straight line to $0.4f_t$ at $4\epsilon_{cr}$, and again in a straight line to 0 at $10\epsilon_{cr}$, the changes in slope indicate the position of reinforcement in each layer.

Figure 2.10 (b) displays the stress block by Carreira and Chu (1986) [14], which consist of a nonlinear ascending part and a gradually descending part. This model was later modified and improved by Prakhya and Morley (1990), by fitting it with available experimental results.

Figure 2.10 (c) and (d) show two stress blocks proposed by Damjanic and Owen (1984) [23], and Schnobrich (1985), both consisting of a linear ascending part and bi-linear/linear descending part, respectively.

The last tensile stress block (f) in Figure 2.10, outlined in BS 8110 (BSI, 1985) [73], is a linear ascending curve without a descending branch, indicating that concrete is treated as a brittle material that fails completely once the stress reaches its strength, without considering the tension stiffening effect.

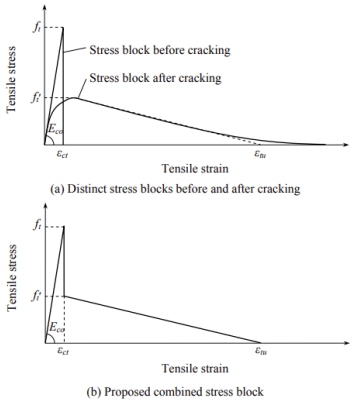

Figure 2.11: Tensile stress block proposed by Ng. P. L et al.

$$f_t^{'} = \alpha_1 \times f_t \tag{2.2}$$

$$\epsilon_{tu} = \alpha_2 \times \epsilon_{ct} \tag{2.3}$$

In Figure 2.11, Ng. P. L et al. proposed a tensile stress block that combines stress-strain curves of both uncracked and cracked concrete. The values of a_1 and a_2 coefficients in above equations depend on the type of loading and are determined based on numerical results obtained from FEA. For instance, "for beams subjected to a point load,a_1 and a_2 may be taken as 0.4and 18, respectively, and for beams subjected to a uniformly distributed load,a_1 and a_2 may be taken as 0.5 and 14,respectively" [60].

The stress-strain relationship of concrete in tension is also influenced by fracture energy, which depends on the strain softening tangent modulus, the peak stress (tensile strength), and the width of the fracture process zone. One of the first two variables may alternatively be replaced by the area under the stress-strain diagram [78].

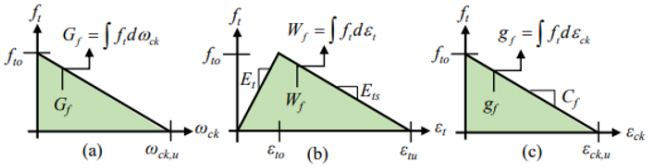

Figure 2.12: Tensile stress block: (a) stress-cracking displacement diagram. (b) stress-strain diagram. (c) stress-cracking strain diagram

It can be demonstrated that the fracture energy of plain concrete G_f (defined as the area under the post-cracking stress-displacement curve in Fig. 2.12 (a)), is related to the fracture energy density g_f (defined as the area under the stress-cracking strain diagram in Fig. 2.12 (c)), by the following expression:

$$G_f = w_c \times g_f \tag{2.4}$$

Furthermore, since $\epsilon_{ck,u} = \epsilon_{tu}$, the area under the total stress-strain diagram in Fig. 2.12 (b), W_f, is equivalent to the area under the stress-cracking strain diagram in Fig. 2.12 (c), g_f.

$$G_f = w_c \times W_f \tag{2.5}$$

Consequently, using Eq. 2.5, the fracture energy G_f can be related to the area under the total stress-strain diagram W_f, by considering the width of the crack band zone. This relationship is crucial for generating the complete tensile stress-strain curve for concrete.

2.4.3. STEEL MATERIAL BEHAVIOUR

The material behaviour of steel is well defined in Eurocode 1993 [34]. Unlike concrete, steel exhibits greater ductility and is highly effective in handling tensile stresses. Eurocode 1993-1-5 outlines different types of stress-strain relationships for steel, varying according to the required accuracy and permissible strain for analysis::

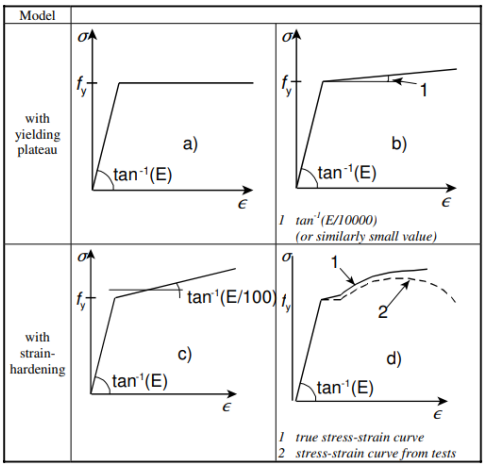

Figure 2.13: Stress-strain relationship for steel material

Steel materials must satisfy specific ductility requirements, including conditions such as the ratio of ultimate strength to yield strength, the minimum elongation at failure, and the ratio of strain at yielding to strain at failure:

$$\frac{f_u}{f_y} \geq 1.15 \tag{2.6}$$

$$e_f \geq 15\% \tag{2.7}$$

$$\epsilon_u \geq 15 \times \epsilon_y, \quad where \quad \epsilon_y = \frac{f_y}{E} \tag{2.8}$$

Where f_u is the ultimate strength and the f_y is the yield strength of the steel, e_f is the elongation at failure, ϵ_u is the strain at ultimate strength and ϵ_y is the strain at yield strength. E is the young modulus of the steel.

The modulus of elasticity and Poisson's ratio of steel are typically 210GPa and 0.3 respectively. The yield strength varies among materials, and the specific values can be found in the respective material codes.

2.5. PEIKKO - CIRCULAR ECONOMY

THE company Peikko is a leading worldwide provider of slim floor structures, as well as cutting-edge solutions for wind energy applications and connection technology, serving both precast and cast-in-situ construction methods[64].

They offer a range of demountable connections that enable the disassembly and reusability of bolts, providing flexibility and sustainability in construction, and aiming to enable circularity without compromising performance. Bolted connections have great potential in supporting Design for Disassembly.

Peikko conducted a series of experiments on the reliability of demountable connections on concrete foundation blocks, including on-sites and laboratory tests.
Two types of connections were used: HPM® 16 L Anchor Bolts and COPRA® 16 H Anchoring Couplers[77].

Figure 2.14: HPM® 16 L Anchor Bolts and COPRA® 16 H Anchoring Couplers

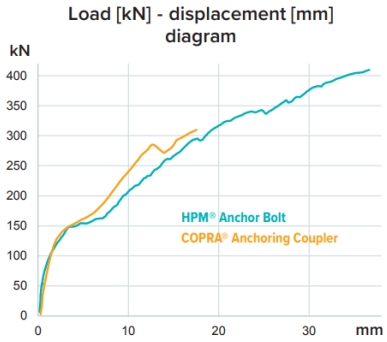

Figure 2.15: Load - Displacement of connections

The results indicate that no substantial difference between these two types of connections. However, it can be suggested that COPRA® 16 H Anchoring Couplers are a more preferable choice due to the potential risk of damage to HPM® 16 L Anchor Bolts during the disassembly process.

A summary table 2.1 below shows the comparison of the two types of connections.

Name	Demountability	Method of demount	Reusability	Rigid behaviour
HPM® 16 L Anchor Bolts	Yes	Direct screw out	Yes	100–150 kN
COPRA® 16 H Anchoring Couplers	Yes	sawing required	Yes	100–150 kN

Table 2.1: Comparison between PM® 16 L Anchor Bolts and COPRA® 16 H Anchoring Couplers

There are other types of demountable connections provided by Peikko for installation in beams, columns, foundations, or even concrete slabs.

2.6. EXISTED BOLTED SHEAR CONNECTIONS SOLUTIONS

2.6.1. STEEL CONCRETE DEMOUNTABLE CONNECTION

Abdolreza Ataei [7] performed an extensive parametric study on steel-to-concrete demountable connections with 12 push-out tests, to examine how different parameters influence the behaviour of the connections. He also compared the studied connection with traditional headed studs.

Analysis was performed by using Abaqus FEM, as shown in Figure 2.16 [3]
, employing the concrete damage plasticity (CDP) model with stress-strain relationships proposed by Carreira and Chu [14] as mentioned earlier in 2.4, in a displacement control manner. The results obtained from FEM were validated by laboratory tests using both cyclic loading control and displacement control methods.

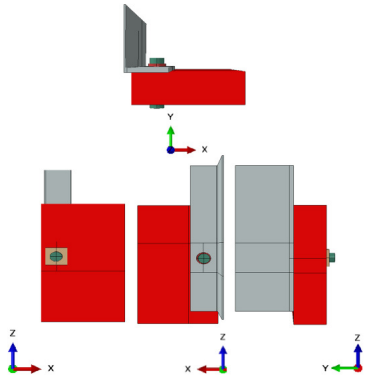

Figure 2.16: FEM model of the bolted shear connector in question[7]

After running a series of analyses, it can be concluded that numerical analysis can predict the behaviour of demountable connections at both local and global levels.

The author compared several parameters of the connections, with the result showing that:

1. The load capacity increases with bolt size, as well as the slip capacity.
2. The shear load capacity and corresponding slip increases as the bolt grade increase, but the initial stiffness and slip in the slipping stage are not affected.
3. Increasing the pretension of the bolt does not significantly influence the maximum shear force capacity and corresponding slip.

[3] Figure 2.16 in this chapter have been published in Journal of Constructional Steel Research, volume 198, title Modelling of demountable steel-concrete composite connections: Validation of finite element model and parametric study [7].

4. With increasing the clearance between connections greatly increases the ductility of the connection.

5. With a higher grade of concrete, the maximum shear capacity of the connection increases, but it also becomes more brittle and reduces the maximum slip capacity.

Several equations for bolted shear connectors, proposed by different researchers using Eurocode EC4 [43] and AISC code [35]. One of the equation proposed by Chen et al [18]. based on both experimental and numerical results is shown as below:

$$Q_u = 0.23d^{1.78} f_{cu}^{0.29}(0.0007 f_s + 0.53) \tag{2.9}$$

The equation proposed by the author can be written as equation 2.10, the accuracy of the results are verified by FEM models.

$$Q_{u,RD} = 0.6345 A_{sc} f_u \tag{2.10}$$

2.6.2. BOLTED SHEAR CONNECTORS VS HEADED STUDS BEHAVIOUR

Dallam [22] observed that high friction grip bolts can exhibit up to double the shear resistance compared to traditional headed studs of the same dimensions.
Similarly, Hawkins [38] conducted experiments finding that bolted shear connectors without embedded nuts achieve approximately 80% of the shear resistance at only 15% of the shear stiffness compared to welded headed studs.

M. Pavlović et al [62] utilized M16 grade 8.8 steel bolts to investigate the use of bolted shear connectors in prefabricated concrete slabs. Their goal was to understand the distinctions between these two connection types, including failure modes, to establish design recommendations.

Laboratory tests show that regardless of the various parameters of the tested specimens, the size and pattern of concrete failure remained consistent, with no concrete cone push-out failure or global failure observed.

The numerical results showed that the shear resistance of both connections is approximately the same, but bolted shear connectors have less stiffness at serviceability load than the headed studs. They also exhibit smaller initial stiffness and earlier non-linearity compared to the latter.

Figure 2.17 shows the FEM model of bolted shear connector configuration, they described thoroughly the damage model used for both steel and concrete materials. [4]

[4] Figure 2.17 in this chapter have been published in Journal of Constructional Steel Research, volume 88, title Bolted shear connectors vs. headed studs behaviour in push-out tests [62].

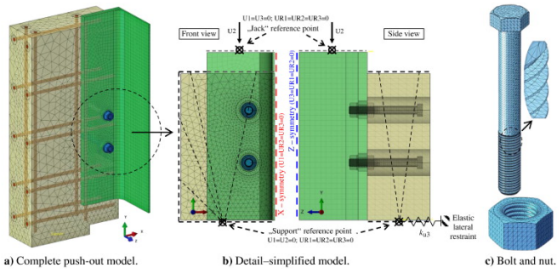

Figure 2.17: FEM model geometry and boundary conditions for bolted connector by M.Pavlović et al[62]

However, full bearing can be achieved after gap closing of the tolerance of the bolt hole, resulting in increased stiffness at the ultimate loading condition. It is observed to have 95% shear resistance of the welded headed studs.
Furthermore, the ultimate slip of the bolted shear connectors is less than 6mm, classified as a brittle connection according to EC4 [43].

It is noteworthy that a local confinement effect can be observed in the vicinity of the shear connector, induced by the pry-out effect from the concrete. This is explained by the concrete being subjected to a triaxial stress state, resulting in stress levels that exceed the strength of the concrete itself, as noted by Malecot et al [54].

2.6.3. DEMOUNTABLE SHEAR CONNECTORS UNDER MONOTONIC/REPETITIVE LOADING

Experiments conducted by W. Wang et al [74] explored the difference between monotonic loading and cyclic loading in the context of demountable shear bolt connections. The study included various bolt grades with different loads, involving a total of 21 specimens. The experimental setup connected two concrete slabs to a central steel beam using demountable shear bolt connections.

The results from these 21 specimens demonstrated that bolt fracture through shearing can be observed at the interface between the concrete and the steel beam. Additionally, as noted by Abdolreza Ataei et al. [8], an increase in the diameter of the bolt leads to greater pressure within the bolt hole, which in turn increases the occurrence of concrete spalling.
Y.J. Zhang et al. [79] also conducted a similar experimental study on the behaviour of demountable shear connectors. They found that high-strength friction grip bolt (HSFGB) connections have better shear properties than traditional welded headed studs.

Their conclusions include:

1. The diameter of the bolt does not affects the concrete damage area next to the bolt

hole.

2. The pretension load can increase the load at initial slip as well as the shear stiffness, but it has little effect in increasing shear capacity.

3. Increasing the diameter of the bolt results in higher shear strength, greater stiffness, increased ultimate slip under monotonic loads, and enhanced shear capacity under cyclic loads.

4. Ductility also increases with increasing bolt diameter.

Existing experiments and parametric studies highlight the increasing popularity of demountable shear connectors as a prominent research focus due to their potential for disassembly and sustainable advantages. Drawing insights from these research methodologies, objectives, and findings, this thesis will also concentrate on investigating the performance of modularised floor system.

2.7. RESEARCHES AND APPLICATION DONE IN CONCRETE HALF-JOINT CONNECTION

The proposed concrete to concrete joint has a similar design as the half joint connection in concrete structural design. Therefore, literature study on this topic is also included.

Half joint concrete (can also be called dapped-end concrete) elements were widely used because they can be prefabricated and are relatively simple to apply. Many researchers are now focusing on the design phase of the half-joint connection, particularly on the cracks development [12][75] and strengthening techniques of the joints [29][67].

As mentioned by Gary Klein et al. [36], "field performance of dapped ends suggests a need for improved dapped-end reinforcing details, which are not yet standardized within the precast concrete industry". Thus, they provided a design code for dapped-ends of pre-stressed concrete, aiming to identify the most effective reinforcement schemes and develop design guidelines for dapped ends.

2.7.1. BRIDGES WITH GERBER BEAMS

Concrete half joints can also be called as dapped-end or Gerber joints, which is taking the name of its inventor: Heinrich Gottfried Gerber [39].

Although the geometry of half joints can vary, according to Desnerck et al [27], the height reduction of it is recommended as 50% or higher, and the length-to-height ratio of the nib is recommended to be equal or higher to 1. The geometry of a half joint can be seen in Figure 2.18.

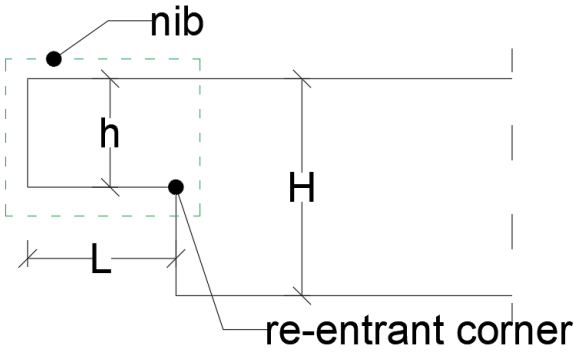

Figure 2.18: Geometry of concrete half joint

The application of Gerber beams is advantageous when the joints are located at the zero bending moment location, allowing minimum bending moment at the joints, resulting in beneficial static performance, since the Gerber beam can act like simply supported

beam in a continuous slab system, and reduce the potential damage done to the joint. However, one disadvantage is the lack of universal rules or standard codes defining the reinforcement layout of concrete half joints.

The Concorde overpass, see Figure 2.19, built in 1968 and collapsed in 2006, is one of the examples that highlighting inadequate construction codes of the time. The fundamental reasons of failure were identified as
1. Absence of shear reinforcement [20] and
2. Inadequately calculated loading conditions (neglecting load contributions from concentrated moment and shear from skew supports) [55]

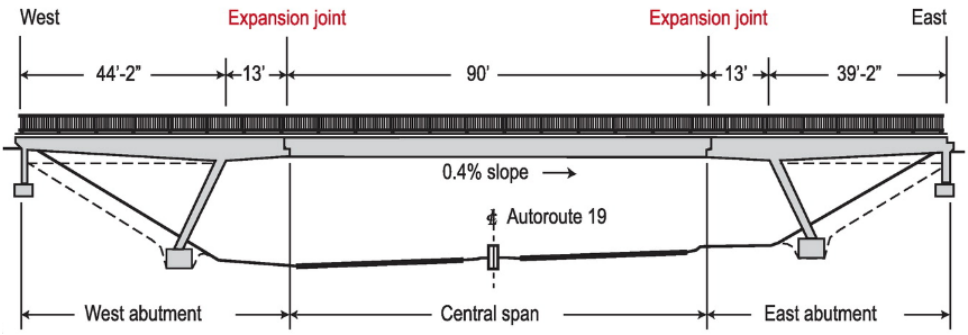

Figure 2.19: Elevation view of Concorde overpass [55]

Modern codes emphasize that for Gerber beams, minimum shear reinforcements are always required, with precise guidelines on anchorage design. For skew bridges, more limitations regarding load distribution and detailing are required.

Another example of Gerber beam is the Annone Overpass, built in 1962 and collapsed in 2016, during it's life time, it went though multiple times of repairing work. The failure was due to degradation of the materials and reduced strength of the joint [28]. However, lack of attention to controlling the bearing capacity of the overpass also played a significant role in the collapse, especially as traffic loads had increased dramatically in recent decades.

From the late 1960s, increasing number of researchers have focused on half joints, Rebecca Asso notes, that "Strut and tie model is an important method to design and assess regions where the Euler-Bernoulli hypothesis in Timoshenko beam theory is not fulfilled" [4]. This method also allows for use in discontinuity of half joint geometry.

In 1976, Mattock concluded that [3], following stress flow, the possible crack location can be identified, and the required amount of steel reinforcement determined based on moment equilibrium in the crack cross section. In 1983, Liem [68] introduced diagonal reinforcement to avoid large cracks at reentrant corners. In 1984, the strut and tie

method in concrete half-joint design was introduced by Canadian codes.

Tests conducted by Moreno-Martinez and Meli [56] in 2014 showed the diagonal reinforcement can reduced crack formation at the reentrant corners. Desnerck et al. [27] found out that nib reinforcement can affect crack patterns.

2.7.2. RESEARCH ON HALF-JOINT ASSESSMENT OF CONCRETE BRIDGES

Numerical analyses conducted by Rebecca Asso [4] validated that various reinforcement layout are possible, all of which can be applied to the proposed models. Prestressing reinforcement can also increase the ultimate resistance of the dapped-end joint.
Validation was achieved by comparing the load/displacement curves and load/crack width curve results from ATENA FEM software with tests conducted by Desnerck et al.
According to the Rebecca Asso, the numerical analyses align well with Desnerck et al. laboratory test. The ATENA 2D post-processing could highlight assumptions made in the analytical analyses, such as crack location, failure mode, and stirrups' contribution in the model trusses.

The author also suggests that future studies are needed in multiple aspects, such as concrete protection, re-bar corrosion protection, external prestressing of re-bar elements, and the influence of joint geometry.

Research in the filed of concrete half joints is ongoing. However, as mentioned in the Introduction chapter in section 1.3, these studies focus on concrete decks that are much larger than those in the floor system studied in this thesis. Therefore, only a very simplified solution for the reinforcement layout can be provided in this thesis, offering a preliminary estimation for such demountable connection designs.

Further investigations on the proper reinforcements design of the concrete half-joint in floor system are needed. However, this topic can become quite complex and detailed, which is beyond the scope of a master's thesis. Therefore, detailed calculations will not be conducted here.

2.7.3. POSSIBLE REINFORCEMENT LAYOUT FOR LARGER SCALE CONCRETE DECKS

"A reinforced concrete half-joint beam has a complex geometry that includes both a locally disturbed nib region and a full depth section. While this configuration simplifies the design and construction procedures, half joint structures rely on the internal steel reinforcement to transfer force from the nib into the bulk of the beam." – Desnerck et al [27].

Four different reinforcement layouts, tested by the group, are shown in Figure 2.20, to identify the impact of specific reinforcing bars.

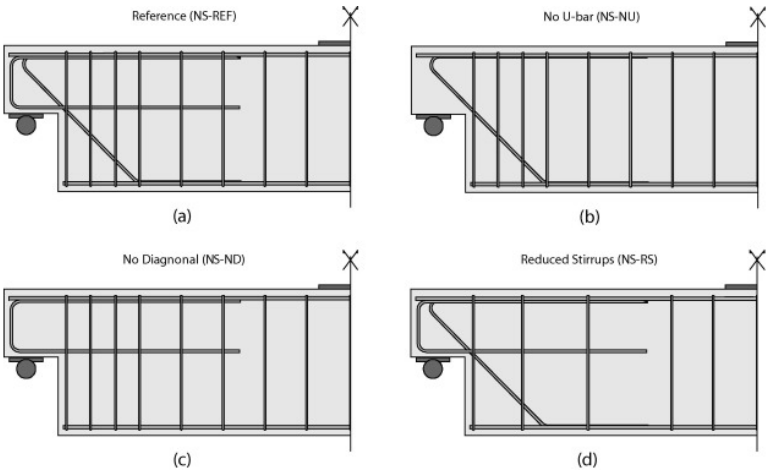

Figure 2.20: Reinforcement layouts for the different test scenarios by Desnerck et al[27]

Results indicate that the cracking at the reentrant corner of dapped-end concretes usually appears at 20-33% of the load capacity with an angle of approximately 40-45 degrees relative to the longitudinal direction.
Lack of reinforcement at the dapped-end joint results in a reduction of load capacity and influences the failure modes of the beam.

Proposed by Gary Klein et al. [36], Figure 2.21 shows the reinforcement layout in a dapped-end concrete beam with critical elements in the load path (numbers 1 through 8) and potential crack locations (letters A through C).

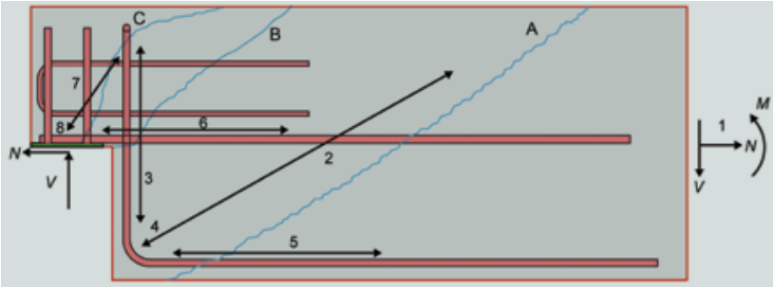

Figure 2.21: Reinforcement layout in dapped-end concrete beam [36]

This paper, developed from extensive three-dimensional non-linear finite element analysis and full-sized specimen tests, provides reinforcement design calculations for each potential crack locations, including serviceability and constructibility recommendations.

Other different reinforcement layouts for dapped-end concrete beams have been explored. Chen et al. [19] tested four different layouts with the same beam geometry but different reinforcement ratios. So [46] investigated different reinforcement details for thin-stemmed PC members using the strut-and-tie model. Nagy-Gyorgy et al. [57] investigated the effectiveness of strengthening dapped-end reinforced concrete beams using externally bonded carbon fiber reinforced polymers (CFRPs).

External prestressing strengthening techniques for dapped-end reinforced concrete beams were investigated by A. Atta and M. Taman [9]. Results showed that the proposed external vertical prestressing technique is very promising, with an increase of up to 82% in the load capacity of the concrete beam compared to the control specimen. However, a new failure mode was observed with the use of external horizontal strengthening techniques, leading to compression failure.

Figure 2.22 shows the strengthening techniques proposed by A. Atta and M. Taman.

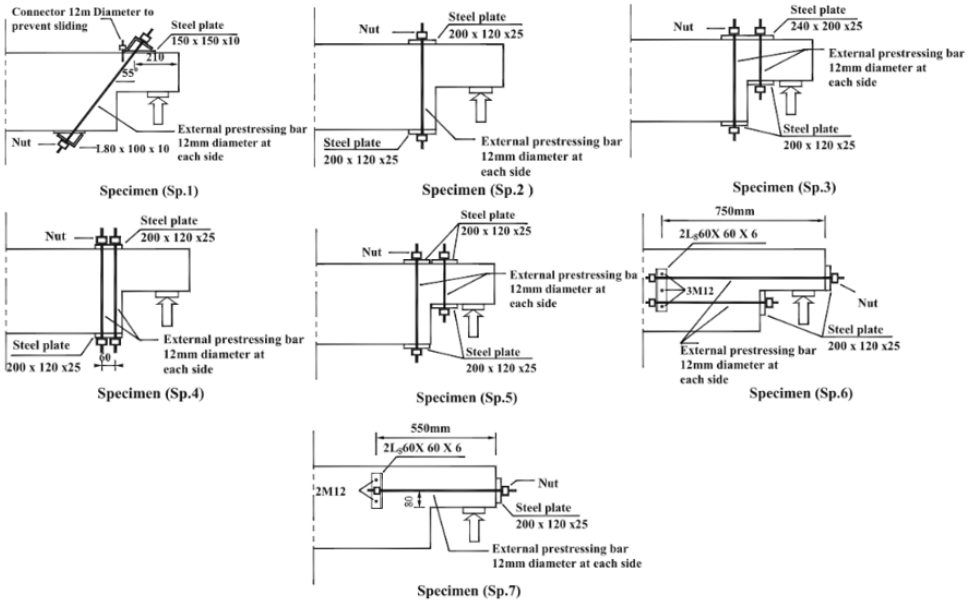

Figure 2.22: Configuration of different strengthening techniques [9]

Concluded by A. Atta and M. Taman, the best technique for strengthening concrete beam with dapped-end joint, considering both the ultimate load capacity and ductility, is using two external prestressing layers: one at the dapped end and the other at the undapped end with two upper separate rigid plates.

3

PRELIMINARY STUDY

Before going deep into details, a simplified comparison is made between conventional deck and demountable connection deck.
This chapter shows in a more global perspective of the difference between two systems. It helps to better understand why and how to create such demountable system.

Most of the floor system nowadays are conventional continuous concrete decks, meaning that they cannot be demounted and reused after the first cycle of life. This significantly increases the CO2 emission during extraction and manufacturing process for new material, also increases the amount of waste material during structure demolish process. It is very harmful for the environment, and it is not sustainable development.

Therefore, alternative floor system needs to be introduced. With demount possibility, the larger part of the concrete deck can be taken out by unhinging from the span after the service life of the structure, it can be reused in other construction after performing strength check.
With this method, less raw materials need to be extracted, less concretes need to be produced, hence sustainable development can be achieved.

In this chapter, you will see several comparisons of these two types of floor system.

3.1. INITIAL PERIMETER AND METHOD USED

3.1.1. INITIAL DATA

The concrete deck is designed for office usage. The concrete class of this deck is taken as C20/25, thickness used is 200mm, the simplified model is built in FEM software - AxisVM, having 2 spans, 5.4m each, which makes a total of 10.8m in length. The width of the span is 8.1m.

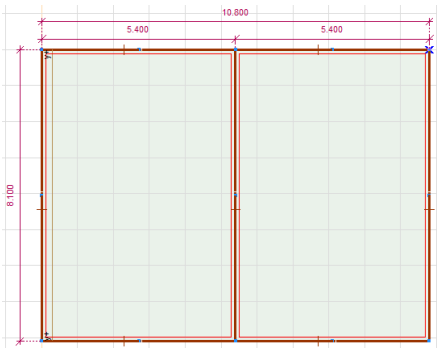

Figure 3.1: Conventional deck

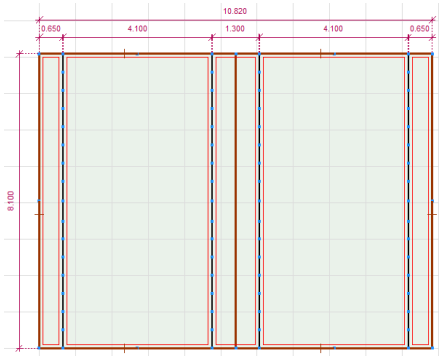

Figure 3.2: Demountable connection deck

The boundary condition for this model is no translation allowed in z direction for 4 edges, nodal supports at half-length of 4 edges are used to restrain model moving in horizontal plan.

Self-weight and live load are applied to the model.

Demountable connection deck consists of 2 parts, 4.1m demountable part and 1.3m composite floor part sitting on top of the steel column. They are connected by bolts spreading along the width, with the spacing of 500mm. 5mm gap between 2 parts is taken as construction tolerance.

3.1.2. METHOD

By setting up 2 different models, several things can be compared, of which the deflection of the system is the most important. Then surface internal force mx and my, sensitivity of the spacing of the bolt will also be analysed. At last, reinforcement pattern and amount can be calculated according to the results from two models.

In this way, without checking into the details, a global view can be formed to see the characteristics of the demountable floor system.

3.2. MODEL SET UP AND RESULT

3.2.1. BEFORE RUNNING

Self-weight of the concrete is 2500kg/m3. Live load of 2.5kN/m2 is applied as office live load according to Eurocode.
To check if the model contains singularity, uniform mesh size of 0.1m is used to get a more accurate result.
Simply supported deck is built for both models before going into continuous deck, to see if the deflection and moment obtained are reasonable.

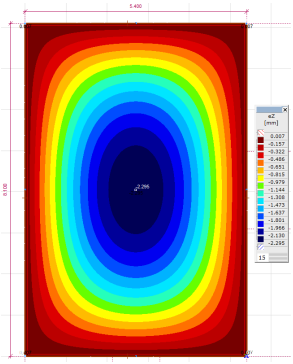

Figure 3.3: Deflection of conventional deck – simply supported

Deflection of this simply supported deck is 2.295mm, for continuous deck the deflection should be smaller.

3.2.2. AFTER RUNNING - RESULT

Conventional deck:

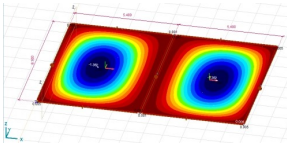

Figure 3.4: Deflection in z direction

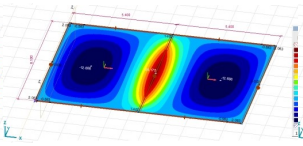

Figure 3.5: Flexural moment mx: around y axis

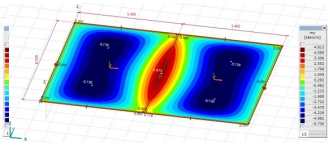

Figure 3.6: Flexural moment my: around x axis

Maximum deflection for this model is 1.362mm, which is smaller than simply supported deck 2.295mm, reasonable.

Demountable connection deck:

Bolt spacing of 500mm is used for this model, simulated as link element with 5mm gap between 2 parts. Link element fixed translation in xyz direction, of which the stiffness is used as default rigid connection given in the software 1E+7kN/m.

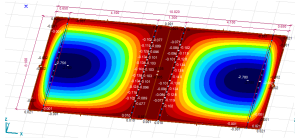

Figure 3.7: Deflection in z direction

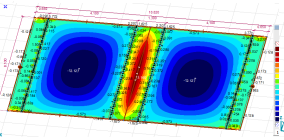

Figure 3.8: Flexural moment mx: around y axis

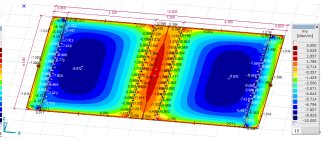

Figure 3.9: Flexural moment my: around x axis

Maximum deflection for this model is 2.780mm.

Summary of the obtained data:

Comparison of obtained results for 2 models.						
	Displacement	Flexural moment		Torsional moment	Reinforcement design moment	
	eZ [mm]	mx [kNm/m]	my [kNm/m]	mxy [kNm/m]	mxD [kNm/m]	myD [kNm/m]
Conventional slab	1.362	24.175	4.813	7.086	24.175	6.587
		-12.679	-5.733	-7.086	-12.716	-8.122
Demountable connection slab	2.780	13.153	8.909	28.360	30.565	26.497
		-12.127	-18.352	-28.360	-27.084	-32.665

Table 3.1: Comparison of obtained results for 2 models.

Explanation of obtained result:

Moments can be found at corners even though the boundary conditions do not restrain edges from rotation because of the torsion of the deck.

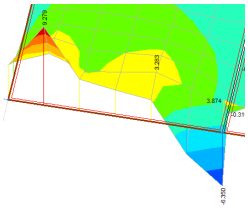

Figure 3.10: Corner moment mx – demountable connection deck

The reason could be: when uniformly distributed load is applied on the deck, the deck is trying to bend in both directions in the plane, but the deformation at the corner is fixed

by the adjacent constrains at edges. Hence torsional moment is induced by uniformly distributed load.
Therefore, the corner moment obtained in mx and my are logical and should be taken into account in reinforcement calculation.

The possibility of singularity is also checked by reducing mesh size, result shown moment at the corner doesn't go into infinity, which is opposite as the definition of singularity: smaller mesh size causing steeper slope of stress which eventually go into infinity.

3

Point support at nodes instead of line support is also tried in the model, to see if the moment at corner changes and because in software how line support works is like many points supports line up together so unsurprisingly the result shows it does not change much.

3.2.3. REINFORCEMENT CALCULATION

Reduced reinforcement design method is used by averaging moment to have a more economical layout. (By securing reinforcement area).
For both decks, concrete cover is 20mm and the reinforcement steel bar used is diameter pi=8mm, spacings are different of course, calculation shown in annex B.

Conventional deck:

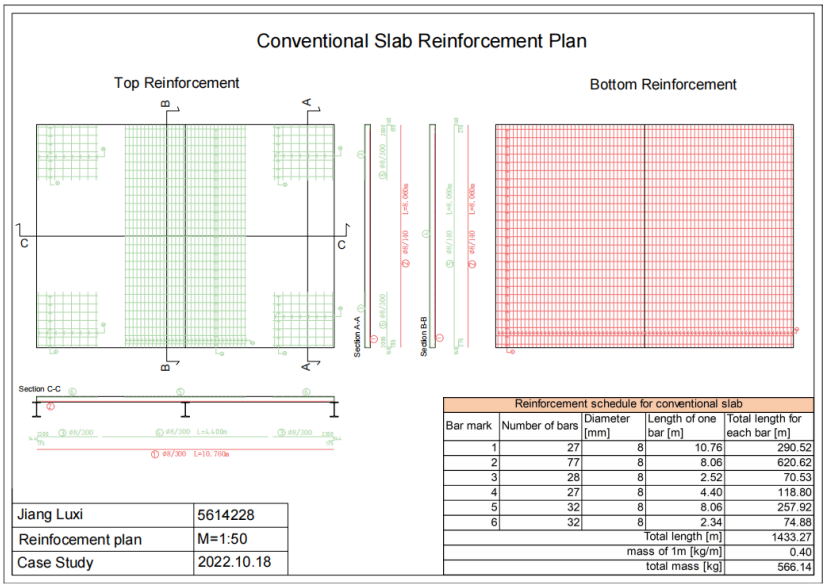

Reinforcement schedule for conventional slab

Bar mark	Number of bars	Diameter [mm]	Length of one bar [m]	Total length for each bar [m]
1	27	8	10.76	290.52
2	77	8	8.06	620.62
3	28	8	2.52	70.53
4	27	8	4.40	118.80
5	32	8	8.06	257.92
6	32	8	2.34	74.88
			Total length [m]	1433.27
			mass of 1m [kg/m]	0.40
			total mass [kg]	566.14

Figure 3.11: Reinforcement plan – Conventional deck

Demountable connection:

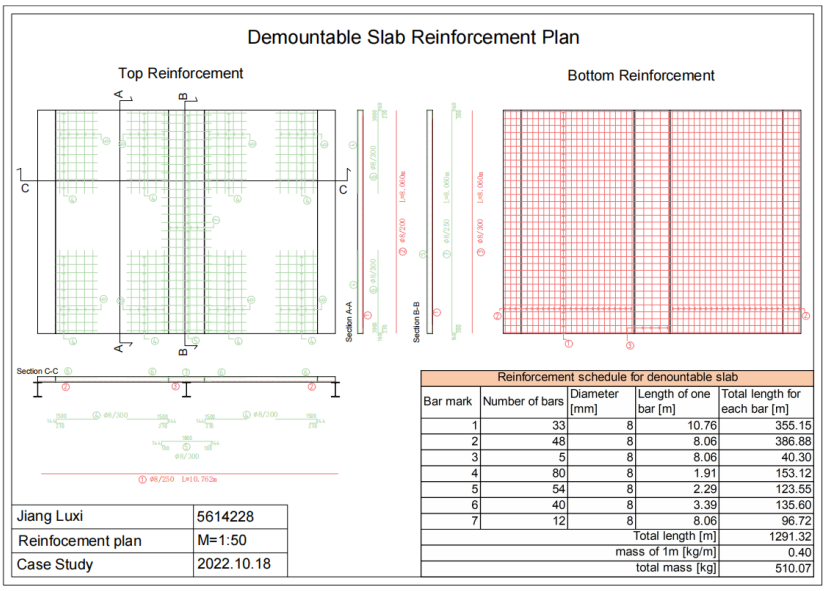

Reinforcement schedule for denountable slab

Bar mark	Number of bars	Diameter [mm]	Length of one bar [m]	Total length for each bar [m]
1	33	8	10.76	355.15
2	48	8	8.06	386.88
3	5	8	8.06	40.30
4	80	8	1.91	153.12
5	54	8	2.29	123.55
6	40	8	3.39	135.60
7	12	8	8.06	96.72
			Total length [m]	1291.32
			mass of 1m [kg/m]	0.40
			total mass [kg]	510.07

Figure 3.12: Reinforcement plan – Demountable connection deck

As shown in the Figure 3.11 and 3.12, the total mass of the reinforcement steel bar for conventional deck is 56kg more than demountable deck, which was not in expectation, therefore I double checked the moment diagram, and concluded as below:

For both decks my diagram are similar, because along y direction the boundary conditions are the same, there is no cut neither hinge connection. But for mx, although the moment in the middle of the decks is similar, but since there is discontinuity in x direction, therefore along the internal support, the conventional deck is almost double of the demountable deck. The reasons can be:
1. Demountable deck has less stiffness than conventional deck, therefore the moment is less.
2. The width of the deck (lever arm) for demountable deck is smaller which also produced less moment.

Since demountable deck has less moment, the reinforcement amount needed is less as well, especially for bottom reinforcement. But the shape of the reinforcement is more complicated than conventional deck.

3.2.4. SENSITIVITY ANALYSIS

THICKNESS TO DEFLECTION:

With all other data staying the same, bolt spacing of 500mm with default stiffness, the thickness of the deck is modified to see how deflection changes when increasing or decreasing the thickness.

Modifying the thickness of the slab:				
Demountable connection			Conventional	
Thickness [mm]	Deflection [mm]		Thickness [mm]	Deflection [mm]
170	3.921		170	1.986
180	3.461		180	1.738
190	3.081		190	1.533
200	2.763		200	1.362
210	2.494		210	1.218
220	2.265		220	1.096
230	2.069		230	0.991
240	1.899		240	0.901
250	1.752		250	0.822
260	1.623		260	0.754

Table 3.2: Thickness vs. Deflection.

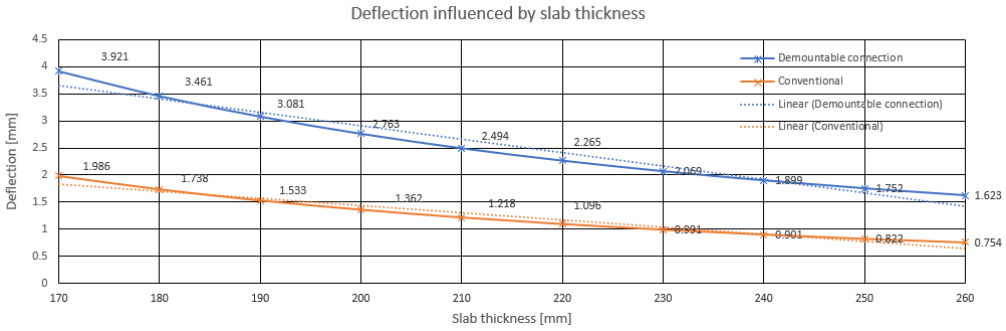

Figure 3.13: Deflection influenced by deck thickness

As the graph above shown, the deflection is reduced by thickening the deck, but the changes are getting smaller as the slope gets flatter.
The demountable connection deck is influenced more by thickness compare to conventional deck. by increasing thickness from 170mm to 260mm, the demountable connection deck deflection drops from 3.921mm to 1.623mm, a total of 2.298mm.
But for conventional deck it drops from 1.986mm to 0.754mm, with a total of 1.232, only half of the demountable deck.

SPACING TO DEFLECTION:

Rigid element:
Rigid element and different diameter of the bolts are used to see how spacing and stiffness influence deflection.

Rigid	
spacing [mm]	deflection [mm]
50	1.384
100	1.396
180	1.477
270	1.546
324	1.567
405	1.608
540	1.674
675	1.735
810	1.779
1350	1.963
1620	2.047
2025	2.163
2700	2.387
4050	2.880

Table 3.3: Spacing vs. Deflection - Rigid.

Theoretically speaking, if the bolts are infinitely rigid, and the spacing of them are very small, the structure will act like conventional deck with the same deflection. But in real life the bolts will never be infinitely stiff, not to mention the spacing, therefore the deflection also will never be the same as continuous conventional deck.

Shown in Tab 2.3, when bolts are set to rigid element in AxisVM, meaning they are restrained in all 6 degree of freedom, with the spacing of 50mm, the deflection is 1.384mm, which is very close to conventional deck of 1.362mm.
Different spacings of the bolts are tested out, ranging from 50mm up to 4050mm, which is not realistic, but for the sake of comparison, the summary is made on the table to the left.

Spacing of 25mm is also analysed, given result of 1.373mm, but the element size is too short which causes issue when meshing the domain, and 25mm is also not realistic, therefore the result is not included. Just to show the two models are getting more and more similar with smaller spacing.

Hinged link element:
Bolt diameter of 10mm, 20mm, 40mm and unrealistic 100mm are used.

	Hinged 6deg/3deg of freedom							
Spacing [mm]	Diameter [mm]	stiffness [kN/m]	Diameter [mm]	stiffness [kN/m]	Diameter [mm]	stiffness [kN/m]	Diameter [mm]	stiffness [kN/m]
	10	8.00E+04	20	3.00E+05	40	1.30E+06	100	8.25E+06
	Deflection [mm]		Deflection [mm]		Deflection [mm]		Deflection [mm]	
50	1.385	2.736	1.386	2.726	1.383	2.722	1.383	2.720
100	1.421	2.764	1.435	2.748	1.430	2.741	1.396	2.739
180	1.519	2.782	1.489	2.758	1.480	2.749	1.478	2.746
270	1.607	2.798	1.563	2.764	1.550	2.752	1.547	2.748
324	1.643	2.808	1.588	2.767	1.571	2.754	1.568	2.750
405	1.695	2.823	1.632	2.773	1.613	2.757	1.609	2.752
540	1.787	2.847	1.705	2.782	1.681	2.761	1.675	2.756
675	1.872	2.872	1.773	2.791	1.744	2.766	1.736	2.759
810	1.941	2.898	1.824	2.802	1.790	2.772	1.781	2.764
1350	2.218	3.012	2.033	2.853	1.980	2.806	1.966	2.793
1620	2.346	3.083	2.129	2.894	2.066	2.838	2.050	2.823
2025	2.527	3.181	2.263	2.945	2.187	2.875	2.167	2.857
2700	2.853	3.459	2.515	3.154	2.417	3.065	2.391	3.041
4050	3.520	3.939	3.057	3.492	2.921	3.362	2.886	3.328

Figure 3.14: Spacing vs. Deflection – link element.

Bolt stiffness is calculated as area of bolt times young's modulus of bolt over thickness of

the clamped material.

$$k_b = \frac{A_b * E_b}{t_p} \tag{3.1}$$

Since in real life, even though there is only tension and shear in bolt, it will still surfer from moment because of the decks it is connected are trying to bend. Therefore, fixed in 6 degrees of freedom and hinged in 3 degrees of freedom are both analysed.

When diameter of 100mm is used, the deflection is very similar as rigid element, since the stiffness of the bolt is very close to default rigid element.
As diameter gets smaller, the deflection gets bigger.

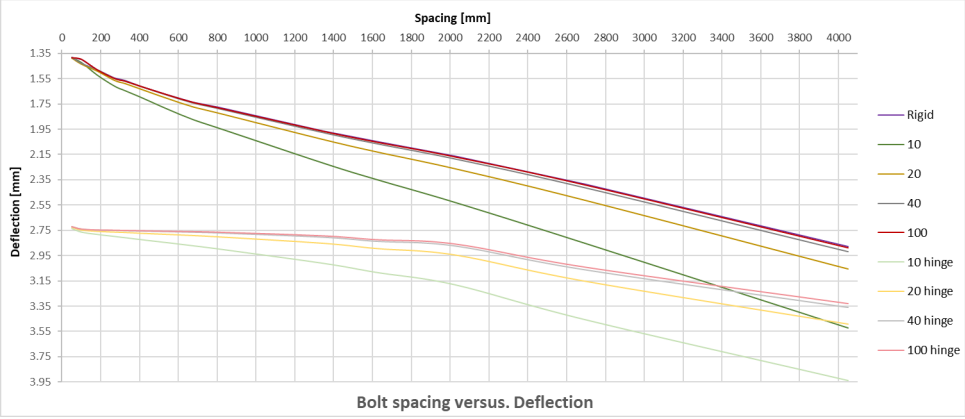

Figure 3.15: Deflection influenced by spacing

As Figure 3.15 shown, deflection of rigid element and 100mm bolt are very similar that they are overlapping.

Diameter of 10mm bolt deflection increases the most with increasing the spacing. For hinged bolt, the deflection stays almost the same until spacing around 810mm, the slopes become steeper after that. However, for fixed bolt, the deflection increases almost linearly with increase of spacing.

MAXIMUM DEFLECTION:

As stated in Eurocode, the maximum deflection of concrete deck is L/250.
In this case, the spans of conventional deck and demountable connection deck are both 5.4m, calculated the maximum deflection is 21.6mm.

The analyses are all within the range of validity, but in real life case, wind load, accidental load, horizontal deformation and so on should also be taken into consideration. This

factor may influence the maximum deflection of the deck.

The spacing and stiffness also influence the load in bolts such as tensile force and shear force, the further the spacing, the bigger the load in bolt, therefore bolts should also be checked for strength limit state.
Since this model is simplified and it is much more complicated to calculate how much force and moment each bolt takes, the most favorable spacing and diameter cannot be chosen by this model.

3.3. CONCLUSION

As shown in this chapter, one can find the difference between the two systems from a broader perspective. Without delving into the specific intricacies of the connection itself, a conclusion can be drawn.
Although the deflection of the demountable deck system is double the deflection of the conventional deck system, the dead load and required reinforcement amount is less compare to the latter, this leads to a more economically efficient configuration. Furthermore, a noteworthy attribute of the demountable deck system is its potential for removal and subsequent reuse after its initial life cycle. This aspect stands as the main focus of this research investigation.

4

NUMERICAL MODELS

The previous chapter provides a global overview of the differences between demountable and traditional concrete decks. Preliminary observations yield a more general understanding of the deck with demountable connection.

This understanding highlights the advantages of employing demountable floor system. To further advance this objective, a comprehensive examination focused on the performance of the connection between the composite beam and concrete deck is needed.

Consequently, the subsequent phase involves studying the behaviour of the connection from every perspective.

Two types of analyses are conducted to examine the mechanical behaviour of such connections: one is connection subjected to shear, providing confidence in modelling and the other one is a connection subjected to bending, which presents the most critical aspect for investigation.

This chapter summarises the input parameters for analytical models used in subsequent chapters, such as dimensions, material properties, boundary conditions, interactions and so forth.

4.1. GEOMETRY

4.1.1. SHEAR MODEL

THE shear model is built as a small specimen in finite element model. This specimen consists of two L-shape concrete blocks (similar to half joint in concrete), connected by a demountable shear connector (bolt) in the middle, which can be unscrewed and demounted later. The dimensions of these concrete block are 350mm and 250mm for the longer and shorter edges, and 250mm for both height and width. Figure 4.1 below illustrates a more direct view of the specimen.

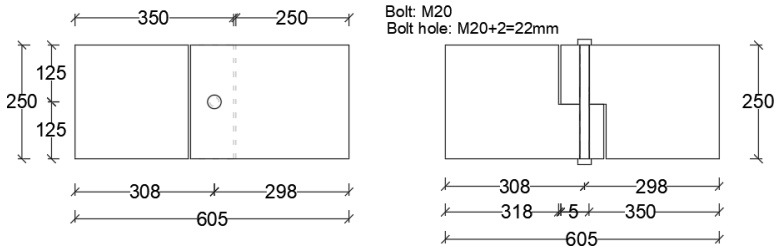

Figure 4.1: top view (top) and cross section (bottom) of the shear model

4.1.2. BENDING MODEL

The bending model is built as a 500 mm wide strip taken from an entire concrete deck in the finite element model. This section also consists of three L-shaped concrete blocks, the joints of which are connected by demountable shear connectors at both ends.
The span and depth taken for this model is 3910 mm and 160 mm, respectively. Figure 4.2 below provides a more direct view of the specimen.

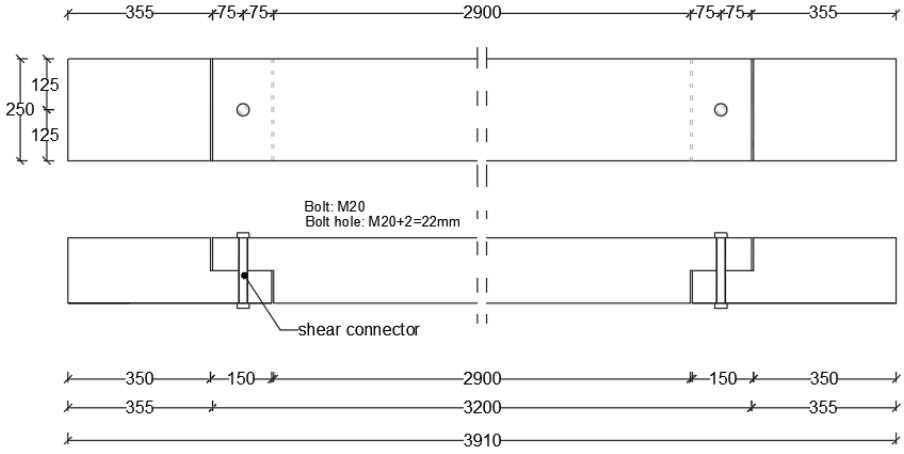

Figure 4.2: top view (top) and cross section (bottom) of the shear and bearing model

4.2. MATERIAL PROPERTIES

4.2.1. INTRODUCTION

As discussed in chapter two literature review under the section material properties 2.4, about the steel and concrete material properties, a more detailed parameters are listed in this section.

Abaqus finite element modelling is utilized for the numerical analysis.
Abaqus/Explicit is a powerful tool for structural analysis, particularly in situations involving dynamic events, impact, and transient loading. Its capabilities in handling nonlinear behaviour and contact interactions make it an essential tool in various industries, from automotive and aerospace to civil engineering and biomechanics.

Steel materials are assumed to follow plastic non-linear behavior, including steel bolts, washers (when used), and reinforcement bars, while fracture analysis with damage material model such as concrete damage plasticity (CDP) non-linearity for concrete material.

4.2.2. STEEL MATERIALS

In this thesis research, the density for steel materials is taken as 7.85E-09 ton/mm^3, initial modulus of elasticity is E which equals to 210000 MPa, and Poisson's ratio is 0.3 taken for steel bolt and other Isotropic steel parts such as washer and re-bars.

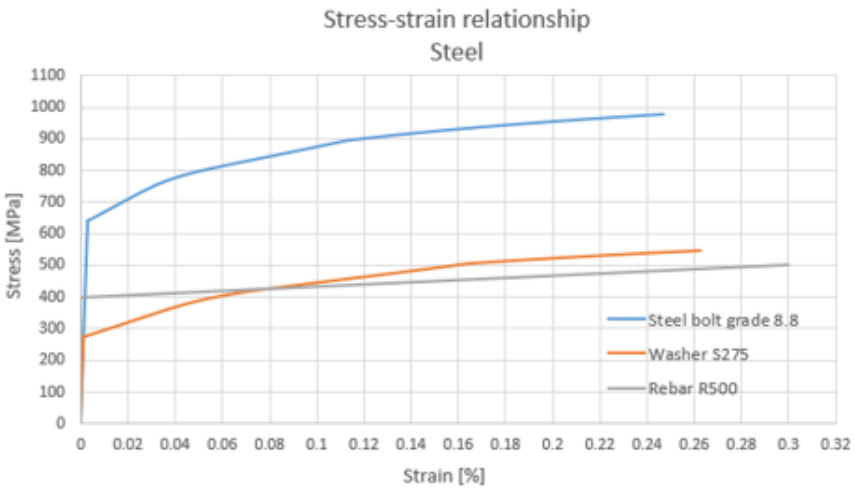

Figure 4.3: Stress strain relationship for steel materials

Figure 4.3 above shows the stress-strain relationship for different steel materials used in this research.

The steel bolt is taken as grade 8.8, M20, with clearance of the bolt hole of 22mm, grade 8.8 denotes that the steel bolt has a yield strength of 640 MPa and an ultimate strength of 800 MPa, and M20 represents the diameter of the bolt.
The washer, considered as a steel plate with grade S275, possesses a yield strength of 275 MPa and an ultimate strength of 430 MPa, in accordance with Eurocode 3 [34].
For the reinforcement bars, R500 steel material grade is employed, with a yield strength of 400 MPa and an ultimate strength of 500 MPa at an equivalent strain of 0.1.

The stress strain relationship for steel materials consists of two ascending parts, the first part is linearly increasing up to the yield strength of the material, after which it transitions into a non-linear increase until failure of the steel.
Since the data required for Abaqus is true stress strain relationships, therefore in the Figure 4.3 does not clearly show the ultimate strength point nor fracture point of the material.

4.2.3. CONCRETE MATERIALS

Initially, concrete grade C20/25 was chosen because the strength requirement for office building is not as strict as for industrial building. However, considering the potential for demounting and reuse after the service life of the structure, an higher grade C40/50 of concrete is chosen at the end.

Concrete is a heterogeneous material that consists of water, cement and aggregates, which the determination of failure or plastic yielding is determined by pressure model, as defined by Drucker–Prager yield criterion [30] theory.

Concrete density taken is 2.45E-09 ton/m^3, the initial modulus of elasticity E is 35000 MPa, and the Poisson's ratio is taken as 0.2.

In order to input the compressive and tensile stress strain behaviour of the concrete, CDP model is employed for the analysis, requiring additional parameters:

1. Dilation angle ψ measured in the p–q plane at high confining pressure.
2. Flow potential eccentricity ϵ
3. Biaxial/uniaxial ratio of compressive yield stress f_{b0}/f_{c0}
4. Ratio of the second stress invariant on the tensile meridian to the compressive meridian K_c
5. Viscosity parameter for relaxation time of the viscoplastic system μ

These parameters are determined based on empirical studies and Abaqus guidelines, as shown below in table 4.1:

Parameter	Value	Reference
ψ	40	Ranges from 36° to 40° by Kmiecik P, Kamiński M.[45]
ϵ	0.1	Usually 0.1, but can go up to 1, by Labibzadeh, Mojtaba et al.[47] and Abaqus standards [69]
f_{b0}/f_{c0}	1.16	Taken from Abaqus standards [69]
K_c	0.667	Ranges from 0.5 to 1, in Abaqus standards [69] the default value of 2/3 is taken
μ	0	No viscoplastic regularization is performed

Table 4.1: CDP parameters adopted values and references

The behavior of concrete in compression in Abaqus/explicit CDP model is defined as the relationship between compressive stress and inelastic strain, while behaviour in tension is defined by the relationship between tensile stress and cracking strain. Both curves should represent true stress-strain state, rather than engineering stress-strain state, allowing Abaqus to compute the plastic strain internally. Difference models are explained in chapter 2.4.

$$\epsilon_c^{pl} = \epsilon_c^{in} - \frac{d_c}{1-d_c}\frac{\sigma_c}{E_0} \tag{4.1}$$

$$\epsilon_t^{pl} = \epsilon_t^{ck} - \frac{d_t}{1-d_t}\frac{\sigma_t}{E_0} \tag{4.2}$$

Equation 4.1 and 4.2 shows the relationship between plastic strain and inelastic/cracking strain of concrete in terms of damage parameters d_c and d_t in compression and tension, respectively. These will be explained later.

True stress-strain relationship can be derived from laboratory results if experiments are conducted. In this case, with only numerical analysis performed, conversion from engineering to true stress strain curve is necessary.

The inelastic strain and cracking strain are calculated as engineering strain minus the elastic strain:

$$\epsilon_c^{in} = \epsilon_c - \epsilon_{0c}^{in} \tag{4.3}$$

$$\epsilon_t^{ck} = \epsilon_t - \epsilon_{0t}^{ck} \tag{4.4}$$

Where the elastic strain is stress over modulus of elasticity: (Note that the modulus of elasticity is the same for concrete in compression or in tension).

$$\epsilon_{0c}^{in} = \frac{\sigma_c}{E_0} \tag{4.5}$$

$$\epsilon_{0t}^{ck} = \frac{\sigma_c}{E_0} \tag{4.6}$$

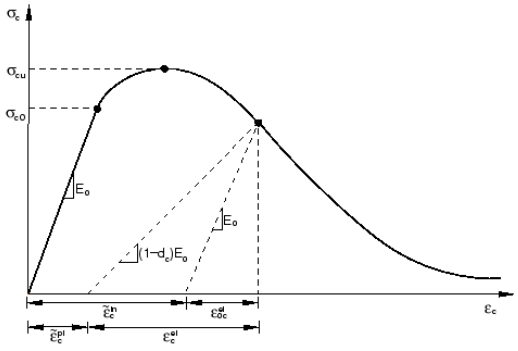

Figure 4.4: Definition of the compressive inelastic (or crushing) strain in compression hardening model

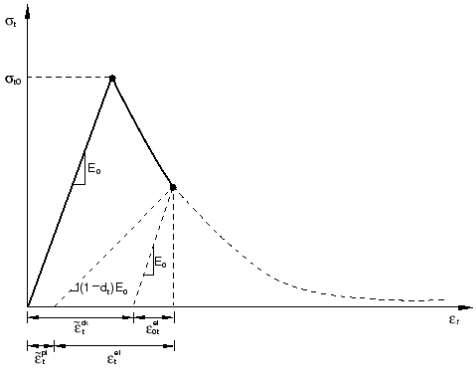

Figure 4.5: Definition of the cracking strain in tension stiffening model

Figure 4.4 and 4.5 shown below gives an expression on the definition of inelastic strain and cracking strain in concrete compression hardening and tension stiffening model. The plasticity model cannot define the descending part of the stress-strain curves, therefore, damage model is used instead. Damage material parameters are defined as the reduction of initial modulus of elasticity E, with the expression of $(1-d_c)E_0$, where the d_c, or in case of tension d_t, is the artificial damage variable, as shown in figure above.

The damage variable is equal to zero within the strength of the material, it starts increasing after the ultimate strength is reached, d_c or d_t goes up to 1, meaning the full degradation of the material stiffness. In Abaqus, it is suggested that the damage variable does not surpass 0.99, to avoid critical effect on the rate of convergence. The damage evaluation can also be displacement or fracture energy controlled, in this way, the mesh dependency due to strain concentration can be omitted [69], but due to the lack of experimental data, strain controlled damage evaluation is chosen.

The compressive and tensile damage parameters d_c and d_t can be obtained from material tests where cyclic loading is applied, with the following equation[1]:

$$d_c = 1 - \frac{E_i}{E_0} \tag{4.7}$$

Where E_i is the stiffness of the concrete after each cycle of loading/unloading, and E_0 is the initial stiffness of the concrete as in the modulus of elasticity.
But in the absence of such data, for example in this thesis research, the following equation can be adapted:

$$d_c = 1 - \frac{\sigma_i}{\sigma_{cu}} \tag{4.8}$$

[1] Mentioned by Dr. Ahmed Elkady in the lecture of ABAQUS Tutorial: Defining Concrete Damage Plasticity Model + Failure and Element Deletion

Where σ_i is the stress at each loading/unloading state and σ_{cu} is ultimate compressive stress. This equation works as the same for tensile damage parameter.

There are many different stress-strain relationships for concrete in compression and tension, mentioned in chapter 2.4, with contributions from different researchers. These variations primarily arise from differences in methodology, experimental findings, empirical formulations, or a mix of these factors.

Ahmed Elkady [31] has developed practical tools, shown in Figure 4.6 and Figure 4.7, that enables the generation of stress-strain curves for both steel (left) [53] and concrete (right) [66][15][16][37] by inputting essential material parameters, including yield strength, ultimate strength, and strain at ultimate strength, among others.
The goal is to combine these engineering stress-strain relationships with equations 4.1 to 4.8 to derive true stress-strain curves suitable for use in Abaqus. These tools are particularly beneficial for individuals without access to testing data, which is suitable in this case that since only numerical analyses are performed.

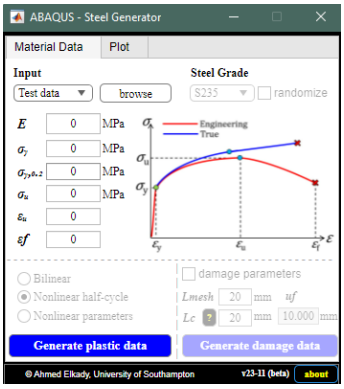

Figure 4.6: Abaqus steel generator

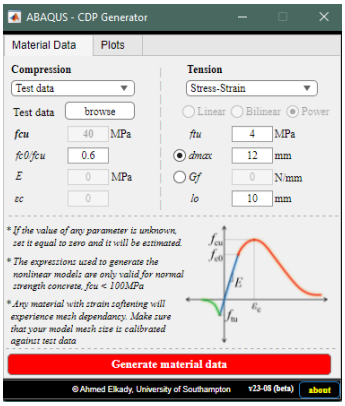

Figure 4.7: Abaqus concrete CDP generator

Stress strain curves for concrete in compression and tension:

The stress-strain curves in this research for both concrete in compression and tension are shown below in Figure 4.8 and Figure 4.10, respectively, accompanying by the damage parameters models in Figure 4.9 and Figure 4.11 as well.

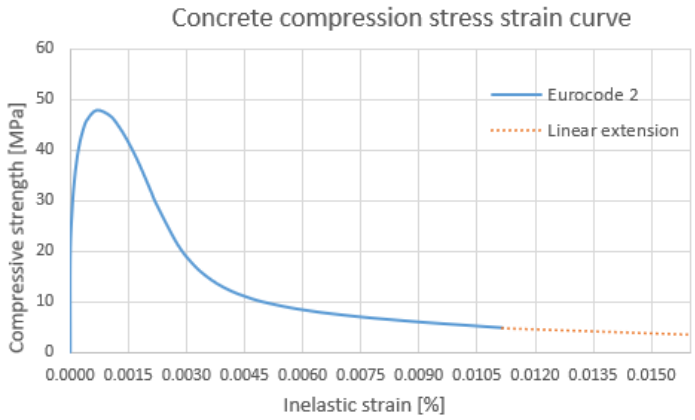

Figure 4.8: Concrete compression stress strain curve

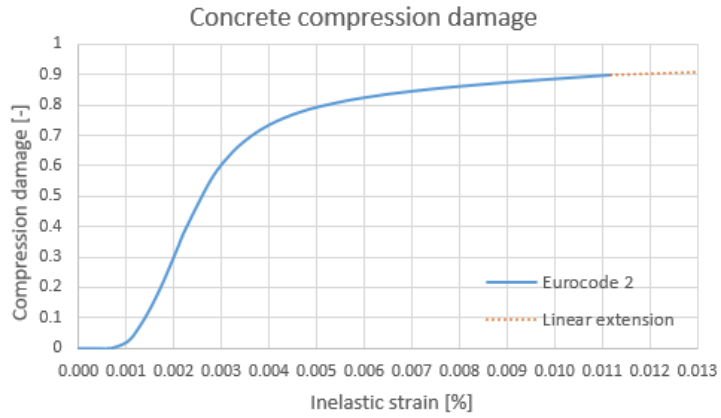

Figure 4.9: Concrete compression damage

The behavior of concrete in compression in Abaqus is defined as a function of compressive stress and inelastic strain. According to Eurocode 2, the stress-strain relationship for concrete in compression is divided into three segments, with two ascending and one descending parts.
Initially, it grows linearly up to $0.4 f_{cm}$, with an initial modulus of elasticity. This region is referred to as the elastic deformation zone.
Subsequently, it increases non-linearly until reaching the compressive strength f_{cm}, at the strain of ϵ_{c1}, where the f_{cm} is the mean compressive strength at 28 days, according to table 3.1 in Eurocode 2 [71]. Compression plasticity curve also starts at this point, for

the input in Abaqus.
After this point, it follows a sinusoidal decrease in stress until it reaches a strain of 0.01. In the end, the curve is extended linearly to strain of 0.1, it is so called residual branch, large value strain of 0.1 is chosen so that it is not to be achieved in the analyses [62].

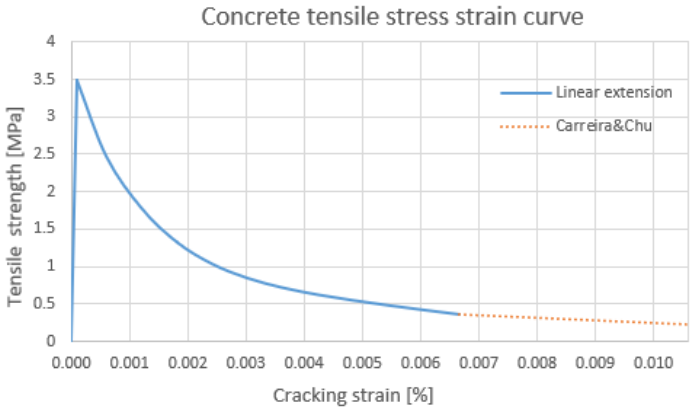

Figure 4.10: Concrete tension stress strain curve

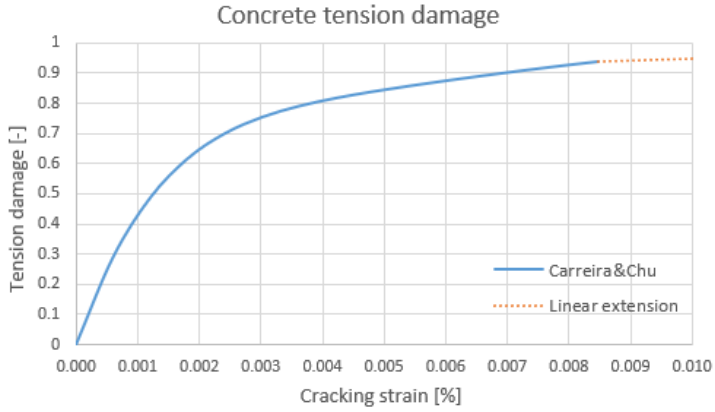

Figure 4.11: Concrete tension damage

The behavior of concrete in tension in Abaqus is defined as a function of tensile stress and cracking strain.
The stress increases linearly until the mean value of axial tensile strength of concrete f_{ctm}, given in table 3.1 in Eurocode 2 [71].
After that point, tension softening appears due to cracking, the stress descends in sinusoidal manner according to Carreira and Chu [14] until strain of 0.01. At last, the curve is extended linearly to reach the strain of 0.1 instead of zero, for the purpose of numerical stability.

4.3. BOUNDARY CONDITION AND LOADING

BOUNDARY conditions in structures refers to the the restrain or limitations on edges or surfaces that affects how it responds to loads or external forces.
It is crucial to apply correct boundary conditions in numerical analyses to accurately simulate structure's behaviour.

Before adding boundary condition, two reference points RP are made for the left and right faces in y-z plane, in the center of the faces, coupling constraints are then added to the RP and the corresponding faces, with all six degrees of freedom constrained. This approach avoids stress concentration effects that could arise from directly applying boundary conditions to the faces.

The boundary conditions are applied to the reference points in a displacement-controlled manner, increasing the stability of the analysis, by avoiding possible convergence issue.

For shear model in Figure 4.12, the boundary conditions on the two RP are fixed, u1, u2 and u3 are restrained in the initial step. For step-1, load is added through displacement control by pulling both concrete blocks horizontally 3mm in opposite directions. This means that for the RP on the left face, the boundary condition for step-1 is u1=-3mm, u2=u3=0, and for the RP in the right face, the boundary condition is u1=3mm, u2=u3=0. There is also boundary condition of u3=0 added to the four edges along x-axis length to avoid deformation along -axis, maintaining rather pure shear in the connection.

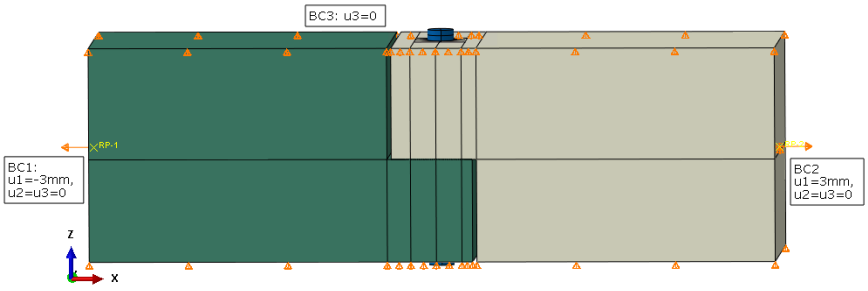

Figure 4.12: Boundary condition of shear model

For the bending models, RP are are similarly defined on both faces and restrained in all six degrees of freedom, making the section act as a continuous beam. As these models represent a strip taken from a concrete deck, y-symmetric boundary conditions are also applied to both faces in x-z plane, which is u2=ur1=ur3=0, along the span of the concrete. In order to reduce computational time, the total span is cut in half, to obtain the same result, x-symmetric boundary condition is added to the middle of the span, which is u1=ur2=ur3=0.

There is an additional RP added on the middle of the top surface of the loading plate,

coupling restrained in all 6 degrees of freedom as well.

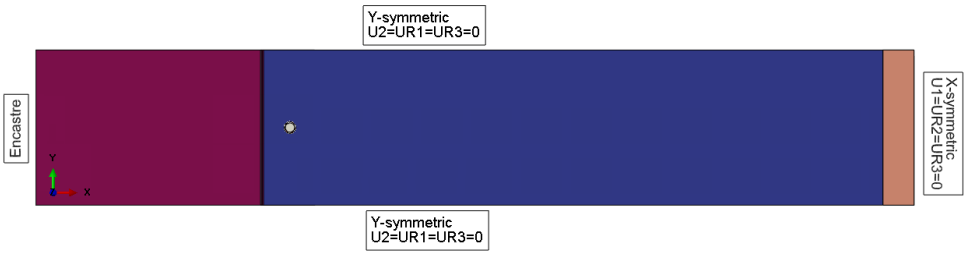

Figure 4.13: Boundary condition of bending model-top view

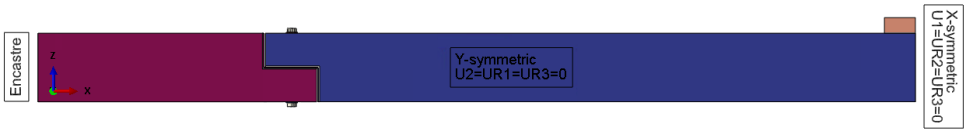

Figure 4.14: Boundary condition of bending model-front view

The loading plate here is defined as an infinitely stiff steel plate with dimension of 200mm*250mm*50
for length, width and height, respectively.
It provides a smoother loading surface for the applied displacement.
Bending is added through the loading plate, after the coupling constraint of the third RP and the top surface of the loading plate, a negative 10mm displacement is applied to step-1 in the u3 direction.

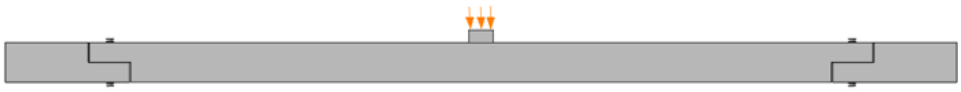

Figure 4.15: Three point bending for bending model

For step-1, dynamic, explicit model is selected with a time period equals to 1. Mass scaling is enabled with a scale of 10 to reduce computational time.
For Abaqus/explicit model, an amplitude tabular for loading is required, and a smooth step type of amplitude is chosen for both model, with value of 0 0, 1 1.

Computation time is related to the minimum stable time increment that requires Abaqus to perform the analysis, larger the time increment, smaller the computational time.
There are multiple ways of increasing minimum stable time increment for running the analysis. Including, but not limited to increase loading rate or density, mass or time scaling, avoiding small local meshes. Among these, mass scaling is used here.

Equation 4.9 shows the relationship between minimum stable time increment with each parameters:

$$\Delta_t = L^e \sqrt{\frac{\rho}{E}} \tag{4.9}$$

$$L^e = \sqrt[3]{Volume} \tag{4.10}$$

Where Δ_t is the minimum stable time increment, L^e is the characteristic length of element, also called the mesh size, ρ is the density of the element, and E is the modulus of elasticity.

Looking at the equation 4.9, the most efficient way to increase minimum stable time increment is to increase the characteristic length of the element, but in most of the cases it cannot be achieved, since fine mesh is required for the area where it is point of interest. And the value of L^e is taken as the minimum element size in the model. The so called density scaling is to increase ρ - density of the element, this also increase the minimum stable time increment, but since it is under the square root, the effect is less noticeable than changing the element size.

Mass scaling works similar to density scaling, but smarter. With mass scaling function, the whole model or even a particular set can be scaled by a given factor or a given target time increment manually.

It is important to know that using mass scaling function might affect the simulation result and the result is need to be checked. It is important to choose a mass scaling factor that reduce efficiently the computational time without too much sacrificing of the accuracy of the result.

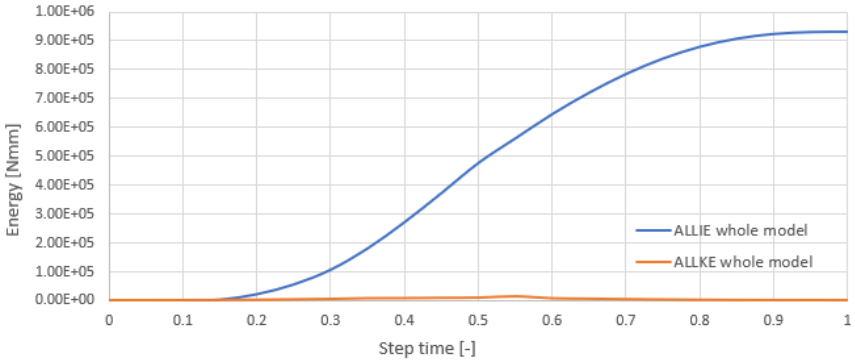

Figure 4.16: Inertia energy vs. Kinetic energy - whole model

To maintain the accuracy of the results by using mass scaling, it is advised that the kinetic energy stays smaller than 5% of inertia energy. Figure 4.16 shows the comparison

of inertia energy and kinetic energy for bending models.

The chosen mass scaling factor of 10 is being tested against the analysis ran without any mass scaling, and after comparing the results from both model, it can be concluded that the difference between the two models is acceptable.

4.4. MESH AND INTERACTION

4.4.1. MESHING

According to Abaqus recommendation [69], hexahedral C3D8R element type with linear integration is the most appropriate for Abaqus/explicit analyses.
C3D8R is an 3 dimensional continuum (solid) element type that consists of 8 nodes, with reduced integration. However, in order to capture more accurate results, small element sizes are required for this element type.

For Abaqus models, a global element size of 20mm is applied generally, but it can be differ in different areas. For example, at or near the critical area, the mesh size is smaller. Several partitions are made to get better control over the element size.

A gradually reduced element length from 10mm to 8mm is applied to the L joint part of concrete where hole exists, because extra attention needs to be paid at the change of geometry. Figure 4.17 and Figure 4.18 shows the mesh density for the whole bending models in front and top views.

Denser mesh elements can be seen near the critical region, such as around bolt hole or concrete half joint, while for the rest region, global seeding of 20mm is assigned.

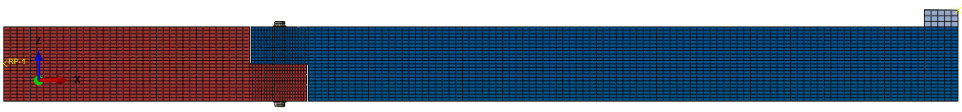

Figure 4.17: Element size for bending model - front

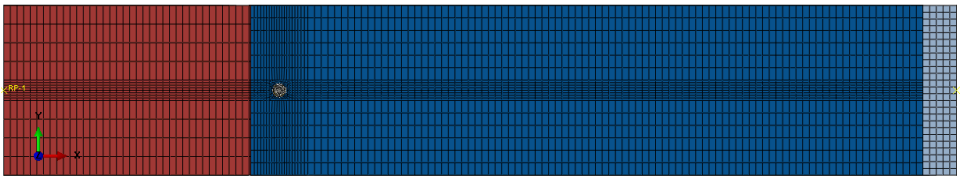

Figure 4.18: Element size for bending model - top

Sweep technique with medial axis and minimized mesh transition is used around the hole, see in Figure 4.19, with element size smaller for inner circles and gradually in-

creased from 3mm to 6mm towards outer circles.
The element size of the steel bolt is applied as 8mm for both bolt shank and bolt nut, see in Figure 4.20.

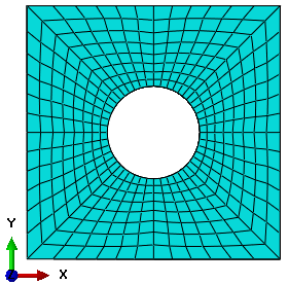

Figure 4.19: Element size near the hole in concrete

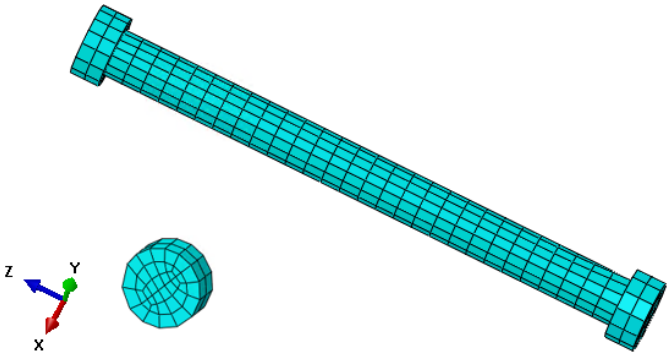

Figure 4.20: Element size of bolt shank and bolt head

Rebar reinforcements are modeled as wired truss elements, with cross sectional areas assigned depends on the diameter of the re-bars. The mesh element size assigned for re-bars are 50mm. Since it is modeled as a wire, no 3D model can be seen for mesh element for reinforcements.

4.4.2. CONTACT INTERACTION

Contact interaction in Abaqus defines the behavior of different surfaces or bodies when in contact, separate or interact with each other. There are several types of contact, the contact type used in these shear models and shear and bending models is the recommended general contact (explicit) from the Abaqus manual.
General contact allows contact between many or all regions of the model with a single interaction. Surface pairs with different attributes can also be manually selected to assign with different interaction properties.

For this research, tangential behaviour of penalty frictional formulation and normal behaviour of hard contact is defined to simulate the contact between each surfaces. "Hard contact relationship minimizes the penetration of the slave surface into the master surface at the constraint locations and does not allow the transfer of tensile stress across the interface."[2]. The definition of friction is the force that resists the sliding or rolling of one solid object over another, as expressed in equation 4.11:

$$F_f = \mu N \tag{4.11}$$

Where F_f is friction, μ is friction coefficient and N is normal force.

[2] Part of this paragraph is cited from Abaqus Analysis User's Manual, under section 30 Contact Property Models[69].

Three interaction properties with different friction coefficients are defined in the models. For pairs between concrete and concrete, between steel bolt nut/shank and concrete, and between steel bolt nut and steel washer. Cohesion properties are fairly difficult to define and it is not the point of interest in this thesis, therefore, cohesion related parameters are not included. The contact interaction properties can be seen in table 4.2:

Contact pairs	Tangential behaviour	Normal behaviour	Reference
Concrete to concrete	Penalty: $\mu = 0.6$	Hard contact	ACI 318. 11.7.4.3[1]
Steel bolt head/shank to concrete	Penalty: $\mu = 0.3$	Hard contact	Empirical data
Steel bolt head and washer	Penalty: $\mu = 0.2$	Hard contact	MIL-HDBK-60[32]

Table 4.2: Contact interaction properties

Since the analyses conducted in this research is mainly focusing on the failure mechanisms of the connection, therefore the modeled is assumed as a perfect structure without any imperfection, such as the unevenness of the concrete surface and so on.

4.4.3. REINFORCEMENT EMBEDMENT

The "embedment region" constraint technique in Abaqus allows an element or a set of elements is embedded in "host element". According to Abaqus Manuel, this technique can be used to model rebar reinforcement.
By defining embedment constraint, the translational degrees of freedom are constrained to the host element, while rotational degrees of freedom are not constrained by the embedment.

For the reinforcement used in both shear and bending models here, embedment constraints are set for re-bars with concrete being the host elements.

4.5. REINFORCEMENT

4.5.1. REINFORCEMENT CALCULATION

Hand calculations according to Eurocode 2 [71] can determine the required amount of reinforcement for a conventional concrete deck. Additional reinforcement at the nib section should be tailor-made for demountable "concrete to concrete" connection.

With applied three point bending, the maximum hogging/sagging bending moment can be calculated as following:

$$M_{hog} = F * \frac{L}{8} \tag{4.12}$$

Where M_{hog} is the hogging bending moment of the concrete strip, F is the point load in the middle of the span and L is the length of the span.

Weather or not compression reinforcement is needed can be calculated by the K factor, when K is lesser than 0.155, then compression reinforcements are not required:

$$K = \frac{|M_{hog}|}{b * d^2 * f_{ck}} \tag{4.13}$$

$$d = h_c - cover - \frac{\phi}{2} \tag{4.14}$$

Where b is the width of the concrete strip, h_c is the height of the concrete and d is the effective depth of the concrete. Cover means the concrete cover for the reinforcement, in this analysis, the concrete cover is taken as 20mm.

At the end, the required area of reinforcement can be calculated by:

$$A_{s.req} = \frac{|M_{hog}|}{0.87 * f_{yk} * z} \tag{4.15}$$

Where $A_{s.req}$ is the required area of reinforcement, f_{yk} is the characteristic yield strength of the steel bars and z if the lever arm of the internal forces in a reinforced concrete which can be calculated as z = 0.95*d.

Based on the required area and diameter of the reinforcements, the spacing and numbers of re-bars can be determined.

For the calculated reinforcement, deflection check also need to be performed by calculating allowable modified ratio, this ratio shall be larger than the ratio of $\frac{L}{d}$.

For one way slab, reinforcements spanning in both longitudinal and transversal direction is not required, however, the distributional steel, or with another name which is temperature steel, is still required in transversal direction.
The minimum required area of this distributional steel reinforcement can be calculated as:

$$A_{smin} = 0.0013 * b * h_c \tag{4.16}$$

The spacing and numbers of required re-bars can be determined with the same method as earlier.

4.5.2. REINFORCEMENT LAYOUT

Figure 4.21 shows the reinforcement added to the demountable connection bending models in longitudinal direction. The diameter and spacing of the re-bars are shown in the figure.

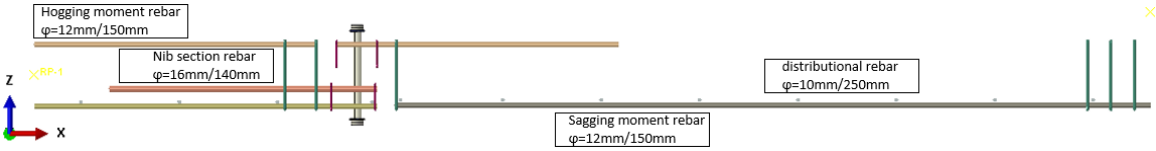

Figure 4.21: Reinforcement for bending model - front

In the hogging and sagging bending moment zones of the concrete decks, longitudinal reinforcement bars are strategically placed. These bars have a diameter of 12mm and are spaced 150mm apart from each other.

Nib section (L joint of concrete) is reinforced to mitigate potential damage caused by direct shear cracks and reentrant corner cracks. The diameter of the four reinforcement bars at this location is 16mm with spacing of 140mm, 150mm and 140mm between each bars, accounts for the presence of the concrete bolt hole in the middle of the section.

Above the longitudinal bottom reinforcement, transversal distributional bars are placed. These bars have a diameter of 10mm and are spaced 250mm apart, extending along the entire span of the concrete.

Stirrups are placed to hole the reinforcement bars in position, the diameter for bigger stirrups at the constant thickness of concrete are 8mm and the diameter for smaller stirrups at the half joints are 6mm.

Figure 4.22 shows a three dimensional layout of the reinforcement bars for the concrete strip modeled in bending.

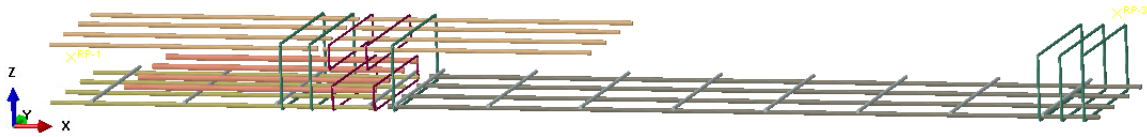

Figure 4.22: Reinforcement for bending model - 3D

This reinforcement plan is tailor-made specifically for the concrete with demountable connection which can be newly crafted from scratch.

For existing concrete decks that are to be reused after their initial cycle of life, should be cut into half joint to have a demountable connection. This implies that only reinforcement bars in hogging and sagging bending moment location exist, leaving the half joint vulnerable under loading conditions. Therefore, additional enhancements shall be applied, such as adding steel plates at the reentrant corners to protect against potential damage to the connections.

The same reinforcement layout is applied in the shear model, see in Figure 4.23.

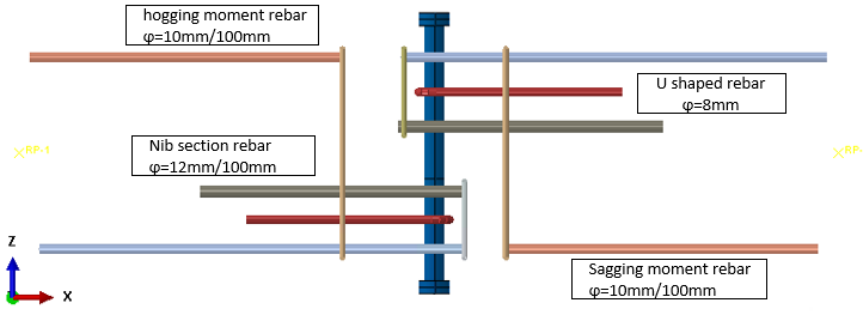

Figure 4.23: Reinforcement for shear model

In the shear model, in the hogging and sagging moment zones, rebars with 10mm diameter and a spacing of 100mm is used.
At the nib section, four 12mm diameter re-bars are used with spacing of 100mm, 160mm and 100mm, due to the steel bolt in the middle, at the L joint section for both left and right concrete blocks.
Additionally, a single U-shaped reinforcement is added around the steel bolt to hold concrete together near the bolt hole.

5

RESULTS

The results presented in this chapter are derived from two sets models mentioned earlier: the shear model of two concrete blocks and the bending model of a modularised floor system, which consists of composite beam and concrete decks.

By combining outcomes from both models, the failure mechanisms of the demountable connection are summarised at the end of this chapter.

5.1. SHEAR MODEL

THE primary goal of developing a simple shear model is to have a step-by-step increase in the level of complexity of the proposed structure to gain confidence in the numerical modelling rather than being a realistic loading condition, mentioned in section 1.5.3.

Applying displacement control of 3mm by pulling both concrete blocks apart from each other, results in this concrete block suffer from tensile stress. Considering the concrete's tensile strength of 3.5 MPa, the connection is extremely brittle.

To achieve force equilibrium, for the right side concrete, the load is transferred from the boundary of the concrete, along the span, to the shear connector. This results in the shear connector resisting a reaction force at the location of one-quarter of the shank. Due to the 2mm bolt hole clearance and friction between the bolt nut and concrete, the bolt nut also bears some force. However, since the weight of the bolt nut and the friction between it and the concrete surface are minimal, this reaction force due to friction is also very small. The same principle applies to the left side concrete block.

Shearing of the steel bolt causes the shank of the bolt to rotate in a small angle, along with the bolt nut, resulting in compression stress at the contact location between the steel nut and the top surface around bolt hole. As the load increases, the stress at this location increase as well, eventually leading to the crushing of concrete under bolt nut, as shown in Figure 5.1. Higher stresses are accumulated under the bolt nut, which becomes one of the failure modes in the bending model.

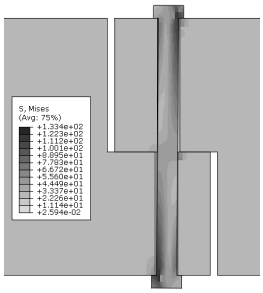

Figure 5.1: Von mises stress in bolt prior to failure

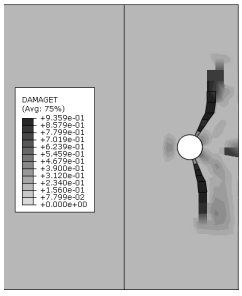

Figure 5.2: top view: Left side concrete block cracking right after failure

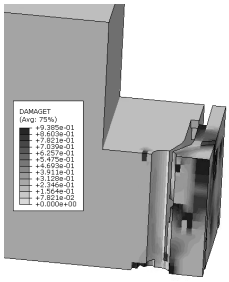

Figure 5.3: Total failure of left side concrete block

Figure 5.1 illustrates that the maximum stress in the steel bolt prior to concrete failure is only 133 MPa, far less than the resistance of the steel bolt. This indicates that the critical aspect of this connection is the concrete elements, according to Figure 5.2 and Figure 5.3. When the concrete block is pulled, the entire concrete is under tensile stress, while the steel bolt is under shear. As the concrete tensile strength is much lower than the strength

of the steel bolt, the rupture of the edge occurs, leading to the total failure of the concrete.

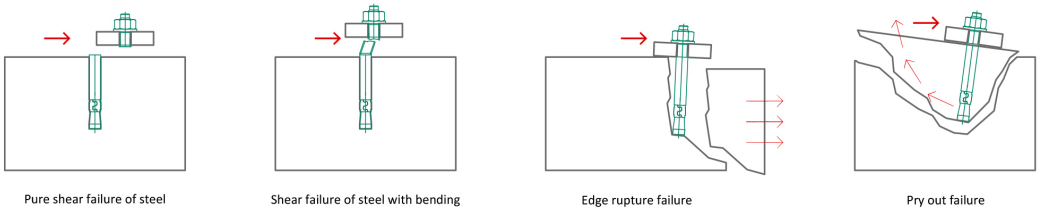

Figure 5.4: Failure mode of connection under shear

As shown in Figure 5.5, the maximum load this connection can resist is 12kN, the load starts increasing gradually until reaching the displacement of 1mm, where the concrete begins to contact the steel bolt (due to 2mm clearance in the bolt hole, the concrete and steel bolt do not touch initially). The force then increase rapidly.
At a displacement of 1.5mm, the load stops increasing and drops linearly, where the concrete failure happens. Concrete fails at this point without early warning due to its brittleness in tension; once the strength is reached, cracking occurs.
At around 2.1mm of displacement, the load drop becomes flatter. At this point, the vertical crack along the bolt hole has reached the total nib height of the concrete, resulting in the splitting of the concrete.

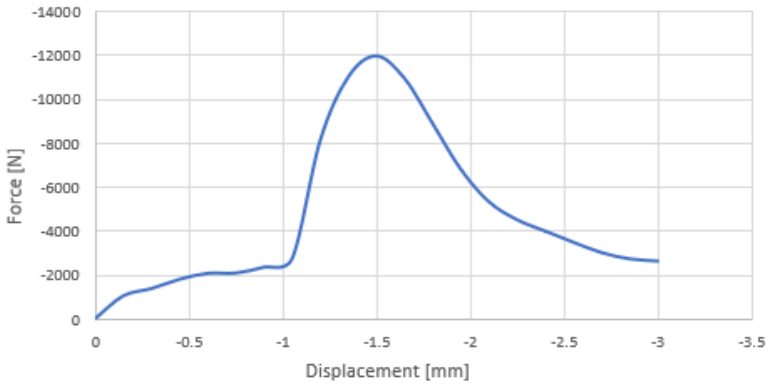

Figure 5.5: Force to displacement curve of shear model

At around 1.8mm of displacement, due to the rotation of the steel bolt, stress concentrates at the contact area of concrete and bolt nut, leading to concrete crushing around the bolt nut, see Figure 5.6. The stress starts dropping prior to this crush due to the concrete damage plasticity model. With increasing compressive damage at this point,

the stiffness within the concrete reduces, and crushing occurs when the maximum compressive damage is reached.

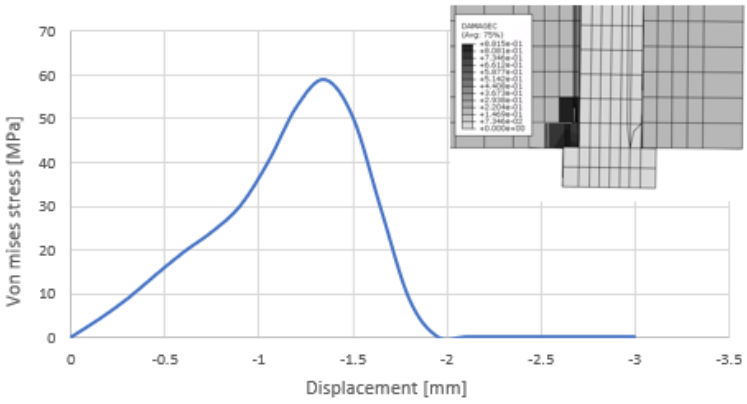

Figure 5.6: Stress to displacement curve at crushing of concrete

From the shear model, it is evident that, instead of steel bolt, the main failure modes of the connection occur in the concrete:

1. Concrete crushing at the mid plane due to the rotation of the steel bolt, resulting in the failure of surrounding concrete due to rapture of the edge
2. Concrete crushing under steel bolt nut due to compression stress.

5.2. BENDING MODEL

In commercial buildings such as office buildings, high load capacity is typically not required. The surface load applied to this concrete deck is calculated by summing the dead load and live load:

$$w = 1.35 * w_g + 1.5 * w_l = 13.41 \frac{kN}{m^2} \tag{5.1}$$

Where w_g represents the sum of the dead load from self weight of concrete deck and the self weight of partition walls, and w_l represents the applied live load in accordance with human action, as specified in Eurocode 1991-1-1 [70]. Coefficients of 1.35 and 1.5 represent the safety factor for dead load and live load, respectively.

This research concentrates on the failure mechanism of the connection between the composite beam and concrete deck; therefore, three-point bending is employed as the loading scenario instead of applying regular surface loads.

The loading behaviours of the three point bending and uniformly distributed surface load are different. However, this is not the central interest of this research. Three-point bending represents the most pessimistic scenario that the deck must withstand. Thus, if the load capacity is sufficient for a three-point bending case, it will also be adequate for surface loads.

Several bending models are built and analysed to observe the influence of the aspects listed below:

1. Length of the span.
2. The distance between the nib edge and middle of the bolt (edge distance).
3. Conventional deck

The term "edge distance" is illustrated in the figure. 5.7 below.

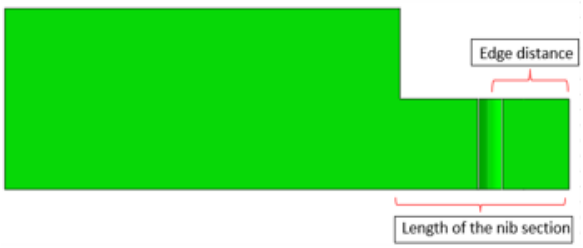

Figure 5.7: Edge distance

5.2.1. BENDING MODEL FOR 3910MM SPAN CONCRETE STRIP

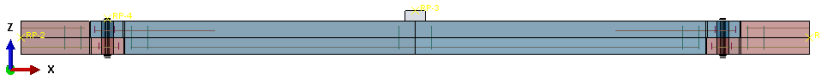

Figure 5.8: Front view of the 3910mm span

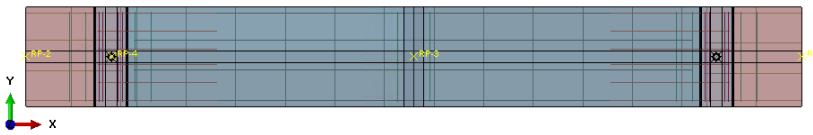

Figure 5.9: Top view of the 3910mm span

The first set of models comprises three strips of concrete decks, each with varying edge distances and dimensions of 3910mm in span, 500mm in width, and 160mm in height. Assigned edge distances are 70mm, 80mm and 90mm. This connection is located at 8% of the span of the strip.

Refer to Figure 5.10 for the load to displacement curves of these three models. The results indicate minimal variance in load capacity among them.

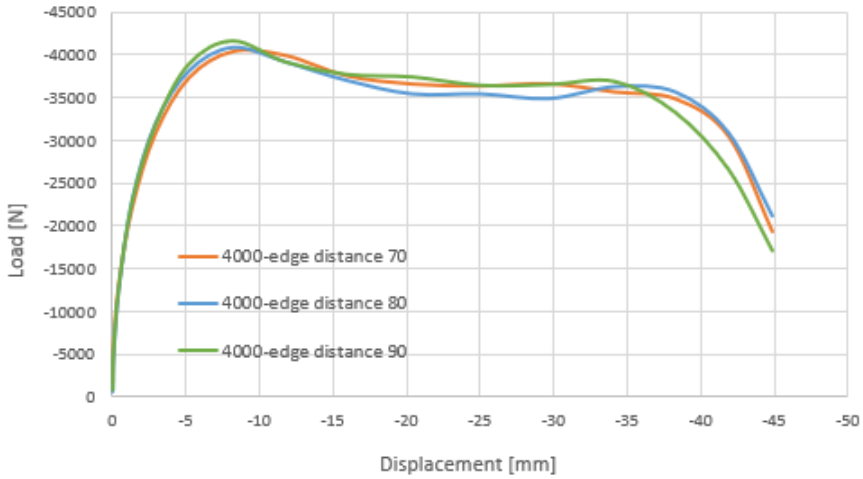

Figure 5.10: Load to displacement diagram for 3.91m span

Load capacity of 40.2kN, 40.7kN and 41.6kN can be read from the model, respectively. The first crack occurs at a displacement of 3mm, with the force increasing linearly up to this point. After cracking, the model enters the tension stiffening stage, where the reinforcing steel within the concrete begins to carry the tensile forces.

At a displacement of 8mm, local cracks appear in the nib region, as shown in the Figure 5.11. Two failure modes are observed in this part: a shear crack at the reentrant corner and concrete crushing at the mid plane due to rotation of steel bolt, as mentioned in section 5.1.
Total failure occurs at approximately 35mm displacement for the 90mm edge distance model and around 38mm for the 70mm and 80mm models. From this point on, the load starts to decrease rapidly.
This failure is characterized by rapid load reduction due to multiple cracks forming in the deck, which significantly reduce concrete stiffness, or when the steel reinforcing bar begins to yield and deform.

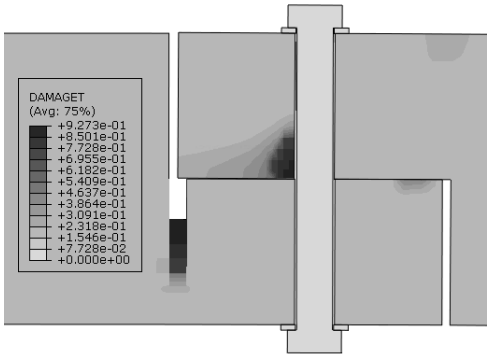

Figure 5.11: Local failure at the nib region for edge distance 70mm

This set of models also demonstrates concrete crushing under washer. Notably, a larger edge distance, increasing the length of the nib section, leads to a higher bending moment at the reentrant corner. In addition with shear force from global loading, direct shear crack and splitting of the concrete occur, as shown in Figure 5.12.

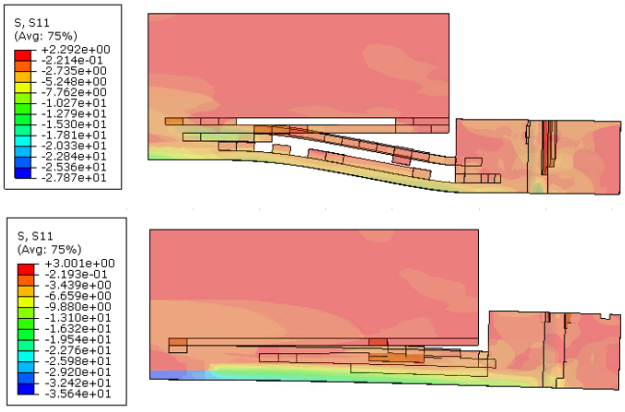

Figure 5.12: Deform shape at total failure of concrete: edge 90mm (up); edge 70mm (down)

A limitation of this model set is the height of the concrete deck (160mm), which restricts the nib section height to 80mm. This makes it challenging to embed sufficient reinforcement bars to resist tension and compression forces, especially in the nib region. Increasing span of the deck can increase the height of the concrete and load capacity, but this also increases the weight of the deck.

5.2.2. BENDING MODEL FOR 5670MM SPAN CONCRETE STRIP

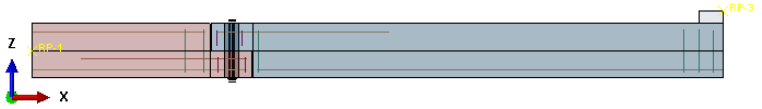

Figure 5.13: Front view of the 5670mm span

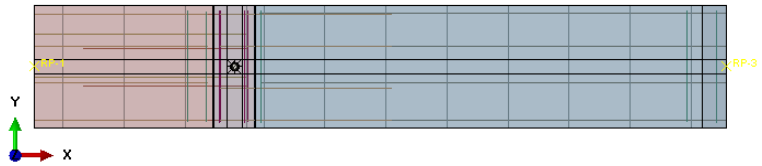

Figure 5.14: Top view of the 5670mm span

The second set of models, designed with a span of 5670mm, features an increased concrete height to 220mm while maintaining a width of 500mm. To reduce computational time, these models are built with symmetric boundary condition on the rightmost side, which does not affect the results.

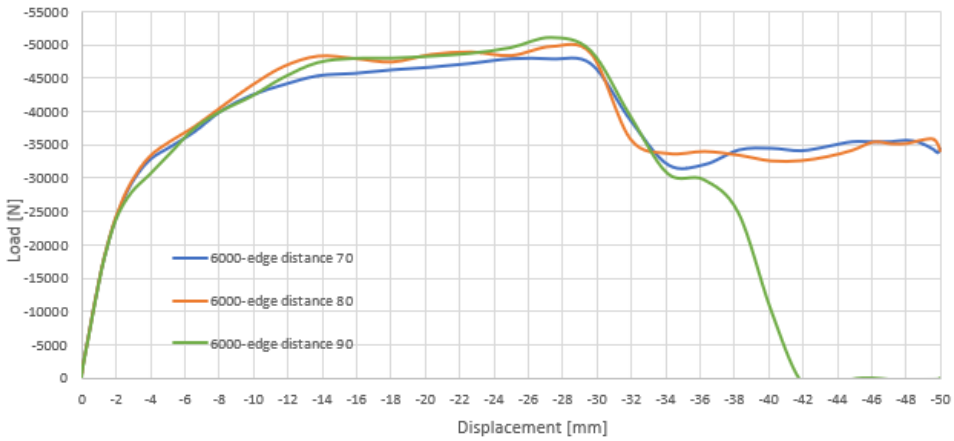

Figure 5.15: Load to displacement diagram for 5.67m span

Different edge distances are also designed for this set of models, same as previous one,

70mm, 80mm, and 90mm. This connection is located at 15% of the span.

The load to displacement curves are shown in Figure 5.15. The load capacity varies slightly with the change in edge distance, which is 48kN, 49kN, and 51kN respectively.

The curves show very similar trend for all three edge distances, except for a total failure in the concrete with the 90mm edge distance occurring at around 34mm displacement.

This load to displacement curve for concrete deck with 5.67m length also consists of four stage. The first stage is linear, with no cracking of the concrete deck. The first crack in all three models occurs at a displacement of 4mm, corresponding to a tensile crack at the middle of the span due to the maximum load being in the middle in three-point bending.

Beyond this point, the model enters the tension stiffening stage. As previously explained, this implies that the reinforcing bars begin to carry tensile force after cracking of the concrete, gradually increasing the load capacity during this stage.

At approximately 14mm displacement, local cracking appears at the reentrant corner for models with larger edge distance (80mm and 90mm). Longer nib sections result in higher bending moments at the reentrant corners, as shown in Figure 5.16 (a). Instead of cracking at the corner, for edge distance of 70mm, the crack happens at displacement of 25mm at the hogging moment location of the demountable deck, see Figure 5.16 (b).

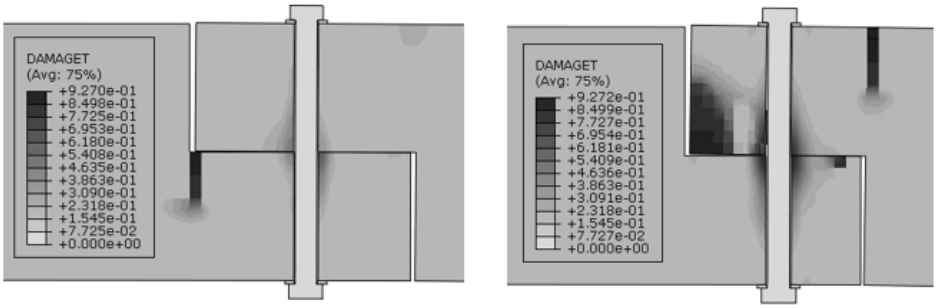

(a)Crack at reentrant corner (b) Crack at hogging moment location

Figure 5.16: Crack at the reentrant corner and hogging moment zone

Around 30mm displacement, there is a rapid drop of force due to concrete crushing under the washer, marking the tension softening stage.
After this point, edge distance of 70mm and 80mm enter another stabilized crack formation stage.

However, a complete failure is observed for the edge distance of 90mm at displacement of 34mm. The nib section of the demountable deck part breaks due to the shear force

and hogging moment from global loading in addition to extra bending moment arise from the increased length of the nib section. Figure 5.17 illustrates the failure of the 90mm edge distance concrete deck at the connection.

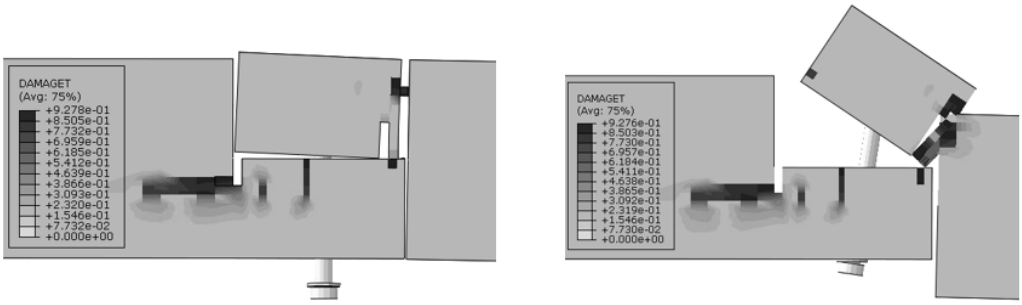

(a) At displacement of 34mm

(b) At displacement of 50mm (total failure)

Figure 5.17: Total failure of the edge distance of 90mm deck

5

Special attention needs to be paid to the reentrant corners in the half joint connection. As the corners are subjected to tension and compression, see Figure 5.18, cracking will occur at these points. While placing reinforcement at the corners may not prevent cracking, it can reduce the crack width, according to American society of concrete contractors [21]. Compression at reentrant corner leads to crushing of the concrete, while tension at reentrant corner leads to cracking of the concrete.

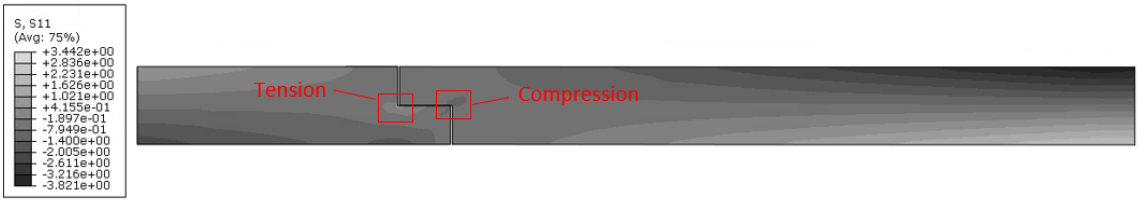

Figure 5.18: Compression and tension at reentrant corners

Compared to the previous set of models of 3910mm span, only an increase in load capacity is observed, with similar failure modes. For the 3910mm set, total failure occurred in all three models, whereas in 5670mm set, total failure only happened for edge distance of 90mm connection.

However, The ductility of the 3910mm set seems to be better, the total displacement from the peak load until the start of failing of the concrete is around 30mm. While for 5670mm set, the total displacement from peak load until first rapid drop of load is around 18mm.

But for edge distance of 70mm and 80mm, the second stabilized crack formation zone is

formed, instead of total failure shown in other cases.

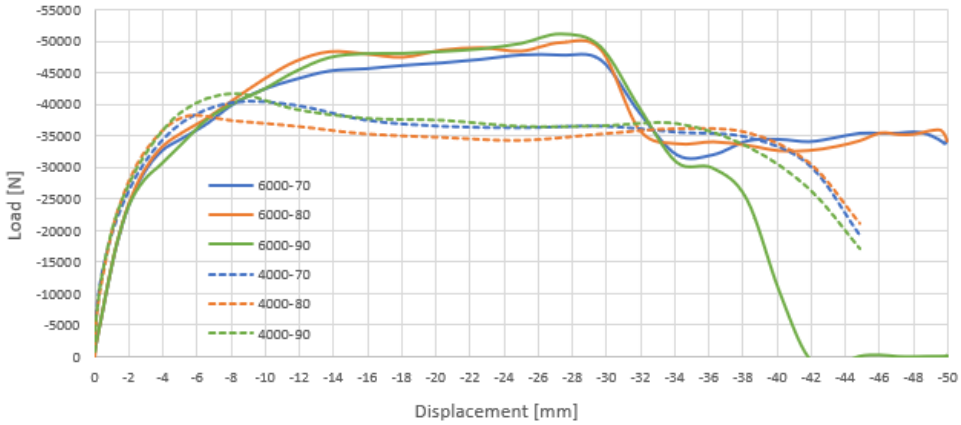

Figure 5.19: Comparison of 3.91m and 5.67m span concrete deck

For the 5670mm set, shown in Figure 5.15, in the stage of tension stiffening, which is from the first crack at displacement of 4mm to the rapid drop in load at displacement of 28mm, the load capacity is increased by 20kN, which is 40% of the total load capacity.

While for the 3910mm set, see Figure 5.10, only experiences a 10kN increase in load capacity from the first crack at displacement of 3mm to maximum at displacement of 8mm, which is 23% of of the total load capacity.

The allowable total deflection requirement stated in Eurocode for the concrete deck is L/250, where L is the span of the concrete deck. For 5.67m span concrete deck, the allowable deflection is calculated as 23mm, which is much less than the available deflection shown in the models, indicating that the deflection requirement is adequately met according to Eurocode.

5.2.3. BENDING MODEL FOR CONVENTIONAL CONCRETE STRIP WITH 5.67M SPAN

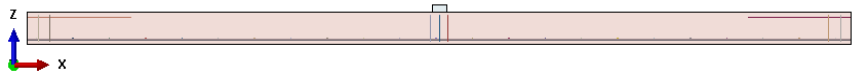

Figure 5.20: Front view of the 5670mm conventional deck

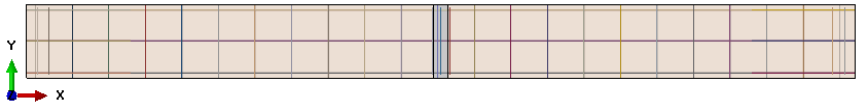

Figure 5.21: Top view of the 5670mm conventional deck

For comparison purposes, a conventional concrete deck strip model with a total span of 5.67m was built and analyzed. This conventional concrete deck does not include a demountable connection; it is a simple strip of reinforced concrete that are clamped at both ends.

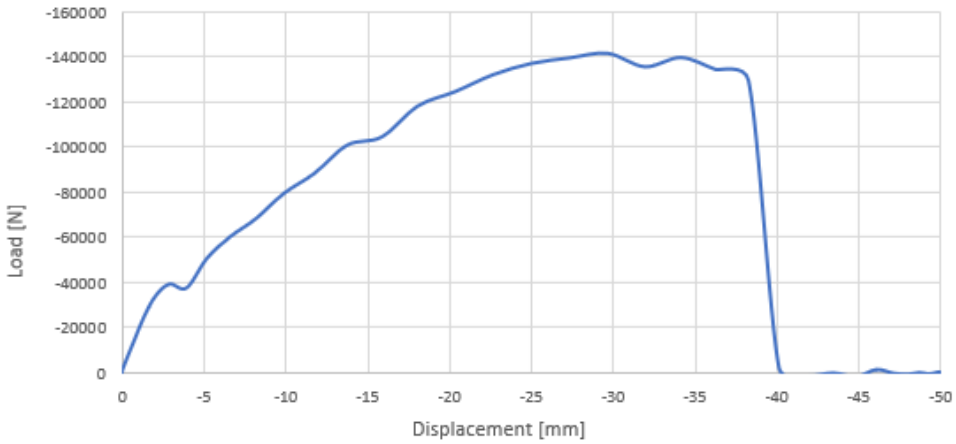

Figure 5.22: Load to displacement curve for continuous deck

Same as other models, the first crack occurs at a displacement of 4mm in the middle of the span at the sagging bending moment location. The load level achieved at this point is 40kN.

During the tension stiffening stage, the load increases by 100kN, from 40kN to the maximum of 140kN.

Second set of cracks appears at the ends of the concrete deck, which is the hogging bending moment location. Cracking at both the sagging and hogging bending moment location can be mitigated by embedding additional longitudinal reinforcement bars in the middle and two ends of the concrete deck.

Total failure of this conventional concrete deck occurs at a displacement of 38mm, in the middle of the deck, due to combined high shear force and bending moment.

Compared to the model with a connection at the zero bending moment location, this conventional deck shows an 85kN higher load capacity. However, its ductility is much lower.

The conventional concrete deck experiences total failure at a displacement of 38mm while no total failure is observed at the applied displacement of 50mm for model with connection at zero bending moment location.

6

IMPROVEMENT OF THE CONNECTION

Based on the previous chapter, five failure modes can be identified:

1. Cracking at the reentrant corners due to large edge distance and stress concentration.
2. Cracking of demountable concrete at the nib section due to hogging bending moment.
3. Crushing of concrete at the mid plane around the bolt hole due to movement of the steel bolt.
4. Cracking in transverse direction in nib section due to failure of concrete around bolt hole.
5. Crushing of concrete under the washer due to stress concentration from bending of steel bolt.

Various enhancements to the connection are considered to improve these failure modes. This chapter will focus on examining how these improvements affect the behavior of the connection.

The following improvements are considered:

1. Adding steel plates to the connection.
2. Relocating the connection.
3. Combining relocation of the connection with the implementation of steel plates.

6.1. BENDING MODEL FOR 5670MM SPAN CONCRETE STRIP WITH STEEL PLATE

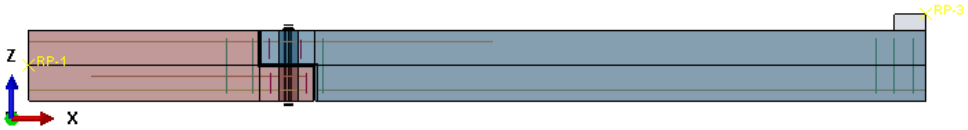

Figure 6.1: Front view of the 5670mm span with steel plate

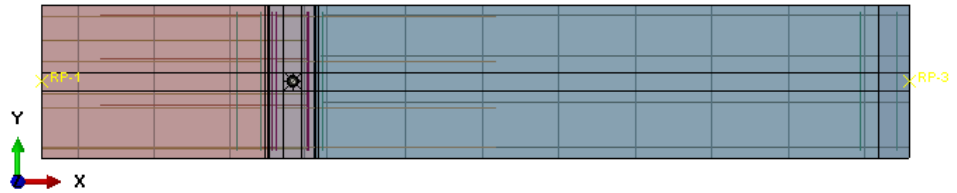

Figure 6.2: Top view of the 5670mm span with steel plate

Learning from the previous two sets of models, it's evident that two of the main failure modes at the connection are crushing of the concrete at the mid plane due to rotation of the bolt and tensile cracking at the reentrant corner. These failure modes develop due to stress concentration at the bolt hole in the mid plane where the bolt touches the concrete, and also stress concentration at the reentrant corners, as shown in Figure 6.3.

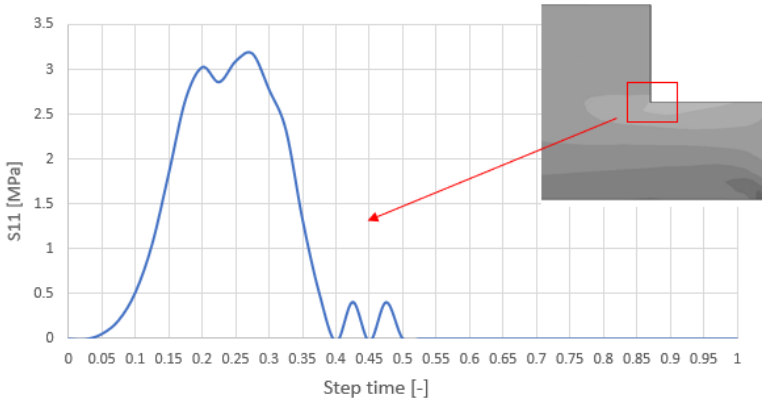

Figure 6.3: Stress concentration at the reentrant corner [6000-80 model]

The stress concentration at the concrete reentrant corners are due to the discontinuity/change of the geometry. As concrete is a brittle material with low tensile strength, it is challenging to bear tensile stresses at the corners. Figure 6.3 shows that stress at the corner continues increasing until the first global cracking occurs. After reaching maximum concrete tensile strength, the stress starts dropping until failure.

Adding a steel plate allows for stress redistribution over a larger area of the concrete deck, effectively reducing stress concentration at the critical locations. Additionally, steel plate is a much more ductile material and effective in handling tensile stress, placing steel plate at the reentrant corner acts like reinforcement, taking over tensile stress and allowing concrete to manage compressive stresses more efficiently. This enhances the structural integrity and durability of the concrete deck.

The third set of models built and analysed, is with the same span length of 5670mm and dimensions of 220mm in height and 500mm in width, includes different edge distances. The connections of these set of models are also located at 15% of the span.
The load capacity for edge distance of 70mm, 80mm and 90mm are 50.3kN, 51.1kN and 52.1kN, respectively. The load to displacement curves are shown in Figure 6.4 below. There are no significant difference in trend and load capacity among the three cases.

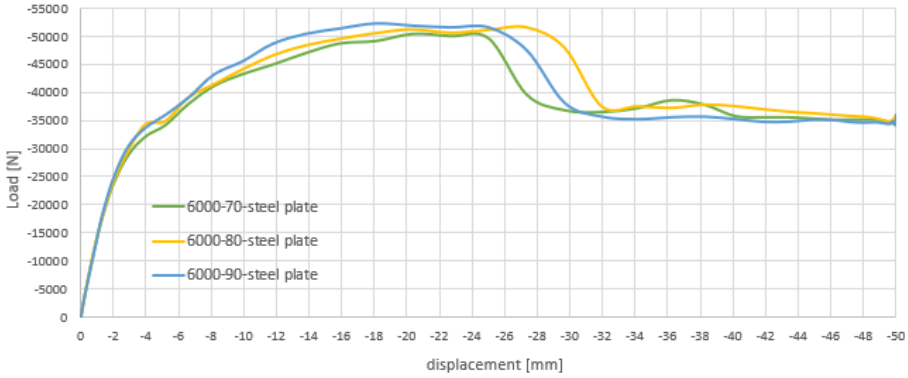

Figure 6.4: Load to displacement curves for 5.67m span with steel plate

The first crack occurs globally at the middle of the deck due to three-point bending at the displacement of 4mm/5mm and around 33kN of load for all models. Up until this point, it is called elastic stage where no cracks are formed.
After the first crack appears, the models enter the tension stiffening stage. The second set of cracks occurs at displacement of 22mm for edge distance of 80mm, and 18mm for the 90mm model, at the tensile location of the nib section of the demountable concrete deck part, refers to Figure 5.16 (b). The load stops increasing at this point.
However, no such crack is observed at this location for edge distance of 70mm deck, where the load continues to increase during the tension stiffening stage.
The load drops at the point of concrete crushing under washer for all three models, occurring at displacement of 25mm for edge distance of 70mm, 30mm for 80mm and 27mm for 90mm.
No total failure of the concrete deck is observed under the applied displacement conditions.

The following figures compare the 5.67m span models with different edge distance of the nib area, with and without the application of steel plates:

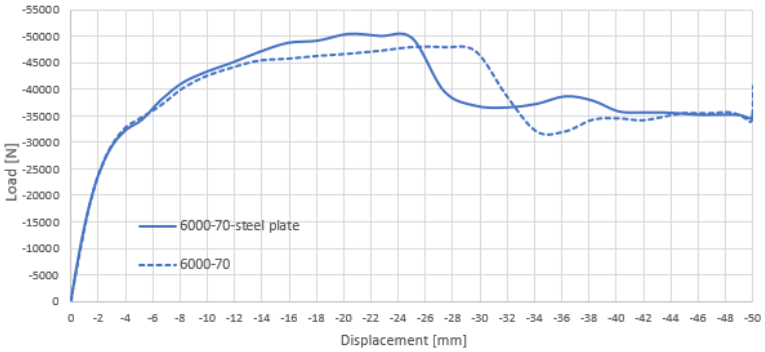

Figure 6.5: Load capacity of 5.67m span concrete deck with/without steel plate for edge distance 70mm

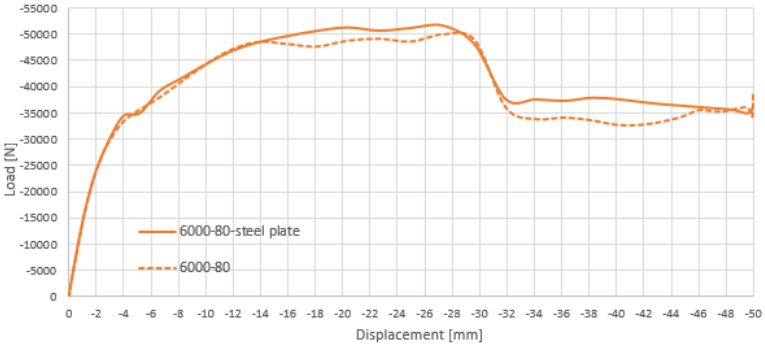

Figure 6.6: Load capacity of 5.67m span concrete deck with/without steel plate for edge distance 80mm

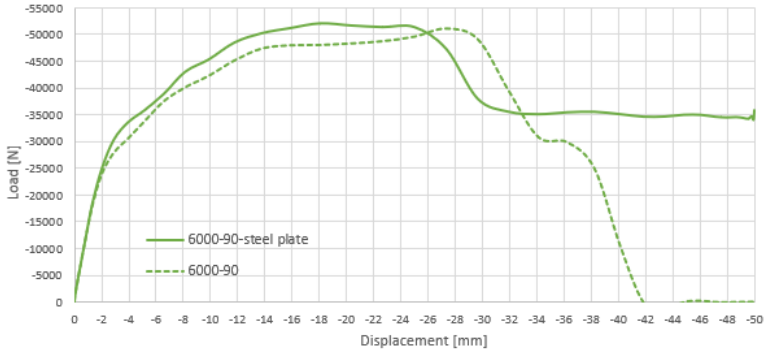

Figure 6.7: Load capacity of 5.67m span concrete deck with/without steel plate for edge distance 90mm

The load capacity for edge distances of 70mm, 80mm, and 90mm without steel plates is 48kN, 49kN, and 51kN, respectively. When a steel plate is applied, these capacities slightly increase to 50.3kN, 51.1kN, and 52.1kN, marking increases of 4.5%, 4.1%, and

2.1% respectively in total load capacity. The modest enhancement, despite the addition of local strengthening steel plates, is due to global cracking in the middle span, leading to significant damage to the concrete deck. Enhancements in load capacity could be achieved by augmenting the deck with additional longitudinal reinforcement bars at critical locations of hogging and sagging bending moments across the entire deck.

From Figure 6.5 and Figure 6.7, although the steel plates slightly increase maximum load capacity, the load drops earlier. The increase in load capacity is due to the strengthening of reentrant corners by the steel plates. The acceleration of load dropping is caused by the concrete crushing under the bolt washer. For the 90mm edge distance concrete deck, the total failure is avoided by the implementation of the steel plates, due to the local strengthening of the connection, preventing the failure shown in Figure 5.17 (b).

See Figure 6.8 and Figure 6.9 below:

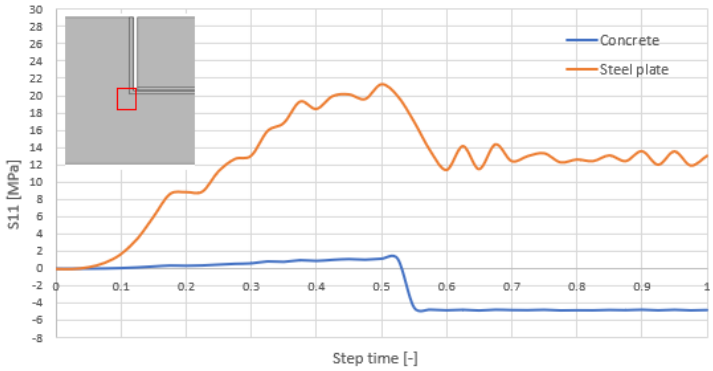

Figure 6.8: S11 of concrete and steel at the reentrant corner-tension

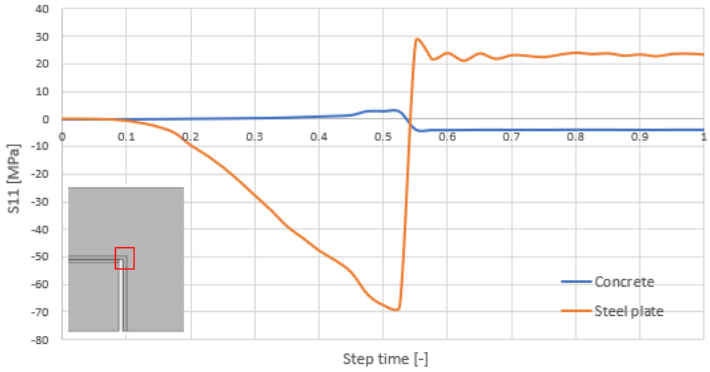

Figure 6.9: S11 of concrete and steel at the reentrant corner-compression

Adding steel plate helps with redistributing the concentrated stresses accumulated at the reentrant corners of concrete. The above figures represent the stresses at the both reentrant corner (tension at the bottom concrete corner and compression at the top concrete corner) of the concrete nib section.

Compared with Figure 6.3, at the tension reentrant corner, the implementation of the steel plates reduces the maximum tensile stress at this location to 1.1MPa, instead of to the maximum tensile strength of the concrete which causes cracking at the reentrant corners.

Instead, with the presence of steel plates, most of the tensile stresses are taken over, as shown in Figure 6.8. A drop in stress at step time 0.55 is due to the crushing of concrete under the washer. The steel plate resists 21MPa of tensile stress before the crushing of concrete.

At the compression part of reentrant corner, the steel plate completely takes over the compressive stress, reaching a maximum of 68MPa before the concrete under the washer is crushed.

This demonstrates that the implementation of steel plates can greatly reduce damage at the reentrant corners, thereby increasing the capacity of the connection.

The concrete crushes under washer happens earlier for connection with steel plates, is due to the strengthening of the nib section, resulting in an increased load carrying capacity of the connection. Without tensile cracks at the reentrant corners, more load can be transferred, leading to higher stress concentration around the concrete bolt hole under the washer.

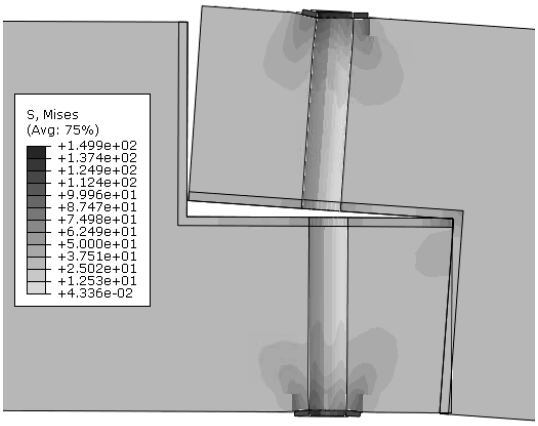

Figure 6.10: Stress concentration under washer M=5

The concrete crushing under washer, as previously mentioned, is a result of stress concentration. Excessive compressive stress are generated by tilting of the bolt nut, this stress is transferred by the washer. When the washer deforms, it pushes the concrete downwards, exceeding the concrete compression strength, leading to crushing.

Figure 6.10shows the stress concentration under the washer just before crushing, depicted in a five times scale for clarity. The stress is higher (indicated by darker color) closer to the washer and gradually reduces in an oval shape moving away from it.

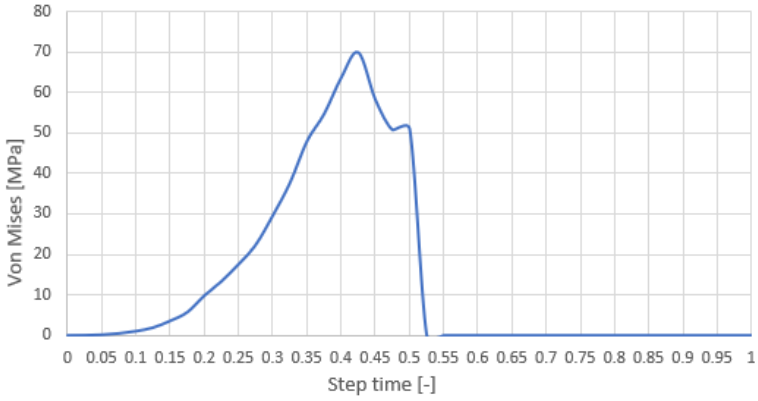

Figure 6.11: Stress under washer for 5.67m span edge distance 70mm concrete deck

Figure 6.11 shows the stress in one of the concrete mesh elements under washer. The stress gradually increases until the step time of 0.425, reaching nearly 70MPa. Due to the concrete damage plasticity model, the stiffness of this element begins to decay, eventually crushing happens very soon at step time 0.5.
It is noted that the maximum compressive strength of this concrete is only 48MPa, however, stress at this point exceeded this limit without failure. This is due to the Drucker-Prager yield criterion [30], that concrete is an non-homogeneous material and the yielding depends on its pressure level.

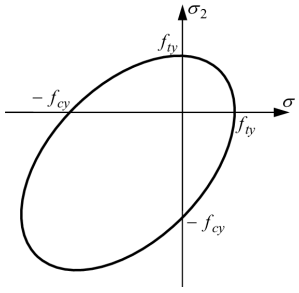

Figure 6.12: Drucker-Prager yield criterion in 2D principal stress space

Figure 6.12 represents the Drucker-Prager yield criterion in 2D, indicating that even when the maximum compressive stress in both direction is reached at the same time, the actual compressive strength can be higher than the set values.

In this particular case, with the load applied in the middle of the deck, the nib section of the demountable part concrete attempts to rotate clockwise, countered by the washer providing an anti-clockwise reaction force. In the transversal direction, the surrounding concrete also restrains the expansion of this part of the concrete, forming a triaxial stress state.
This triaxial stress state provide compressive stress from all three directions, enhancing the bearing strength of concrete at this location. Therefore the concrete at this location only starts to fail at the stress level of 70MPa in this case.

Increasing the thickness or size of the washer can reduce stress concentration by redistributing stresses. However, achieving local confinement state can significantly increase the compressive strength of concrete, which can even prevent crushing in this region. In the case shown earlier, the bearing strength of the concrete only increased by 22MPa, which is from 48MPa to around 70MPa. This increase is attributed to the gap between the bolt and concrete, known as the clearance in the bolted connection.

Local confinement substantially boosts the bearing strength of the concrete by preventing expansion in all three directions. Closing the gap between concrete and steel bolt at the stress concentration area could greatly increase the strength of the concrete. This could be achieved by injecting fiber-reinforced epoxy resin to fill the gap, but as this is beyond the scope of this research, it can be tested by future studies.

6.2. BENDING MODEL FOR 5670MM SPAN CONCRETE STRIP AT ZERO BENDING LOCATION

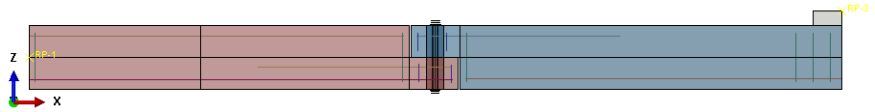

Figure 6.13: Front view of the 5670mm span at zero bending moment location

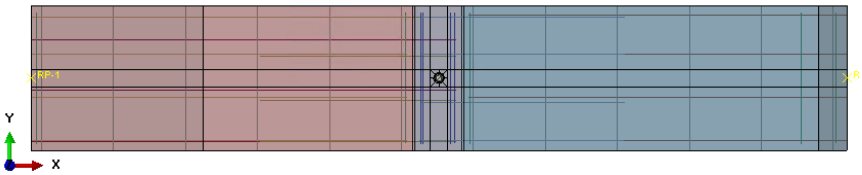

Figure 6.14: Top view of the 5670mm span at zero bending moment location

Considering the bending and shear force diagrams of a continuous beam fixed at both ends and subjected to uniformly distributed load or a concentrated load in the middle, see Figure 6.15 for uniformly distributed load and Figure 6.16 for the concentrated load in the middle of the span.

The zero bending moment occurs at both ends at around 25% of the span of the concrete deck. Also at this point, the shear force is 1/4 of the applied load for uniformly distributed load and 1/2 of the applied load for concentrated load acting in the middle of the span.

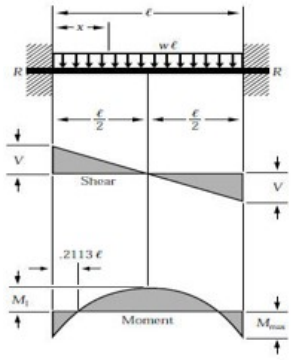

Figure 6.15: Beam fixed at both end with uniformly distributed load

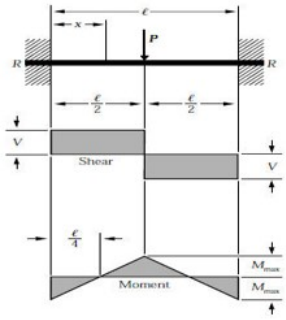

Figure 6.16: Beam fixed at both end with concentrated load

It is wise to choose the location of the connection, the weakest link in this concrete deck,

at the zero bending moment location. At this position, the connection experiences less combined bending and shear force than at other positions.

This section is focusing on 5.67m span concrete deck with the connection at the zero bending moment location, which is at the 25% of the span from both ends.
Figure 6.17 shows the load capacity of 5.67m span for edge distance 80mm concrete deck, with the connection at the zero bending moment location (orange line) and at 15% of the span from the previous set (blue line).

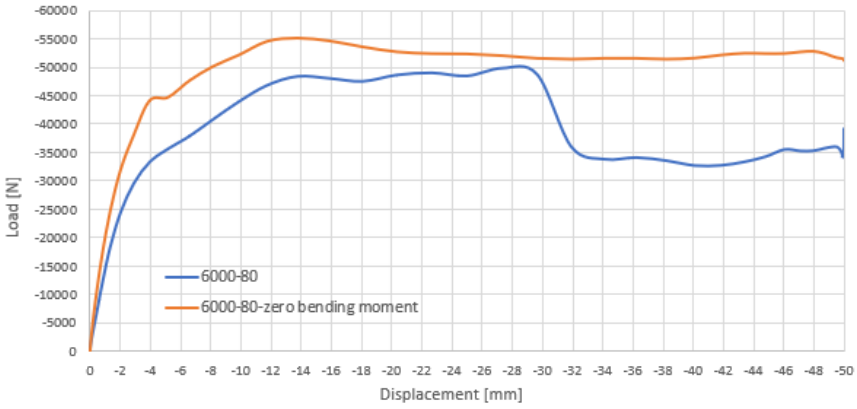

Figure 6.17: Load to displacement curves for 5.67m span edge distance 80mm

First crack in this model also occurs at a displacement of 4mm, at a load level of 45kN. Compared to the model with a connection not at the zero bending moment location, the load at the first crack is increased by 10kN. The first crack is induced by global cracking at the mid span of the concrete deck, similar to the previous models. The load increases by 18% during the tension stiffening stage.
After the elastic stage, it enters the tension stiffening stage with an increased load level. The load peaks at 55kN at a displacement of 14mm for this model, due to cracking at the global hogging bending moment location.
After this point, it enters a stabilized crack formation stage where several cracks form without reducing the capacity of the concrete deck.
Total failure of the concrete deck is not observed for connection at zero bending moment location with the applied displacement control.

The primary failure of this concrete deck occurs at the hogging and sagging bending moment locations, which could be mitigated by adding additional longitudinal tensile reinforcement.

See in Figure 6.18 for connection located further from the zero bending moment location, and Figure 6.19 for connection located at the zero bending moment location. Both model are from a 5.67m span of concrete deck with an 80mm of edge distance, the load applied are both with displacement control of 50mm, the figures show the deformed

shaped of the connection.

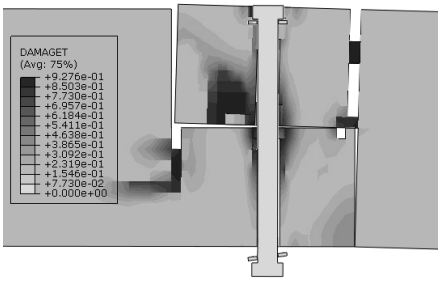

Figure 6.18: Connection located further away from zero bending moment location

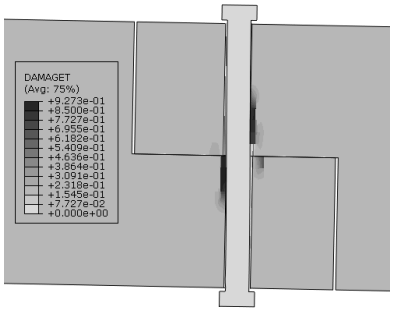

Figure 6.19: Connection located at zero bending moment location

Excessive damage can be observed from the left figure, where the shear force and bending moment combined exceeds the strength of the connection, leading to local failure and reducing the overall capacity of the concrete deck.
No such damage is observed for connection located at the zero bending moment location, as seen in figure to the right. At this location, only 1/2 of the shear force from concentrated load acts, and for uniformly distributed load only 1/4 of shear force is present, significantly reducing the stresses on the connection.

Furthermore, the absence of bending at this location keeps the mid-plane of the connection parallel, resulting in minimal tensile and compressive stresses at the reentrant corners. Due to the minimized force and moment, crushing of concrete under the washer is also not observed.

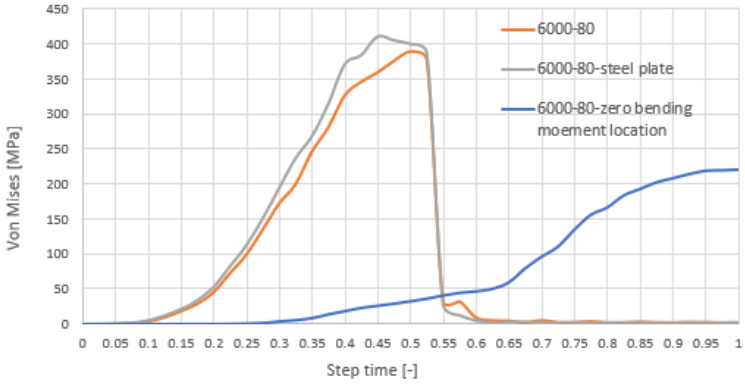

Figure 6.20: Maximum stress in bolt for three different models

Figure 6.20 shows the maximum Von Mises stress in steel bolt. Since the strength of steel bolt is much higher, failure of bolt is not observed in this connection. However, concrete failure can alter the stresses in the steel bolt. For instance, for the edge distance

80mm concrete deck with or without steel plates, the stress in the bolt drops to zero immediately after the concrete under the washer crushes. For the connection at the zero bending moment location, without crushing of the steel bolt, the stress in bolt increases linearly.

The figure also shows that the maximum stress in the bolt is around 400MPa for the former cases and only 220kN for the latter, caused by the presence of only shear force at the zero bending moment location. However, at locations further from this position, the combination of shear force and bending moment induces higher stresses in the connection, leading to the crushing of the concrete under the washer.

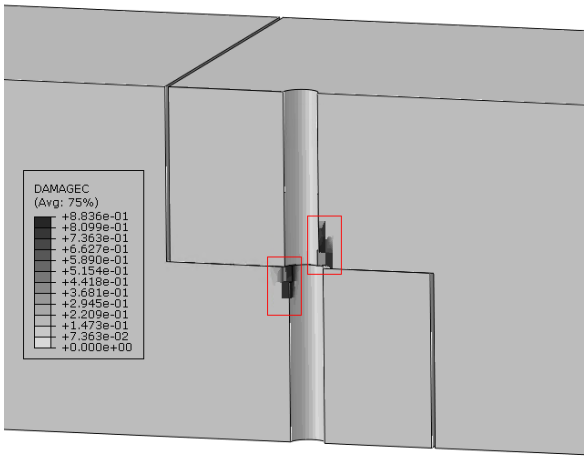

Figure 6.21: Crushing of mid plane of concrete nib section

The change in angle for the increase of stresses in bolt at step time of 0.65 is due to the contact between the concrete bolt hole and steel bolt at the mid-plane of the concrete nib section around the bolt hole, inducing concrete crushing at this location due to stress concentration from the tilting of the steel bolt, see Figure 6.21.

Highly concentrated stresses cannot be avoided here, and concrete is sensitive to concentrated stress at the change of geometry, such as the bolt hole in the middle of the nib section. This leads to crushing of concrete at these positions.
Adding steel plates will be highly effective in connections with stress concentration. As mentioned in section 6.1, a steel plate can redistribute stresses over a larger area and act as reinforcement for concrete, in this case, around the bolt hole.

6.3. BENDING MODEL FOR 5670MM SPAN CONCRETE STRIP AT ZERO BENDING LOCATION WITH STEEL PLATE

An enhanced version of the concrete deck was built and analysed, with connection located at25% of the span, which is the zero bending moment location. Additionally, steel plates were also implemented in the reentrant corner of the concrete nib section.
Another model, embedded with additional longitudinal reinforcement at the hogging and sagging bending moment locations, was also analyzed to assess the increase in load capacity of the concrete deck.

Figure 6.22 shows the load capacity of the aforementioned model, which also has a span of 5670mm and an edge distance of 80mm.

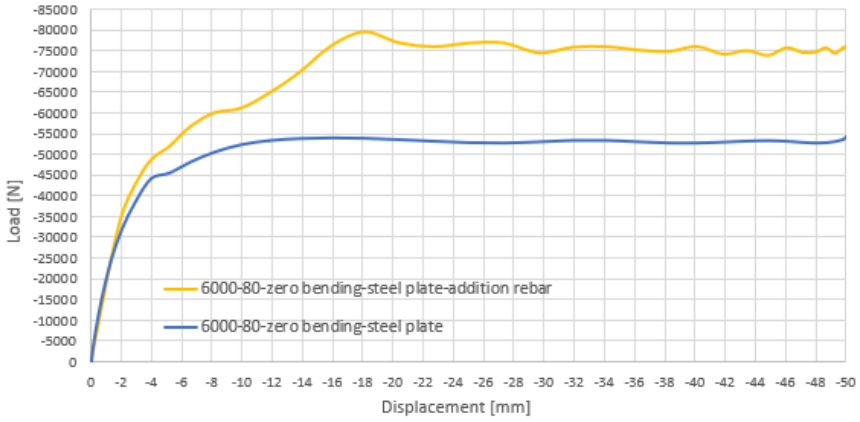

Figure 6.22: Load to displacement curve for 5.67m span edge distance 80mm connection with steel plate

Simply adding steel plates to the connection at zero bending model does not significantly alter the global behaviour, hence there is no increase of the load capacity. However, with additional longitudinal reinforcement bar, the first crack delays to a displacement of 10mm, at a load level of 60kN. During the tension stiffening stage, the load increases by 20kN, reaching a maximum load capacity of 80kN, a 25% improvement.
After reaching this maximum load level, the concrete deck enters the stabilized crack formation zone for the rest of the applied displacement.
No total failure is observed within the total 50mm displacement, either.

Taking a look at the connection, Figure 6.23 and Figure 6.24 represent the tension damage and compression damage at mid-plane of the connection around bolt hole for two sets of models: one set with connections located at 15% of the span, with and without steel plates, and another set at the zero bending moment location, with and without steel plates.
This location is particularly sensitive to damage from the movement of the steel bolt, due

to stress concentration and the inadequate compressive and tensile strength of concrete.

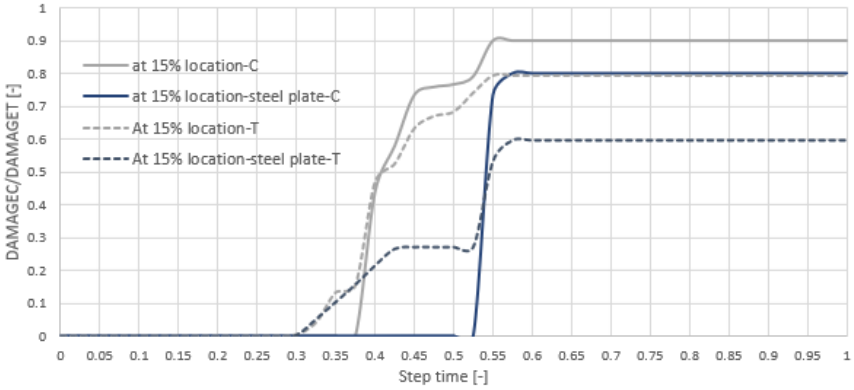

Figure 6.23: Compression and tension damage around bolt hole in mid plane with and without steel plate

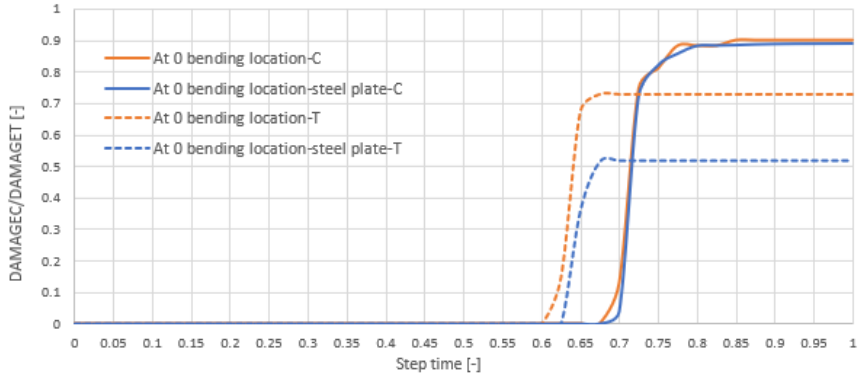

Figure 6.24: Compression and tension damage around bolt hole in mid plane with and without steel plate at zero bending moment location

For models with connection at 15% of the span, the compressive damage is delayed from step time 0.375 which is at displacement of 14mm to step time 0.525 which is at displacement of 27mm, with a total of 48% of increase.
Even though tensile damage happened at the same step time, the maximum tensile damage for connections with steel plates is reduced by 20%
The reason why the damage parameter stop increasing before reaching the maximum level, is the crushing of concrete under washer, which releases the stress that accumulated around the bolt hole.

For models with connection at 25% of the span, a reduce of tensile damage is also observed, with a reduction of 21%. There is no significant difference in compressive dam-

age for this set of models.

As no crushing of concrete under the washer is observed, the bolt can withstand stresses from global loading, as seen in Figure 6.20 from earlier. This results in shearing of the bolt at the mid-plane of the concrete nib section, introducing compression at the contact point between concrete and steel bolt. Consequently, crushing of the concrete occurs once the bearing strength is exceeded.

The Von Mises stress in steel plate at this location reaches 286MPa at step time of 0.657, where the compressive damage of concrete starts to increase. This 286MPa stress in steel plate has exceeded its yield strength, this can be one of the explanations for adding steel plate does not help with compressive damage of concrete at this location.
This could be improved by increasing the yield strength of the steel plate or increasing the thickness of the steel plate. Such parametric studies can be conducted in future research.

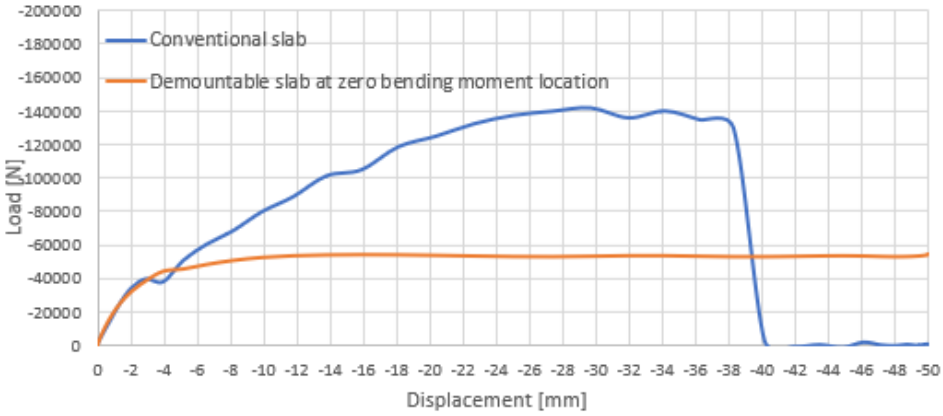

Figure 6.25: Load to displacement curve: conventional deck vs. demountable deck

Figure 6.25 compares the load to displacement curves for conventional deck and demountable deck.
The maximum load capacities are observed to be 140kN for the conventional deck and 55kN for the demountable deck, indicating that the conventional deck has a 60% higher load capacity.

However, total failure occurs at a displacement of 38mm for the conventional deck, but the ductility of the demountable deck is much better with no total failure observed at a displacement of 50mm, which is the maximum load added in the model.

6.4. DISCUSSION BASED ON RESULTS OBTAINED FROM NUMERICAL ANALYSES

Chapter 5.1 and chapter 5.2 presents the behaviour of the demountable connection under shearing and bending, respectively.
As mentioned in section 1.5.3, developing shear model is only to gain confidence in the numerical modelling rather than being a realistic loading condition. Bending model shows the most critical aspects regarding to failure mechanisms of this innovative demountable "concrete to concrete" connection.

After figuring out the failure mechanisms of the connection, Chapter 6 focusing on finding possible techniques to improve/strengthen the behaviour of such connection.

Based on the analyses presented in the previous two chapters, the following conclusions can be drawn:

(1) Observed failure modes for proposed modularised floor system:

1. Cracking at the reentrant corners is caused by a large edge distance and stress concentration.
2. Cracking of the demountable concrete at the nib section occurs due to the hogging bending moment.
3. Concrete crushing at the mid-plane around the bolt hole is due to the movement of the steel bolt.
4. Transverse cracking in the nib section arises from the failure of concrete around bolt hole.
5. Concrete crushing under the washer results from stress concentration due to the bending of the steel bolt.

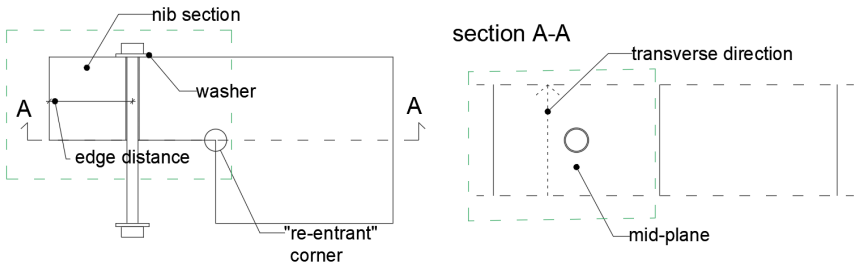

(a) Front view of the nib section

(b) Bottom view of the nib section (section A-A)

Figure 6.26: Front and bottom view of the nib section

(2) Impact of Edge Distance on Failure Mode:
Lager edge distances provide a longer lever arm for the bending of the nib section, which increase tensile stress at the reentrant corner, inducing cracking. Conversely, smaller edge distances in the nib section lead to crushing of the convex edge due to high compressive stresses coming from the bending of the demountable concrete deck.

(3) Benefits of Adding a Steel Plate:
Incorporating a steel plate can greatly mitigate the failure of crushing of concrete around bolt hole in the mid-plane of the nib section and prevent cracking at the reentrant corner due to high tensile stress.
The steel plate redistributes stresses over a larger area and, with its higher tensile strength, can bear tensile stress in place of the concrete, especially at the reentrant corners. Additionally, it provides extra bearing strength, reinforcing and anchoring the concrete.

(4) Placement of Connection at Zero Bending Moment Location:
Locating the demountable connection at the zero bending moment position greatly assists in reducing failure modes such as cracking at the reentrant corner due to tension and crushing at the convex corner due to compression.
This placement also lowers the likelihood of concrete crushing under the washer since, at this location, only half of the shear force for three-point bending (or even less for uniformly distributed load which is 1/4 of the total load) is active, thereby minimizing stress concentration and preventing crushing.

(5) Influence of Steel Plates on Connection Behavior at Zero Bending Moment Location:
In the analysed models, implementing steel plates at the zero bending moment location does not significantly affect the behaviour of the connection. It fails to efficiently reduce compressive damage around the bolt hole in the mid-plane, this can be due to insufficient strength class or thickness of the steel plates.

(6) Load Capacity and Ductility of analysed Concrete Deck:
Although the load capacity of the analysed concrete deck is much less than the conventional concrete deck, its ductility is substantially increased. This attribute can be advantageous in commercial buildings where extreme load capacity is not a primary requirement.
The improved ductility allows the concrete deck to withstand greater deflection before failure, providing more opportunities for damage inspection and repair.

Recommendation:
For optimal performance, it is recommended that the connection in such modularised floor system, which consists of concrete deck and composite beam, be positioned at the zero bending moment location, where the combined effects of bending moment and shear force are minimized.

However, due to the complexity of structures and the uncertainty of configuration of the

structures which will be used in subsequent life cycle, achieving this ideal placement of the connection can be very challenging.

In such instances, employing L-profile steel plates at the nib section of the connection is advisable. This approach significantly reduces stress concentration and consequent damage to the reentrant corner of the concrete, as mentioned before.

7

LIFE CYCLE ASSESSMENT OF PROPOSED CONCRETE DECKS

As explained in section 2.3, Life Cycle Assessment (LCA) is a widely utilized methodology for quantifying the environmental impacts of construction components and entire building structures.
A critical factor in this analysis is the amount of CO_2 embedded in structural elements.

This section aims to highlight the environmental benefits of reusing concrete decks from existing buildings. It involves a comparison with newly designed floor systems and traditional non-reusable concrete floor systems, emphasizing the ecological advantages.

Figure 7.1 presents the calculated CO_2 emissions associated with different concrete decks. For comprehensive data and calculation methodologies, please refer to Annex C, which contains detailed calculation spreadsheets.

Shadow prize (Euro) per kg equivalents		0.05	
Impact category	**Unit**	Global warming (GWP100)	
Unit		kg CO2 eq	
Concrete C45/55 (CEM I-CEMIII)	kg	1.07E-01	
Steel reinforcement for concrete	kg	1.79E+00	
Steel components	kg	1.79E+00	

For 5.67m span concrete deck:

Existed concrete slab	per half meter		
Concrete	1559.25	1.66E+02	
Steel reinforcement	29.27365	5.24E+01	
	sum	219	kg
	For 8m long:	3503	kg
		175.13	Euro

Fully new designed	per half meter		
Concrete	1559.25	1.66E+02	
Steel reinforcement	53.93497	9.66E+01	
Steel components	1.4273	2.56E+00	
	sum	266	kg
	For 8m long:	4250	kg
		212.51	Euro

Reusing existed concrete slab	per half meter		
Steel components	40.88486	7.32E+01	
	For 8m long:	1172	kg
		58.59	Euro

Figure 7.1: CO_2 embedded in different concrete decks

The amount of CO_2 embedded in construction materials per kilogram, as available in

existing literature [24], is a key input for these calculations
To determine the embedded CO_2 in concrete decks, one must first calculate the weight of the concrete and steel reinforcement, including any steel components like bolts and plates, if present. This weight is then multiplied by the CO_2 values for each material.

Assuming each concrete deck has the dimensions of 5.67m by 8m. For existing concrete decks, the embedded CO_2 amount is estimated at 3.5 tonnes.
For the newly designed concrete decks, the focus of this thesis, the embedded CO_2 is approximately 4.25 tonnes. This 0.75 tonne increase is attributed to the tailor-made reinforcement and additional steel components, such as bolts, nuts, and washers required.

Further calculations were conducted for concrete decks cut from existing systems and connected to composite beams, as discussed in section 1.2 and shown in Figure 1.3. The inclusion of extra steel plates and shear bolts in this scenario results in an additional 1.17 tonnes embedded CO_2.

Reusing concrete decks from existing buildings for subsequent life cycles can lead to substantial CO_2 emission reductions. By deducting the additional 1.17 tonnes of CO_2 from the steel components required for connecting the concrete deck with a composite beam, the net CO_2 locked within the reused concrete deck amounts to 2.33 tonnes.
In other words, reusing a concrete deck from an existing building for a second life cycle can save around 2.33 tonnes of CO_2 emissions per deck of size 5.67m by 8m.

CO_2 emission resulting from re-manufacturing process and transportation are not considered in this analysis.
For re-manufacturing of the concrete decks, the use of renewable energy is proposed, which is more environmentally friendly and does not contribute significantly to CO_2 emissions.

While CO_2 emissions from transportation, often significant. In this scenario, it is assumed that the distance between the existing building (from where the concrete deck is sourced) and the construction site (where the deck is reused) is relatively short.
This assumption leads to the conclusion that the CO_2 produced during the transportation process is not substantial.

To optimize environmental benefits, minimizing the distance between the source and reuse sites is recommended, thereby enhancing the CO_2 savings from reusing concrete decks.

Despite the higher embedded CO_2 content in the newly designed decks compared to traditional cast in situ concrete decks, their ability to be reused multiple times until failure, without generating additional CO_2, offsets this initial environmental cost. This is under the assumption that minimal or no extra CO_2 is produced during the re-manufacture and transportation processes, as previously mentioned.

Remarkably, reusing a concrete deck from an existing building for an additional life cycle can reduce CO_2 emissions by 67% compared to a new, cast in situ concrete deck.

It is important to note that the calculations and comparisons presented in this chapter are based on the assumption that a reused concrete deck has the same efficiency with a newly designed concrete deck. However, reusable concrete elements typically have larger thicknesses, implying that the embedded CO_2 emissions would be greater initially calculated. Therefore, the additional CO_2 emissions saved by reusing concrete decks from existing buildings should be calculated on a case-by-case basis.

This chapter offers a general estimation of embedded CO_2 in structural elements, assuming negligible additional CO_2 production during re-manufacture and transportation.

However, future studies should conduct a more comprehensive analysis of CO_2 emissions during these stages to fully assess the environmental impact.

8

CONCLUSION AND FUTURE STUDIES

8.1. CONCLUSION

THIS thesis provides an initial perspective on the modularisation of concrete floor systems. It does so by exploring the integration of newly designed concrete decks with composite beams through a demountable shear connector (bolt), facilitating a circular built environment.

By implementing this innovative "concrete to concrete" demountable connection for composite floor systems in commercial buildings, such as office buildings, it becomes feasible to reuse these elements after their initial life cycle. This approach has the potential to greatly reduce greenhouse gases emissions.

Due to a lack of relevant experiments in literature, this study relied solely on numerical analyses. Nonetheless, the results can serve as a foundation for future research, offering a basis for planning experiments. It should be noted that the design of reinforcement was not the central focus of this research, thus can be further optimized in future studies.

A summary table, presented in Figure 8.1, compares different configurations of the connection for load capacity and failure modes, considering models with an edge distance of 80mm:

Models	Load capacity	±%		Cracking at reentrant corner	Crushing under washer	Crushing at mid plane	Cracking in transversal	Total failure
L08	40.7	-20%		√	√	√	√	√
L15	49	0%		√	√	√	√	
L15S	51.1	4%			√	√		
L25	55	11%				√		
L25S	55	11%				√		
REF	140	65%		-	-	-	-	√

L08 - connection located at 8% of the span
L15 - connection located at 15% of the span
L15S - connection located at 15% of the span with implementation of steel plates
L25 - connection located at 25% of the span
L25S - connection located at 25% of the span with implementation of steel plates
REF - conventional concrete deck with no demountable connection

Figure 8.1: Summary table for edge distance 80mm concrete strips

This table contains six different models analysed previously:
L08 analysed in section 5.2.1, L15 analysed in section 5.2.2 and L25 analysed in section 6.2; with implementation of steel plates for models L15S analysed in section 6.1 and L25S analysed in section 6.3; lastly, REF analysed in section 5.2.3.

Taking L15 (highlighted in blue) as a baseline, adding steel plates increases the load capacity of the concrete deck by 4%; Shifting this connection to the zero bending moment location, with or without steel plates (L25S and L25), increases load capacity by 11%;

However, the capacity of the demountable concrete deck (L15) is only a third of that of the conventional concrete deck with no demountable connection (REF), with 55kN and 144kN, respectively, see Figure 6.25. This is due to the non-continuous nature of the connections in demountable concrete decks, leading to increased deformation and, consequently, a reduction in stiffness.

Placing the connection at the zero bending moment location is optimal in terms of load capacity and failure modes. However, due to the complexity of the second life cycle structure, exact placement at this location is challenging. It is recommended to implement steel plates at the reentrant corners of the "concrete to concrete" connection to mitigate potential failure due to sensitivity of the nib section.

Based on the assumptions outlined, reusing concrete decks can lead to significant savings of CO_2 emissions, as detailed in chapter 7.
For a 5.67m*8m concrete deck, the newly design deck proposed in this thesis, can save approximately 4.2 tonnes of CO_2 emissions per life cycle; For an existing concrete deck that is cut and reused, saving of around 2.33 tonnes of CO_2 emissions per life cycle are achievable with the same area, see in Figure 7.1.
It is also noted in this chapter that reusable concrete elements typically have larger thicknesses, which increases the embedded CO_2. This implies that reusing concrete decks from existing buildings, can result in additional CO_2 emissions savings. However, this additional amount should be calculated on a case-by-case basis.
Such considerable reductions demonstrates the potential of circular built environments through modular floor systems.

8.2. FUTURE STUDIES

8.2.1. OPTIMIZATION

Given that the suggested design of modularised floor system is relatively novel, and it has not yet been used in practice, further research and improvements are necessary for re-manufacturing and optimization.

The addition of an L profile steel plate at the half-joint of the concrete deck effectively reduces or prevents cracking at the reentrant corners and mitigates compressive and tensile damage around the bolt hole in the mid-plane.
The required strength and thickness of the L profile can be further investigated to determine their impacts on damage mitigation.

To enhance cost efficiency, the L profile could be applied only at critical locations around the steel bolt, instead of along the entire transverse direction. However, the influence due to the discontinuity of L profile shall be examined.

Reducing stress concentration under the washer, and thus mitigating concrete crushing, could be achieved by using larger or thicker washers, or even a rectangular steel plate in

place of the washer. However, the benefits of this approach should be weighed against the additional costs.

8.2.2. ALTERNATIVE DEMOUNTABLE CONNECTIONS

As outlined in the beginning of the thesis, in section 1.2, concrete decks cut from existing buildings can be reused by connecting them with composite beams. As shown in Figure 1.3, demountable "concrete to concrete" connection can be achieved by adding steel plates at both the top and bottom surfaces of the end of the concrete deck.

This solution enables the reuse of concrete decks from existing buildings without increasing CO_2 emissions. However, the need for additional steel plates and bolts may need some attention to improve practical appeal.

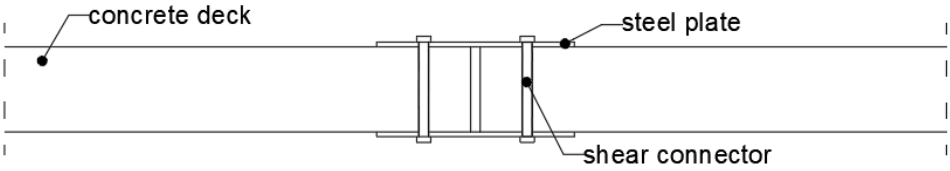

Figure 8.2: Alternative demountable connection 2(a)

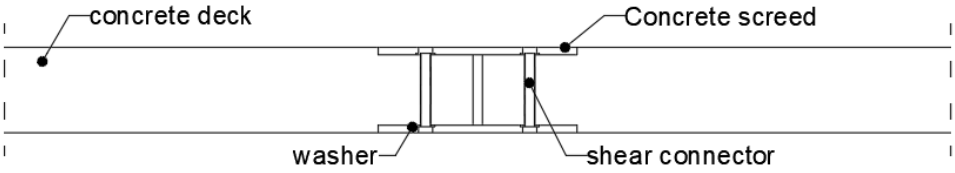

Figure 8.3: Alternative demountable connection 2(b)

Figure 8.3 presents an alternative version of this demountable "concrete to concrete" connection. In this design, the bolt nut is embedded into the concrete deck. Reinforcement is not shown in the figures.
The necessity of implementing steel plates at this configuration should be verified through further numerical analysis or laboratory testing.

There can be multiple alternatives for the concrete deck with demountable connection, each requiring thorough analysis and testing to understand their mechanical behaviours.

Additionally, the practicality of implementing such demountable concrete decks must be assessed, taking into account the cost of achieving these connections and their durability across multiple life cycles.

8.2.3. MODIFYING EXISTING CONCRETE DECKS

This research focuses on constructing demountable concrete decks in a design phase. Adapting existing conventional concrete decks from concrete floor system together with composite beam, into a similar dapped-end joint concrete connection requires additional considerations.

The cutting method of the conventional concrete deck presents challenges. Cutting the deck in one go is difficult and requires safety precondition at a construction site. In addition, it requires specialized machinery to create a zigzag cutting pattern, significantly increasing reuse costs.

As shown in Figure 8.4, the existing conventional deck can be cut in half at the connection location using a concrete cutting saw/blade, however, temporary propping is required. To achieve an L-shaped joint, a small rectangular concrete strip in the transverse direction can then be cut and removed. Subsequently, a bolt hole is drilled at the L joints, allowing a steel bolt to connect the two concrete pieces (reinforcement is not shown in the figure).
This configuration should be compared to that proposed in section 8.2.2, considering the complexity of cutting/drilling methodologies, mechanical behaviour, durability of the connection, and economic viability.

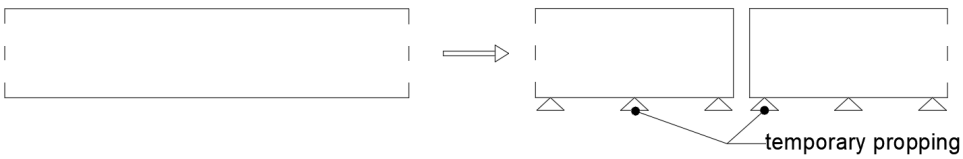

Figure 8.4: Sawing of a conventional concrete deck requires temporary propping

However, conventional concrete decks typically require only top and bottom reinforcements to address hogging and sagging moments. Modifying these decks into the proposed design requires due attention.

In conclusion, disconnecting a concrete deck from existing buildings and integrating it with a composite beam using proposed configuration should be feasible.
However, for future studies, comprehensive numerical analyses and laboratory testing are essential to validate the safety and effectiveness before implementing such modularised floor systems in practice.

BIBLIOGRAPHY

[1] ACI COMMITTEE 318. *ACI 318-05, "Building Code Requirement for Structural Concrete and Commentary"*. 2004.

[2] P.L. Ng A.K.H. Kwan J.Y.K. Lam. "Tension Stiffening in Reinforced Concrete Beams: A New Tensile Stress Block". In: *Advances in Structural Engineering and Mechanics(ASEM'08)* (2008).

[3] Mattock AH. "Design Proposals for Reinforced Concrete Corbels". In: *Prestressed Concr Inst* 21(3) (1976), pp. 18–42. DOI: 10.15554/pcij.05011976.18.42.

[4] Rebecca Asso. "Half-joint assessment of concrete bridges: strut and tie model development and FEM validation". In: *Master thesis, POLITECNICO DI TORINO* (2019/2020).

[5] Rebecca Asso et al. "Behavior of Half-Joints: Design and Simulation of Laboratory Tests". In: *Infrastructures* 7.12 (2022). ISSN: 2412-3811. URL: https://www.mdpi.com/2412-3811/7/12/160.

[6] World Steel Association. "WORLD STEEL IN FIGURES 2018". In: (2018). URL: https://worldsteel.org/wp-content/uploads/2018-World-Steel-in-Figures.pdf.

[7] Abdolreza Ataei. "Modelling of demountable steel-concrete composite connections: Validation of finite element model and parametric study". In: *Journal of Constructional Steel Research* 198 (2022), p. 107585. ISSN: 0143-974X. DOI: https://doi.org/10.1016/j.jcsr.2022.107585. URL: https://www.sciencedirect.com/science/article/pii/S0143974X22004552.

[8] Abdolreza Ataei, Mehran Zeynalian, and Yahya Yazdi. "Cyclic behaviour of bolted shear connectors in steel-concrete composite beams". In: *Engineering Structures* 198 (2019), p. 109455. ISSN: 0141-0296. DOI: https://doi.org/10.1016/j.engstruct.2019.109455. URL: https://www.sciencedirect.com/science/article/pii/S0141029618337209.

[9] Ahmed Atta and Mohamed Taman. "Innovative method for strengthening dapped-end beams using an external prestressing technique". In: *Materials and Structures* 49 (Sept. 2015). DOI: 10.1617/s11527-015-0701-8.

[10] *AxisVM - structural analysis and design software*. 2024. URL: https://axisvm.eu/.

[11] A.F. Barbosa and G.O. Ribeiro. "Analysis of reinforced concrete structures using ANSYS nonlinear concrete model". In: (1998).

[12] Prota A Bossio A Lignola GP. "An overview of assessment and retrofit of corroded reinforced concrete structures". In: *Procedia Structural Integrity* 11.Elsevier B.V (2018), pp. 394–401. DOI: 10.1016/j.prostr.2018.11.051.

[13] Giovanni Brambilla et al. "Environmental benefits arising from demountable steel-concrete composite floor systems in buildings". English. In: *Resources, Conservation and Recycling* 141 (Feb. 2019), pp. 133–142. ISSN: 0921-3449. DOI: 10.1016/j.resconrec.2018.10.014.

[14] Domingo J. Carreira and Kuang-Han Chu. "Stress-Strain Relationship for Reinforced Concrete in Tension". In: *ACI JOURNAL TECHNICAL PAPER* (1985).

[15] J. D. Carreira and K.-H. Chu. "Stress-strain relationship for plain concrete in compression." In: *ACI Journal Proceedings* 82(6 (1985). DOI: 10.14359/10390.

[16] CEB-FIP. “Model code for concrete structures”. In: *International du Beton (CEB) and International Federation for Prestressing (FIP), Lausanne, Switzerland* (1990), pp. 241–263.

[17] Han-Mei Chen et al. “Reclaiming structural steels from the end of service life composite structures for reuse – An assessment of the viability of different methods”. In: *Developments in the Built Environment* 10 (2022), p. 100077. ISSN: 2666-1659. DOI: https://doi.org/10.1016/j.dibe.2022.100077. URL: https://www.sciencedirect.com/science/article/pii/S2666165922000114.

[18] Jun Chen et al. “Behavior of an advanced bolted shear connector in prefabricated steel-concrete composite beams”. In: *Materials* 12.18 (2019), p. 2958.

[19] Breen JE Chen BS Hagenberger MJ. “Evaluation of strut-and-tie modeling applied to dapped beam with opening.” In: *ACI Struct J* 99 (2002), pp. 445–4.

[20] Mitchell D Collins MP. “A Rational Approach to shear design - The 1984 Canadian code provisions”. In: *The American Concrete Institute.* 83 (1986).

[21] American society of concrete contractors. *Finishing Problems and Possible Solutions Chapter 10.* URL: https://slideplayer.com/slide/4149382/.

[22] Lawrence N Dallam. “High strength bolt shear connectors-pushout tests”. In: *Journal Proceedings.* Vol. 65. 9. 1968, pp. 767–769.

[23] F. Damjanic and D.R.J. Owen. “Practical considerations for modelling of post-cracking concrete behaviour for finite-element analysis of reinforced concrete structures”. In: *International Conference on Computer Aided Analysis and Design of Concrete Structures* (1984), pp. 693–706.

[24] TU Delft. “CIE4100 Materials and Ecological Engineering: Concrete LCA dataset”. In: (2021).

[25] *Demountable concrete connection search in ScienceDirect.* 1999-2024. URL: https://www.sciencedirect.com/search?qs=demountable%20concrete%20connection.

[26] *Demountable shear connectors search in ScienceDirect.* 1999-2024. URL: https://www.sciencedirect.com/search?qs=demountable%20shear%20connectors.

[27] Morley CT Desnerck P Lees JM. “Impact of the reinforcement layout on the load capacity of reinforced concrete half-joints”. In: *Engineering Structures* 127 (2016), pp. 227–239. DOI: 10.1016/j.engstruct.2016.08.061.

[28] Martinelli P Di Prisco M Colombo M and Coronelli D. “The technical causes of the collapse of Annone overpass”. In: *SS* 36 (2018), pp. 1–16.

[29] Taher SE-DMF. “Strengthening of critically designed girders with dapped ends”. In: *Proceedings of the Institution of Civil Engineers - Structures and Buildings* 158(2) (2005), pp. 141–152. DOI: 10.1680/stbu.2005.158.2.141.

[30] D. C. Drucker and W. Prager. “Soil mechanics and plastic analysis for limit design.” In: *Quarterly of Applied Mathematics* 10 (1952), pp. 157–165.

[31] A. Elkady. “ABAQUS SteelMat Generator: A tool for generating metal plastic and damage parameters for ABAQUS”. Version v23.04. In: (2023). DOI: 10.5281/zenodo.7756886.

[32] 2019-2023 EngineeringLibrary.org. *MIL-HDBK-60: Threaded Fasteners - Tightening to Proper Tension.* 1990. URL: https://engineeringlibrary.org/reference/threaded-fastener-preload-mil-hdbk.

[33] *Environmental management - Life cycle assessment - Principles and framework.* 2006. URL: https://connect.nen.nl/standard/openpdf/?artfile=481642&RNR=109085&token=8487b49a-0fe7-4564-ab36-0dda350caef1&type=pdf#pagemode=bookmarks.

[34] "Eurocode 3 - Design of steel structures - Part 1-1: General rules and rules for buildings". In: (1993).

[35] James M Fisher. "Specification for structural steel buildings". In: AISC. 2005.

[36] Blake Andrews Gary Klein Amir Botros and Kurt Holloway. "Dapped ends of prestressed concrete thin-stemmed members: Part 2, design". In: *PCI Journal* (2017).

[37] GB. "Code for design of concrete structures." In: *GB 50010-2010, National Standard of the People's Republic of China, Beijing, China.* (2010).

[38] Neil M. Hawkins. "Strength in shear and tension of cast-in-place anehor bolts". In: vol. SP-103. 1987, pp. 233–255. URL: https://www.scopus.com/inward/record.uri?eid=2-s2.0-0012516105&partnerID=40&md5=a051817925cb042ac0c6c2db4f864f33.

[39] "Heinrich Gottfried Gerber - Wikipedia". In: (Accessed June 10, 2020). URL: https://it.wikipedia.org/wiki/Heinrich_Gottfried_Gerber.

[40] IEA. "Energy and Climate Change, Special Report". In: (2015). URL: https://iea.blob.core.windows.net/assets/8d783513-fd22-463a-b57d-a0d8d608d86f/WEO2015SpecialReport.pdf.

[41] IEA. "Net Zero by 2050". In: *IEA (2021)* (2021).

[42] Jason Martinez. Ann E. Jeffer. "Elevated-Temperature Tension Stiffening Model for Reinforced Concrete Structures under Fire". In: *Conference: SiF* (2018).

[43] Roger Paul Johnson and D Anderson. *Designers' guide to EN 1994-1-1: eurocode 4: design of composite steel and concrete structures. General rules and rules for buildings*. Thomas Telford, 2004.

[44] Hiroshi Yokota Ken Watanabe Junichiro Niwa and Mitsuyasu Iwanami. "Experimental Study on Stress-Strain Curve of Concrete Considering Localized Failure in Compression". In: ().

[45] Kamiński M. Kmiecik P. "Modelling of reinforced concrete structures and composite structures with concrete strength degradation taken into consideration." In: *J Arch Civil Mech Eng.* 11(3) (2011), pp. 623–636.

[46] So KMP. "Prestressed concrete members with dappedends." In: (1989).

[47] Mojtaba Labibzadeh, Alireza Firouzi, and Hamid Ghafouri. "Structural performance evaluation of an aged structure using a modified plasticity model in inverse solution method". In: *Inverse Problems in Science and Engineering* 26 (Nov. 2017), pp. 1–30. DOI: 10.1080/17415977.2017.1400028.

[48] J. Y. K. Lam, P. L. Ng, and A. K. H. Kwan. "Tension stiffening in concrete beams. Part 2: member analysis". In: *Proceedings of the Institution of Civil Engineers - Structures and Buildings* 163.1 (2010), pp. 29–39. DOI: 10.1680/stbu.2009.163.1.29. eprint: https://doi.org/10.1680/stbu.2009.163.1.29. URL: https://doi.org/10.1680/stbu.2009.163.1.29.

[49] *Lecture 5-6 LCA ISO1040 procedure and exercise.* 2021.

[50] Fritz Leonhardt. "Cracks and Crack Control in Concrete Structures". In: *PCI Journal 33: 124-145* (1988).

[51] Wu Xiaobao Lin Feng. "Mechanical Performance and Stress–Strain Relationships for Grouted Splices Under Tensile and Cyclic Loadings". In: *International Journal of Concrete Structures and Materials* 10 (2016). DOI: 10.1007/s40069-016-0156-5. URL: https://doi.org/10.1007/s40069-016-0156-5.

[52] Somayeh Lotfi et al. “Mechanical recycling of EOL concrete into high-grade aggregates”. In: *Resources, Conservation and Recycling* 87 (2014), pp. 117–125. ISSN: 0921-3449. DOI: https://doi.org/10.1016/j.resconrec.2014.03.010. URL: https://www.sciencedirect.com/science/article/pii/S0921344914000688.

[53] L. Mak and A. Elkady. “Experimental database for steel flush end-plate connections.” English. In: *Journal of Structural Engineering* 147(7) (2021). DOI: 10.1061/(ASCE)ST.1943-541X.0003064.

[54] Yann Malecot et al. “Strength and damage of concrete under high triaxial loading”. In: 14.6-7 (2010), pp. 777–803. DOI: 10.1080/19648189.2010.9693262. URL: https://www.scopus.com/inward/record.uri?eid=2-s2.0-81255124168&doi=10.1080%2f19648189.2010.9693262&partnerID=40&md5=65821cf39c8730ee537ec558cac9d692.

[55] Croteau P Mitchell D Marchand J and Cook WD. “Concorde overpass collapse: Structural aspects”. In: *Performance of Constructed Facilities* 25(6) (2011), pp. 545–553. DOI: 10.1061/(ASCE)CF.1943-5509.0000183.

[56] Meli R Moreno-Martínez JY. “Experimental study on the structural behavior of concrete dapped-end beams”. In: *Engineering Structures* 75 (2014), pp. 152–163. DOI: 10.1016/j.engstruct.2014.05.051.

[57] Daescu AC et al. Nagy-Gyorgy T Sas G. “Experimental and numerical assessment of theeffectiveness of FRP-based strengthening configurations fordapped-end RC beams.” In: *Eng Struct* 44 (2012), pp. 291–3.

[58] United Nations. “Paris Agreement.” In: *United Nations Treaty Collection* (2021).

[59] Transitieagenda Circulaire Bouweconomie -– Samen bouwen aan de circulaire economie voor Nederland in 2050. (Transition Agenda for the Circular Construction Economy -– Jointly building on the circular economy for the Netherlands in 2050.). “Circular Construction Economy transition team (2018)”. In: (2018). URL: https://www.rijksoverheid.nl/documenten/rapporten/2018/01/15/bijlage-4-transitieagenda-bouw.

[60] P. L. Ng, J. Y. K. Lam, and A. K. H. Kwan. “Tension stiffening in concrete beams. Part 1: FE analysis”. In: *Proceedings of the Institution of Civil Engineers - Structures and Buildings* 163.1 (2010), pp. 19–28. DOI: 10.1680/stbu.2009.163.1.19. eprint: https://doi.org/10.1680/stbu.2009.163.1.19. URL: https://doi.org/10.1680/stbu.2009.163.1.19.

[61] European Parliament. “Circular economy: definition, importance and benefits”. In: (2023). URL: https://www.europarl.europa.eu/news/en/headlines/economy/20151201STO05603/circular-economy-definition-importance-and-benefits.

[62] Marko Pavlović et al. “Bolted shear connectors vs. headed studs behaviour in push-out tests”. In: *Journal of Constructional Steel Research* 88 (2013), pp. 134–149. ISSN: 0143-974X. DOI: https://doi.org/10.1016/j.jcsr.2013.05.003. URL: https://www.sciencedirect.com/science/article/pii/S0143974X13001314.

[63] *PCI DESIGN HANDBOOK, PRECAST AND PRESTRESSED CONCRETE, 7TH EDITION*. 2010. ISBN: 978-0-937040-87-4. URL: https://www.kerkstra.com/wpcontent/uploads/2020/03/Design_Handbook_7th_Edition.pdf.

[64] Peikko. *Peikko Company*. URL: https://www.peikko.com/.

[65] A Purvis. “Steel and CO2 - a global perspective”. In: (20 November 2017). URL: https://iea.blob.core.windows.net/assets/imports/events/245/ISTRM_Session1_A._PURVIS_241117.pdf..

[66] H. W. Reinhardt and H. A. W. Cornelissen. “Post-peak cyclic behaviour of concrete in uniaxial tensile and alternating tensile and compressive loading.” In: *Cement and Concrete Research* 14(2 (1984), pp. 263–270. DOI: 10.1016/0008-8846(84)90113-3.

[67] Popescu C Sas G Daescu C and Nagy-György T. “Numerical optimization of strengthening disturbed regions of dapped-end beams using NSM and EBR CFRP.” In: *Composites Part B: Engineering* 67 (2014), pp. 381–390. DOI: 10.1016/j.compositesb.2014.07.013.

[68] Liem SK. “Maximum shear strength of dapped-end or corbel”. In: (1983).

[69] Michael Smith. *ABAQUS/Standard User's Manual, Version 2023*. English. United States: Dassault Systèmes Simulia Corp, 2023.

[70] EUROPEAN COMMITTEE FOR STANDARDIZATION. *EN-1991-1-1 Eurocode 1, Actions on Structures—Part 1-1: General Actions —Densities, Self-Weight, Imposed Loads for Buildings*. 2002.

[71] EUROPEAN COMMITTEE FOR STANDARDIZATION. *Eurocode 2: Design of concrete structures - Part 1-1: General rules and rules for buildings*. 2005.

[72] *Structural use of concrete — Part 1: Code of practice for design and construction*. 1997. URL: https://crcrecruits.files.wordpress.com/2014/04/bs8110-1-1997-structural-use-of-concrete-design-construction.pdf.

[73] “Structural Use of Concrete, Part 2: Code of Practice for Special Circumstances”. In: *BSI* (1985).

[74] Wei Wang et al. “Repetitive behavior of an advanced demountable bolted shear connection in push-off tests”. In: *Construction and Building Materials* 362 (2023), p. 129656. ISSN: 0950-0618. DOI: https://doi.org/10.1016/j.conbuildmat.2022.129656. URL: https://www.sciencedirect.com/science/article/pii/S0950061822033128.

[75] Dilger WH Werner MP. “Shear Design of prestressed concrete stepped beams”. In: *Prestressed Concreat Inst.* 18(4) (1973), pp. 37–49. DOI: 10.15554/pcij.07011973.37.49.

[76] Kelvin O. Yoro and Michael O. Daramola. “Chapter 1 - CO2 emission sources, greenhouse gases, and the global warming effect”. In: (2020). Ed. by Mohammad Reza Rahimpour, Mohammad Farsi, and Mohammad Amin Makarem, pp. 3–28. DOI: https://doi.org/10.1016/B978-0-12-819657-1.00001-3. URL: https://www.sciencedirect.com/science/article/pii/B9780128196571000013.

[77] Jaakko Yrjölä. *Peikko white paper: Bolted connection for precast concrete structure*. URL: https://media.peikko.com/file/dl/i/YuEX4A/qI7IjmhJ1LlASRrEq_2DFQ/PeikkoWhitePaper_Boltedconnectionsforprecaststructuresenablingcircularity-%20withoutcompromisingperformance.pdf?fv=5474.

[78] Byung Hwan Oh Zdenek P Bazant. “Crack band theory for fracture of concrete.” In: *Mat. Constr. 16* (1983).

[79] Yujie Zhang et al. “Experimental study on shear behavior of high strength bolt connection in prefabricated steel-concrete composite beam”. In: *Composites Part B: Engineering* 159 (2019), pp. 481–489. ISSN: 1359-8368. DOI: https://doi.org/10.1016/j.compositesb.2018.10.007. URL: https://www.sciencedirect.com/science/article/pii/S1359836818330427.

A

ANNEX A-INPUT DATA FOR MATERIAL MODELS IN ABAQUS

This annex aims to show the material properties for concrete and steel of the applied elements in Abaqus FEM software, version of Abaqus/CAE 2022.

A.1. CONCRETE MATERIAL

Concrete is modeled with CDP (Concrete damage plasticity) model by implementing concrete failure, type=strain key attributes. Data of compression and tension damage are shown above.

** MATERIALS
**
***Material, name="Concrete C40"**

*Density
2.4516e-09,

*Elastic
35000., 0.2

*Concrete Damaged Plasticity
40., 0.1, 1.16, 0.66667, 0.

*Concrete Compression Hardening
19.18, 0.
28.4758, 5.19e-05
32.3416, 8.73e-05
35.8849, 0.000132511
39.0703, 0.000188622
41.857, 0.00025686
44.1979, 0.00033866
46.0378, 0.000435696
47.9457, 0.000683664
46.9099, 0.00102117
45.0025, 0.00123219
41.9666, 0.00147753
37.6067, 0.00176314
31.6797, 0.00209642
29.5986, 0.00220972
21.2886, 0.00277814
17.0242, 0.00322352
14.4523, 0.00361741
12.7379, 0.00398523
11.5126, 0.00433816
10.5899, 0.00468189
9.86562, 0.00501959
8.7868, 0.00568374
8.00074, 0.00633898
7.67541, 0.00666454
7.11412, 0.00731295
6.86653, 0.00763615
6.63552, 0.00795884
6.01542, 0.0089247
5.82678, 0.0092461
4.80841, 0.0111711

*Concrete Tension Stiffening
3.5, 0.
2.47862, 0.000605786
1.78793, 0.00121157
1.33612, 0.00181736
1.04514, 0.00242314
0.856103, 0.00302893
0.728018, 0.00363471
0.63428, 0.0042405
0.558764, 0.00484629
0.492474, 0.00545207
0.430946, 0.00605786
0.37239, 0.00666364

*Concrete Compression Damage
0., 0.
0., 2.53e-05
0., 8.73e-05
0., 0.000132511
0., 0.000188622
0., 0.00025686
0., 0.00033866
0., 0.000435696

0.00113088, 0.000683664
0.0227103, 0.00102117
0.0624479, 0.00123219
0.125696, 0.00147753
0.216527, 0.00176314
0.340007, 0.00209642
0.383362, 0.00220972
0.556488, 0.00277814
0.645329, 0.00322352
0.698911, 0.00361741
0.734627, 0.00398523
0.760154, 0.00433816
0.779378, 0.00468189
0.794466, 0.00501959
0.816942, 0.00568374
0.833318, 0.00633898
0.840096, 0.00666454
0.851789, 0.00731295
0.856947, 0.00763615
0.86176, 0.00795884
0.874679, 0.0089247
0.878609, 0.0092461
0.899825, 0.0111711

*Concrete Tension Damage
0., 0.
0.291824, 0.000605786
0.489163, 0.00121157
0.618251, 0.00181736
0.701387, 0.00242314
0.755399, 0.00302893
0.791995, 0.00363471
0.818777, 0.0042405
0.840353, 0.00484629
0.859293, 0.00545207
0.876873, 0.00605786
0.893603, 0.00666364
0.909586, 0.00726943
0.924739, 0.00787521
0.938922, 0.008481

***Concrete Failure, TYPE=Strain**
0.008, 0.0112, 0.94, 0.90

A.2. STEEL MATERIALS

Section A.2 including material properties of all structural steel elements that are used in the Abaqus model, such as steel plate, steel bolt, rebars and loading plates.

***Material, name="Loading plate"**
*Density
7.85e-09,

*Elastic
210000., 0.3

*Plastic
1000., 0.
1100., 0.01

***Material, name="Reinforcement bar"**
*Density
7.85e-09,

*Elastic
210000., 0.3

*Plastic
400., 0.
500., 0.3

***Material, name=Steel**
*Density
7.85e-09,

*Elastic
210000., 0.3

*Plastic
640., 0.
642.048, 0.000152
642.442, 0.000252
665.537, 0.006051
688.829, 0.011816
712.098, 0.017549
734.571, 0.023248
754.815, 0.028916
771.601, 0.034551
784.984, 0.040155
795.964, 0.045728
805.551, 0.05127
814.398, 0.056781
822.863, 0.062262
831.138, 0.067714
839.319, 0.073135
847.463, 0.078528
855.598, 0.083891
863.742, 0.089226
871.905, 0.094533
880.092, 0.099811
888.31, 0.105062
896.558, 0.110286
901.912, 0.117057
907.455, 0.123729
912.745, 0.1304
917.805, 0.137072
922.657, 0.143744
927.316, 0.150415
931.799, 0.157087
936.12, 0.163758
940.289, 0.17043
944.319, 0.177101
948.219, 0.183773
951.997, 0.190445
955.662, 0.197116
959.219, 0.203788
962.677, 0.210459
966.04, 0.217131
969.313, 0.223802
972.503, 0.230474
975.612, 0.237146

***Material, name="washer S275"**
*Density
7.85e-09,

*Elastic
210000., 0.3

*Plastic
275., 0.
275.378, 6.5e-05
275.614, 0.000165
296.853, 0.009039
318.399, 0.017834
340.038, 0.026553
361.013, 0.035197
379.912, 0.043766
395.498, 0.052263
407.789, 0.060688
417.746, 0.069043
426.352, 0.077328
434.247, 0.085545
441.784, 0.093696
449.15, 0.10178
456.443, 0.1098
463.717, 0.117756
471., 0.125649
478.309, 0.13348

B

ANNEX B- REINFORCEMENT CALCULATION

Hand calculation of reinforcements that are required for conventional concrete slab with assigned dimensions is shown in this annex B. This calculation is done using PTC Mathcad Prime 6.0.0.0.

Material properties:

Concrete class: C40/50

Characteristic compressive strength: $f_{ck} := 40 \frac{N}{mm^2}$ $\gamma_c := 1.5$

Design compressive strength: $f_{cd} := \frac{f_{ck}}{\gamma_c} = 26.667 \frac{N}{mm^2}$

Mean tensile strength: $f_{ctm} := 3.5 \frac{N}{mm^2}$

Elastic modulus: $E_{cm} := 35\ GPa$

Steel rebar class: B500

Characteristic yield strength: $f_{yk} := 500 \frac{N}{mm^2}$ $\gamma_s := 1.15$

Design yield strength: $f_{yd} := \frac{f_{yk}}{\gamma_s} = 434.783 \frac{N}{mm^2}$

Geometry of the concrete strip:

Thickness of the concrete: $h_c := 220\ mm$

Width of the concrete: $b := 0.5\ m$

Span of the concrete: $L := 5.67\ m$

Applied loading cases:

Live load: $q_{live} := 3 \frac{kN}{m^2}$ $w_l := q_{live} = 3 \frac{kN}{m^2}$

Dead load:

Unit weight of the concrete: $\gamma_c := 25 \frac{kN}{m^3}$

Concrete self weight: $w_s := \gamma_c \cdot h_c = 5.5 \frac{kN}{m^2}$

Partition wall self weight: $g_{partition} := 1.1\ \frac{kN}{m^2}$ $w_p := g_{partition} = 1.1\ \frac{kN}{m^2}$

Total dead load on concrete slab: $w_g := w_s + w_p = 6.6\ \frac{kN}{m^2}$

Load combination:

Uniformly distributed surface load acting on the slab:

$w := 1.35 \cdot w_g + 1.5 \cdot w_l = 13.41\ \frac{kN}{m^2}$

Line load acting on this 0.5m strip of the concrete slab:

$q := w \cdot b = 6.705\ \frac{kN}{m}$

For three point bending, the load is applied in the middle of the slab as a manner of point load, in which it shows the most pessimistic loading scenario, in order to find out the failure mechanisms of this demountable connection.

Point load: $F := q \cdot L = 38.017\ kN$

Reinforcement calculation:

Main reinforcement:

Sagging bending moment of the slab: $M_{sag} := F \cdot \frac{L}{8} = 26.945\ kN \cdot m$

Hogging bending moment of the slab: $M_{hog} := -F \cdot \frac{L}{8} = -26.945\ kN \cdot m$

Assumed diameter of the rebar: $\phi := 12\ mm$

Concrete cover: $cover := 20\ mm$

Effective depth of the concrete: $d := h_c - cover - \frac{\phi}{2} = 194\ mm$

K capital factor for calculating reinforcement required: $K := \frac{|M_{hog}|}{b \cdot d^2 \cdot f_{ck}} = 0.036$

Arm length of the reinforcement bar:

$z := \frac{d}{mm} \cdot \left(1 + \sqrt{1 - 3.53 \cdot K}\right) = 187.665$ > $0.95 \cdot d = 184.3\ mm$ $z := 0.95 \cdot d = 184.3\ mm$

Required area of the reinforcement bar for 0.5m strip: $A_{s.req} := \frac{|M_{hog}|}{0.87 \cdot f_{yk} \cdot z} = 336.094\ mm^2$

Required area of the reinforcement bar for 1m unit length: $A_{s.req.1m} := A_{s.req} \cdot 2 = 672.187\ mm^2$

Area of single reinforcement bar: $A_s := \frac{\pi \cdot \phi^2}{4} = 113.097\ mm^2$

Bar size	*Spacing of bars (mm)*								
(mm)	50	75	100	125	150	175	200	250	300
6	566	377	283	226	189	162	142	113	94.3
8	1010	671	503	402	335	287	252	201	168
10	1570	1050	785	628	523	449	393	314	262
12	2260	1510	1130	905	754	646	566	452	377
16	4020	2680	2010	1610	1340	1150	1010	804	670
20	6280	4190	3140	2510	2090	1800	1570	1260	1050
25	9820	6550	4910	3930	3270	2810	2450	1960	1640
32	16100	10700	8040	6430	5360	4600	4020	3220	2680
40	25100	16800	12600	10100	8380	7180	6280	5030	4190

Table C Cross-sectional area per metre width for various bar spacing (mm^2)

Assumed diameter of the rebar: $\phi = 12\ mm$

Taken spacing between rebars: $spacing := 150\ mm$

Provided area of reinforcement in 1m: $A_{s.pro} := 754\ mm^2$ > $A_{s.req.1m} = 672.187\ mm^2$

Required number of rebars in 1 meter: $\frac{1\ m}{spacing} = 6.667$ → taken as $n := 8$

Required number of rebars for 0.5m concrete strip: $n := \frac{n}{2} = 4$

<u>Checking if compression reinforcements are needed:</u>

$\delta := 0.8 \qquad K' := 0.6\ \delta - 0.18 \cdot \delta^2 - 0.21 = 0.155$

$K = 0.036$ < $K' = 0.155$ → dont need any compression reinforcement

<u>Deflection check:</u>

Actual span-depth ratio: $\frac{L}{d} = 29.227$

Reference reinforcement ratio: $\rho_0 := \sqrt{\frac{f_{ck}}{MPa}} \cdot 10^{-3} = 0.006$

Required tension reinforcement ratio at mid-span to resist the moment due to the design loads:

$$\rho := \max\left(\frac{A_{s.req}}{b \cdot d}, 0.0035\right) = 0.0035$$

Check: $\rho < \rho_0 = 1$

Allowable modified ratio:

Factor to take into account the different structural systems: $k := 1.5$ (taken from table 7.4N)

According to EC1992-1-1, formula 7.16a is taken:

$$ratio := k \cdot \left(11 + \left(\frac{1.5 \cdot \sqrt{\frac{f_{ck}}{MPa}} \cdot \rho_0}{\rho}\right) + 3.2 \cdot \sqrt{\frac{f_{ck}}{MPa}} \cdot \left(\frac{\rho_0}{\rho} - 1\right)^{\frac{3}{2}}\right) = 64.223$$

$\frac{L}{d} = 29.227$ < $ratio = 64.223$ √

Distribution steel:
(Secondary reinforcement)

Minimum area of reinforcement : $A_{smin} := 0.0013 \cdot b \cdot h_c = 143\ mm^2$

(Formular according to BS8110 table 3.25)

Rebar diameter assumed for distributional bars: $\phi_{dis} := 10\ mm$

Taken spacing between rebars: $spacing.dis := 250\ mm$

Provided area of reinforcement in 1m: $A_{s.pro.dis} := 314\ mm^2$

Distribution rebar: ϕ=10mm/250

Shear check:

Maximum shear force: $V_{max} := 0.5 \cdot F = 19.009\ kN$

Shear stress at the face of the support: $v := \frac{V_{max}}{b \cdot d} = 0.196\ \frac{N}{mm^2}$

Maximum allowable shear stress: $v_u := min\left(0.8 \cdot \sqrt{\frac{f_{ck}}{MPa}}, 5\right) = 5$

Check for shear: v=0.196 < vu=5 √

Values of vc design concrete shear stress:
(BS8110 Table 3.8)

$v_{c.0} := 100 \cdot \frac{A_{s.pro}}{b \cdot d} = 0.777$ < 3 √ $\gamma_m := 1.25$

Based on concrete strength of 25N/mm2:

$$v_c := \left(\frac{0.79 \cdot \left(100 \cdot \frac{A_{s.pro}}{b \cdot d}\right)^{\frac{1}{3}} \cdot \left(\frac{400}{\frac{d}{mm}}\right)^{\frac{1}{4}}}{\gamma_m} \right) \frac{N}{mm^2} = 0.696\ \frac{N}{mm^2}$$

Modification due to increased characteristic concrete strength:

$$v_c := v_c \cdot \left(\frac{f_{ck}}{25 \cdot \frac{N}{mm^2}}\right)^{\frac{1}{3}} = 0.814\ \frac{N}{mm^2}$$

$v = 0.196\ \frac{N}{mm^2}$ < $v_c = 0.814\ \frac{N}{mm^2}$ Shear check is √

Horizontal reinforcement due to nib flexure:

Shear span measured from the vertical reaction to center of hanger reinforcement:

$a := 100\ mm$

Distance from extreme compression fiber to nib flexural reinforcement:

$d_n := 140\ mm$

Force in the nib due to flexure: $F_{As} := \frac{F}{2} \cdot \left(\frac{a}{d_n}\right) = 13.578\ kN$

Assumed diameter of the rebars: $\phi_{nib} := 16\ mm$

Area of single rebar: $A_\phi := \frac{{\phi_{nib}}^2\ \pi}{4} = 201.062\ mm^2$

Area required for nib flexural reinforcement: $A_{s.req} := \frac{1}{0.75 \cdot f_{yd}} \cdot F_{As} = 41.638\ mm^2$

Number of required rebars: $n_{req} := \frac{A_s}{A_\phi} = 0.563$

Number of applied rebars: $n_{app} := 4$

The formular for horizontal reinforcement required due to nib flexure is taken from PCI Design Handbook Eq. (5-57). This formula is typically used for calculating normal dapped ends in concrete.

However, the concrete under consideration has a hole in the middle of the dapped end, along with potential additional normal forces arising from external conditions like deflection or earthquakes.

Therefore, the application of four rebars is considered a conservative approach to ensure adequate reinforcement.

C

ANNEX C- LCA CALCULATION SPREADSHEETS

Fully new designed

reinforcement — density 7850 kg/m3

	diameter [m]	area [m^2]	length [m]	no.	weight [kg]
hogging	0.012	0.00011304	1.307	4	4.63913899
long rebar	0.012	0.00011304	1.477	3	3.93190988
longitudinal	0.012	0.00011304	1.313	4	4.66043573
nib rebar	0.016	0.00020096	0.68	4	4.29089792
higging short	0.012	0.00011304	0.71	4	2.52011376
rectangular big	0.008	0.00005024	1.2	6	2.8395648
rectangular small	0.004	0.00001256	0.984	4	0.38807386
distributional bar	0.01	0.0000785	0.5	12	3.69735
bolt shank	0.02	0.000314	0.22	1	0.542278
bolt nut	0.03	0.0007065	0.0125	2	0.13865063
washer	0.037	0.000694725	0.003	2	0.03272155
SUM rebars	2*				53.9349699
SUM steel comp	2*				1.42730035

Existed concrete deck

reinforcement

	diameter [m]	area [m^2]	length [m]	no.	weight [kg]
hogging	0.012	0.00011304	0.71	6	3.78017064
longitudinal	0.012	0.00011304	5.67	3	15.0940616
rectangular big	0.008	0.00005024	1.2	7	3.3128256
distributional bar	0.01	0.0000785	0.5	23	7.0865875
SUM					29.2736454

Reusing existed concrete deck

	length [m]	width [m]	height [m]	no.	density [kg/m3]	weight [kg]	*2
steel plates	0.26	0.5	0.01	2	7850	20.41	40.82
	diameter [m]	area [m^2]	length [m]	no.	density [kg/m3]	weight [kg]	
steel bolts	0.02	0.000314	0.22	2	7850	0.02169112	0.043382
bolt nut	0.03	0.0007065	0.0125	4	7850	0.008319038	0.016638
washer	0.037	0.0006947	0.003	4	7850	0.002421395	0.004843
						sum	40.88486

Concrete	length [m]	width [m]	height [m]	density [kg/m3]	kg
	5.67	0.5	0.22	2500	1559.25

Shadow prize (Euro) per kg equivalents		0.16	0.05	30	0.09	0.03	0.0001	0.06	2	4	9	SUM
Impact category	**Unit**	Abiotic depletion	Global warming (GWP100)	Ozone layer depletion (ODP)	Human toxicity	Fresh water aquatic ecotox.	Marine aquatic ecotoxicity	Terrestrial ecotoxicity	Photochemical oxidation	Acidification	Eutrophication	
Unit		kg Sb eq	kg CO2 eq	kg CFC-11 eq	kg 1,4-DB eq	kg 1,4-DB eq	kg 1,4-DB eq	kg 1,4-DB eq	kg C2H4	kg SO2 eq	kg PO4--- eq	
Concrete C45/55 (CEM I-CEMIII)	kg	3.05E-04	1.07E-01	4.88E-09	1.12E-02	2.28E-03	3.80E+00	2.01E-04	8.24E-06	2.44E-04	4.29E-05	
Steel reinforcement for concrete	kg	1.54E-02	1.79E+00	7.17E-08	3.81E+00	1.49E+00	1.32E+03	3.18E-02	9.27E-04	7.38E-03	1.34E-03	
Steel components	kg	1.54E-02	1.79E+00	7.17E-08	3.81E+00	1.49E+00	1.32E+03	3.18E-02	9.27E-04	7.38E-03	1.34E-03	
Existed concrete slab	per half meter											
Concrete	1559.25	4.75E-01	1.66E+02	7.62E-06	1.75E+01	3.55E+00	5.93E+03	3.13E-01	1.29E-02	3.81E-01	6.70E-02	
Steel reinforcement	29.27365	4.49E-01	5.24E+01	2.10E-06	1.12E+02	4.35E+01	3.85E+04	9.31E-01	2.71E-02	2.16E-01	3.93E-02	
	kg sum	1	219	0	129	47	44438	1	0	1	0	
	For 8m span:	15	3503	0	2066	753	711005	20	1	10	2	
	Euro:	2.37	175.13	0.00	185.94	22.60	71.10	1.19	1.28	38.23	15.30	**513.15**
Fully new designed	per half meter											
Concrete	1559.25	4.75E-01	1.66E+02	7.62E-06	1.75E+01	3.55E+00	5.93E+03	3.13E-01	1.29E-02	3.81E-01	6.70E-02	
Steel reinforcement	53.93497	8.28E-01	9.66E+01	3.87E-06	2.06E+02	8.02E+01	7.10E+04	1.72E+00	5.00E-02	3.98E-01	7.25E-02	
Steel components	1.4273	2.19E-02	2.56E+00	1.02E-07	5.44E+00	2.12E+00	1.88E+03	4.54E-02	1.32E-03	1.05E-02	1.92E-03	
	kg sum	1	266	0	229	86	78760	2	0	1	0	
	For 8m span:	21	4250	0	3658	1374	1260157	33	1	13	2	
	Euro:	3.39	212.51	0.01	329.21	41.23	126.02	1.99	2.05	50.56	20.35	**787.32**
Reusing existed concrete slab	per half meter											
Steel components	40.88486	6.28E-01	7.32E+01	2.93E-06	1.56E+02	6.08E+01	5.38E+04	1.30E+00	3.79E-02	3.02E-01	5.49E-02	
	For 8m span [kg]	10	1172	0	2495	973	860604	21	1	5	1	
	Euro:	1.61	58.59	0.00	224.52	29.19	86.06	1.25	1.21	19.32	7.91	**429.66**